A CASE OF SPLIT-LINE RESEARCH SPECIMENS RECEIVED FOR FORENSIC ANTHROPOLOGICAL ANALYSIS

Angi M. Christensen, PhD, D-ABFA

FBI, Laboratory Division

Leslie S. Larsen, MAPS

FBI, Detroit Division

Brian F. Spatola, MA

National Museum of Health and Medicine, Defense Health Agency

ISFRI Annual Congress – Albuquerque, NM 2020

Disclaimer

- The content of this presentation is UNCLASSIFIED/FOUO (for official use only).
- The views expressed are those of the authors and do not necessarily reflect the position or views of the FBI, the US DOD Defense Health Agency, or the US Government.
- Names of commercial manufacturers are provided for identification purposes only, and inclusion does not imply endorsement of the manufacturer or its products or services by the FBI or DOD.

"Body Brokers"

- Multiple US federal and state organizations (led by FBI Detroit Division) investigated case 2012 – 2018
- Network of "body brokers" operating in Michigan, Illinois, Arizona

- Suspected of fraudulently obtaining and then dismembering, packaging, selling, and leasing body parts (some carrying communicable diseases)
- Distributed to a vast network of domestic and foreign medical research, medical equipment, and pharmaceutical end users who would otherwise have a difficult time obtaining donated human body parts

- Search executed on Detroit warehouse
- Gray plastic bin with lid discovered under a desk

- Bin contained skeletal material of apparent human origin and described as having a “speckled” appearance
- Remains sent to FBI Laboratory for anthropological analysis

- Remains consisted of an assemblage of more than 60 bones and bone fragments.
- Minimum of 16 individuals represented including adults and subadults
- Fragmentary in nature, overall poor quality, limited quantity of skeletal material for each individual

- Most skeletal material bears regular, dark, linear markings on all surfaces

- Markings also appear on some endocranial surfaces

- Overall poor preservation with warping, cracking, reduction in bone quality and density

- Standard radiographs do not show markings, and illustrate reduction in bone and tooth density and quality

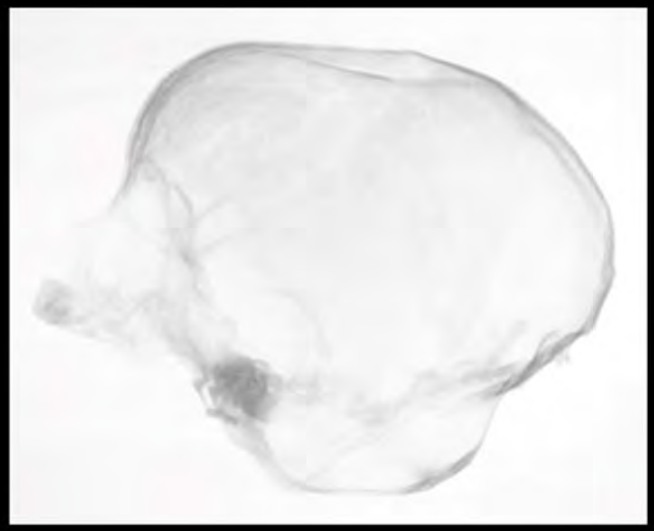

- Markings examined microscopically
- Dark markings are located along the margins of superficial fissures

- Other alterations include
  - Drill holes
  - Hardware
  - Sectioning
  - Cord/string
- Consistent with use as anatomical teaching specimens

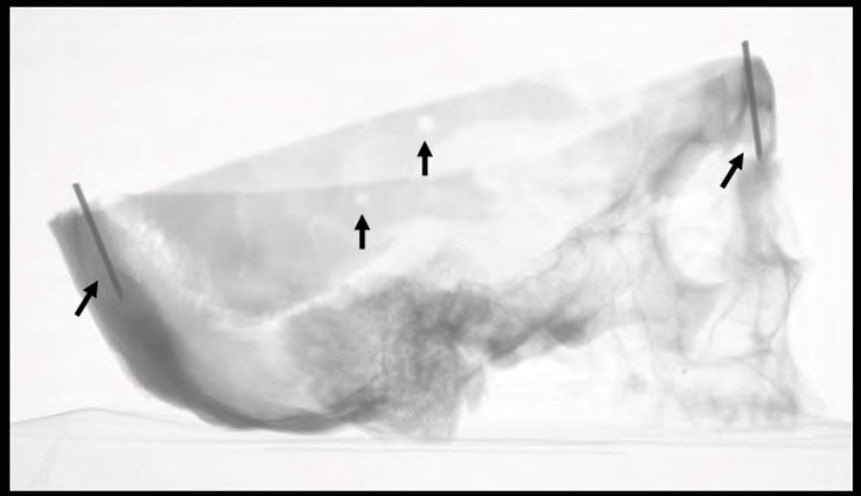

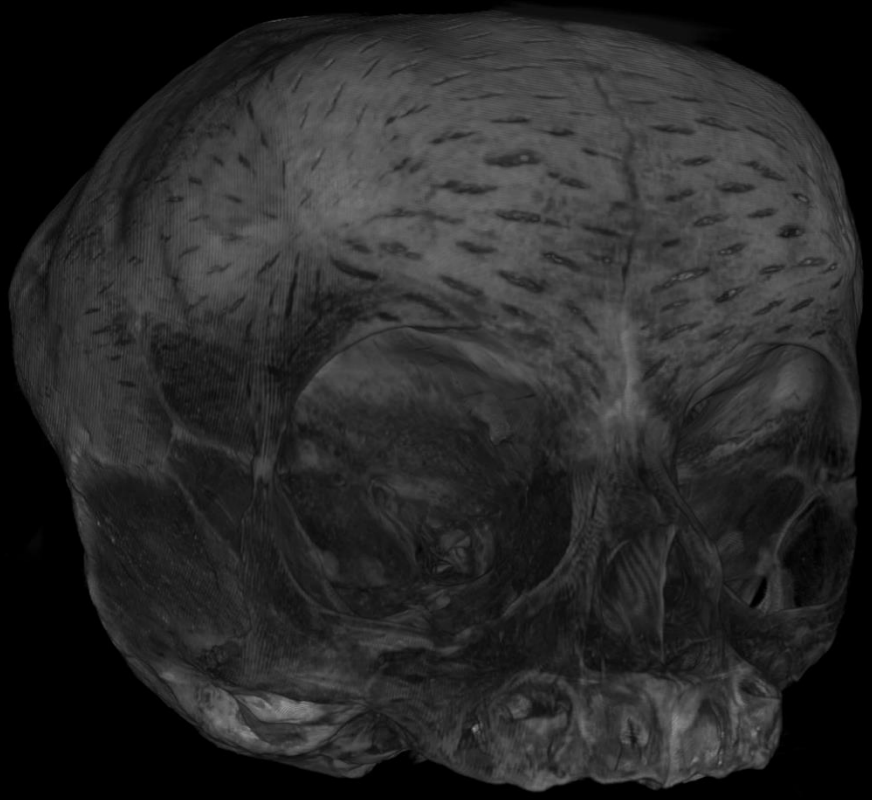

- Several specimens CT scanned, fissures clearly visualized
- CT scans highlight physical alterations of the bones

- Histogram adjustments further enhance the fissures

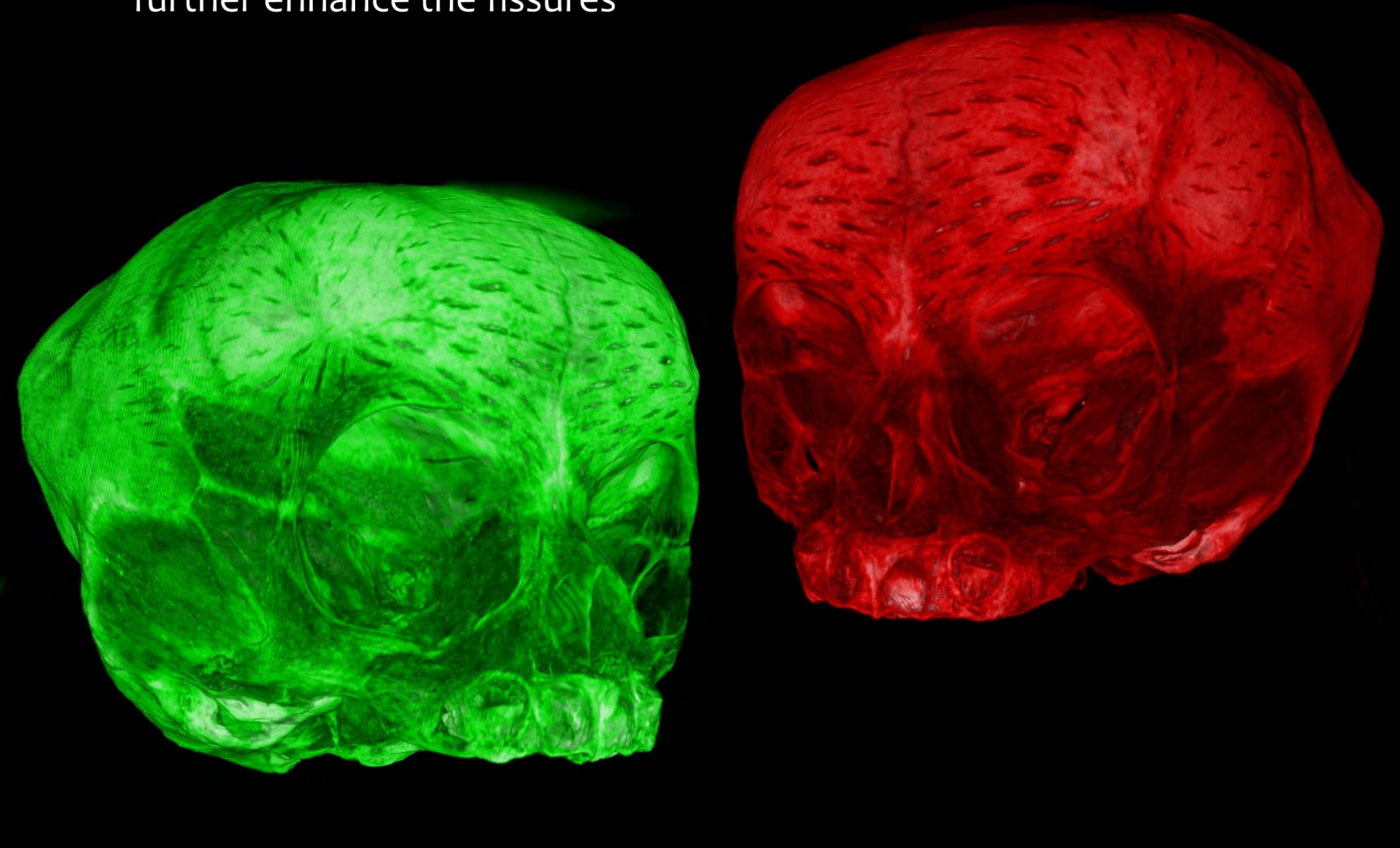

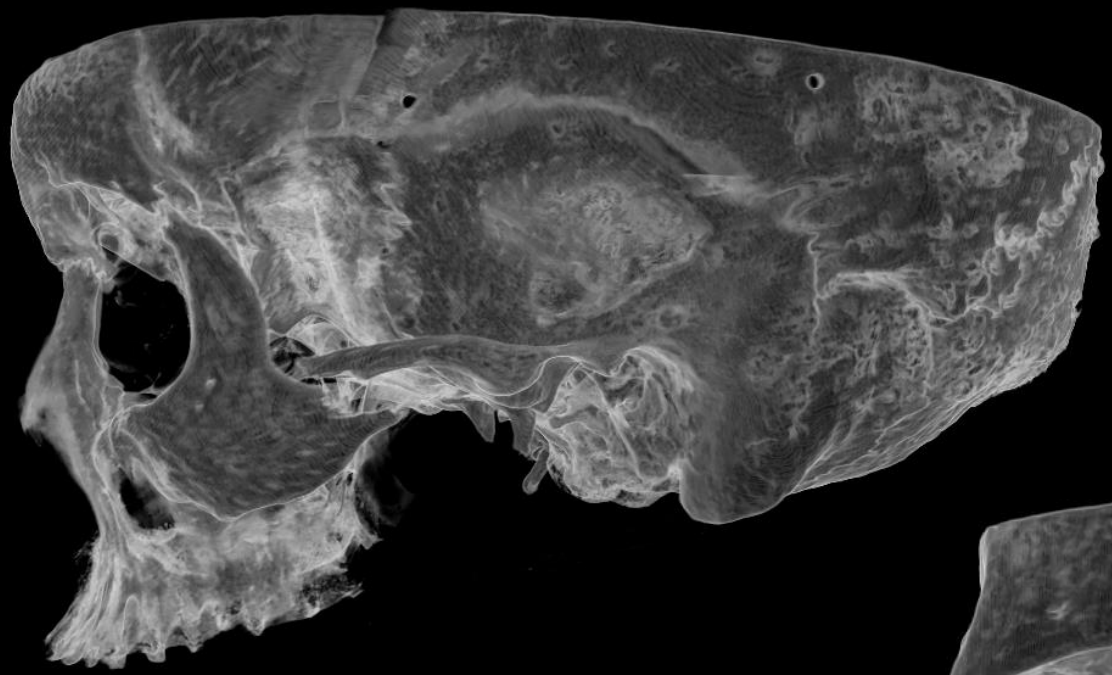

- Poor bone quality can also be appreciated in CT scans
- Fissure and drill holes easily visualized

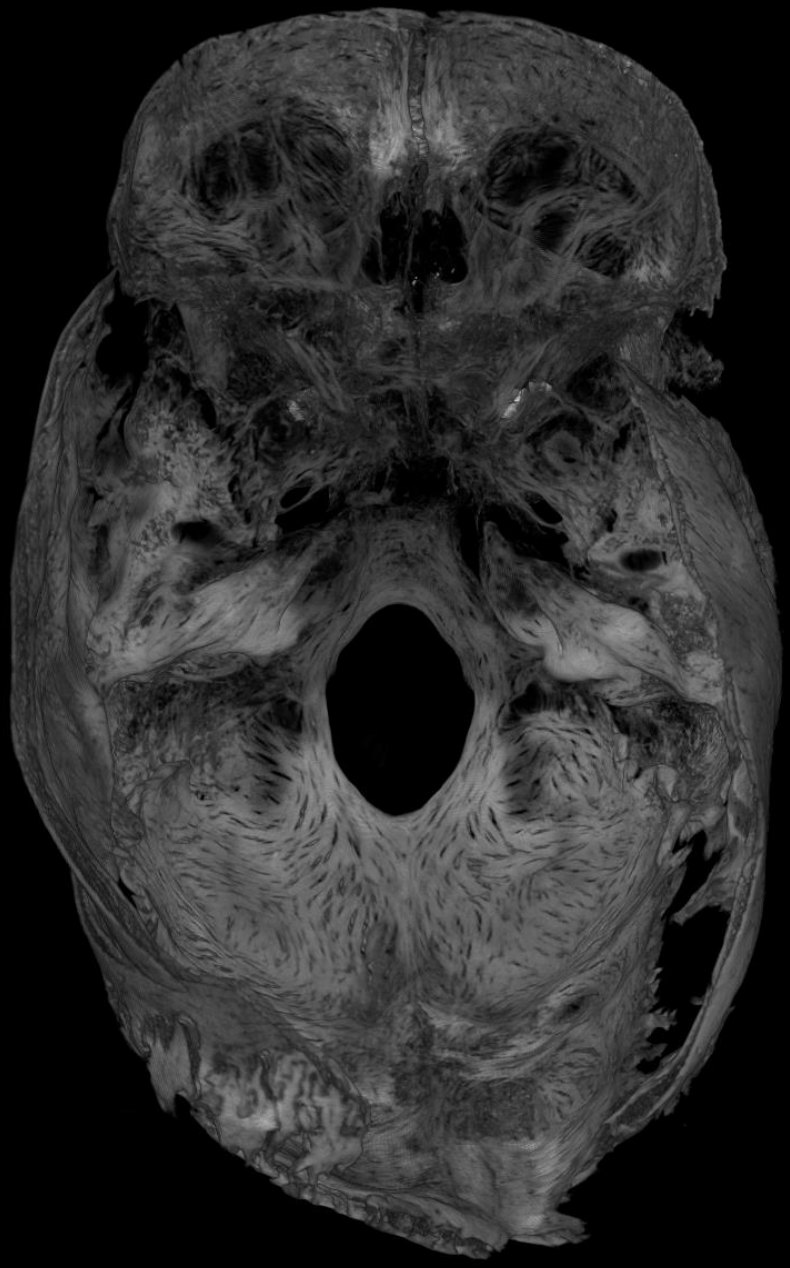

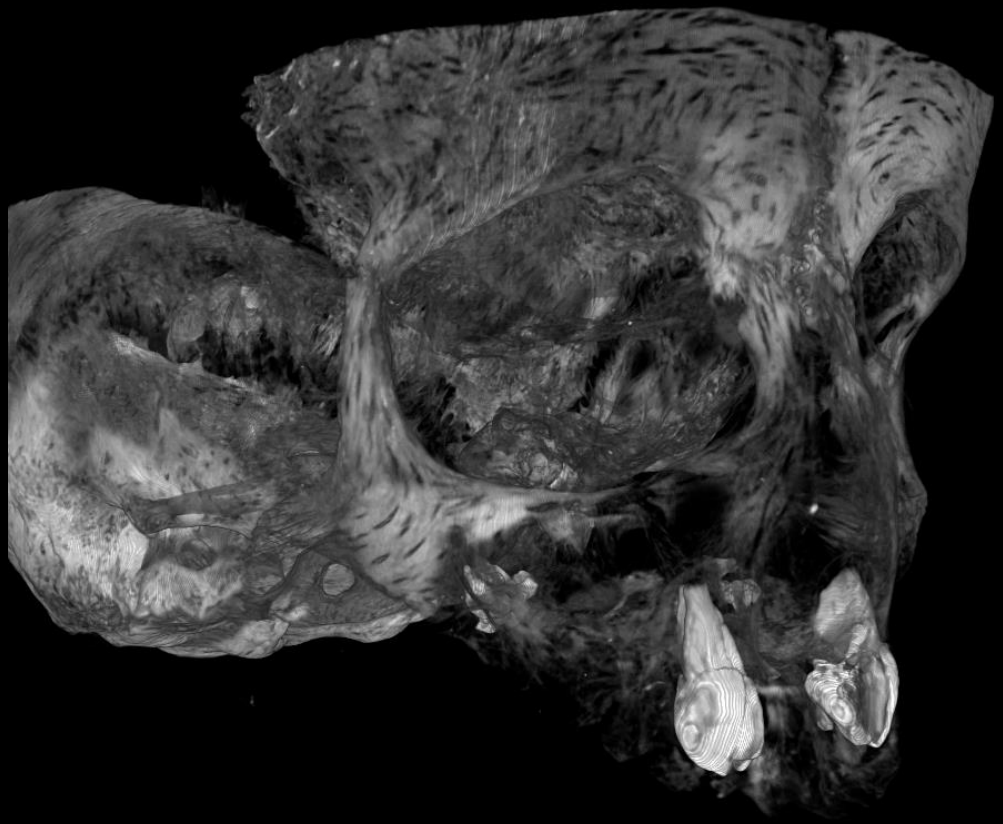

- Endocranial fissures observed
- Poor quality of dental tissue
- Cranial warping

- Through consultation with National Museum of Health and Medicine, this pattern was discovered to be consistent with material utilized in research involving the “split-line” technique
  - Method of assessing biomechanical structure of cortical bone
  - Typically involves puncturing decalcified bone with a needle dipped in India ink to produce linear marks (“split-lines”) that reveal the grain direction of underlying matrix
- This approach explains the patterned markings as well as the poor bone and tooth quality from decalcification process

- X-ray fluorescence spectrometry performed on a clavicle
- Revealed presence of calcium and phosphorus expected for skeletal tissue, as well as sulfur
- No heavy elements detected

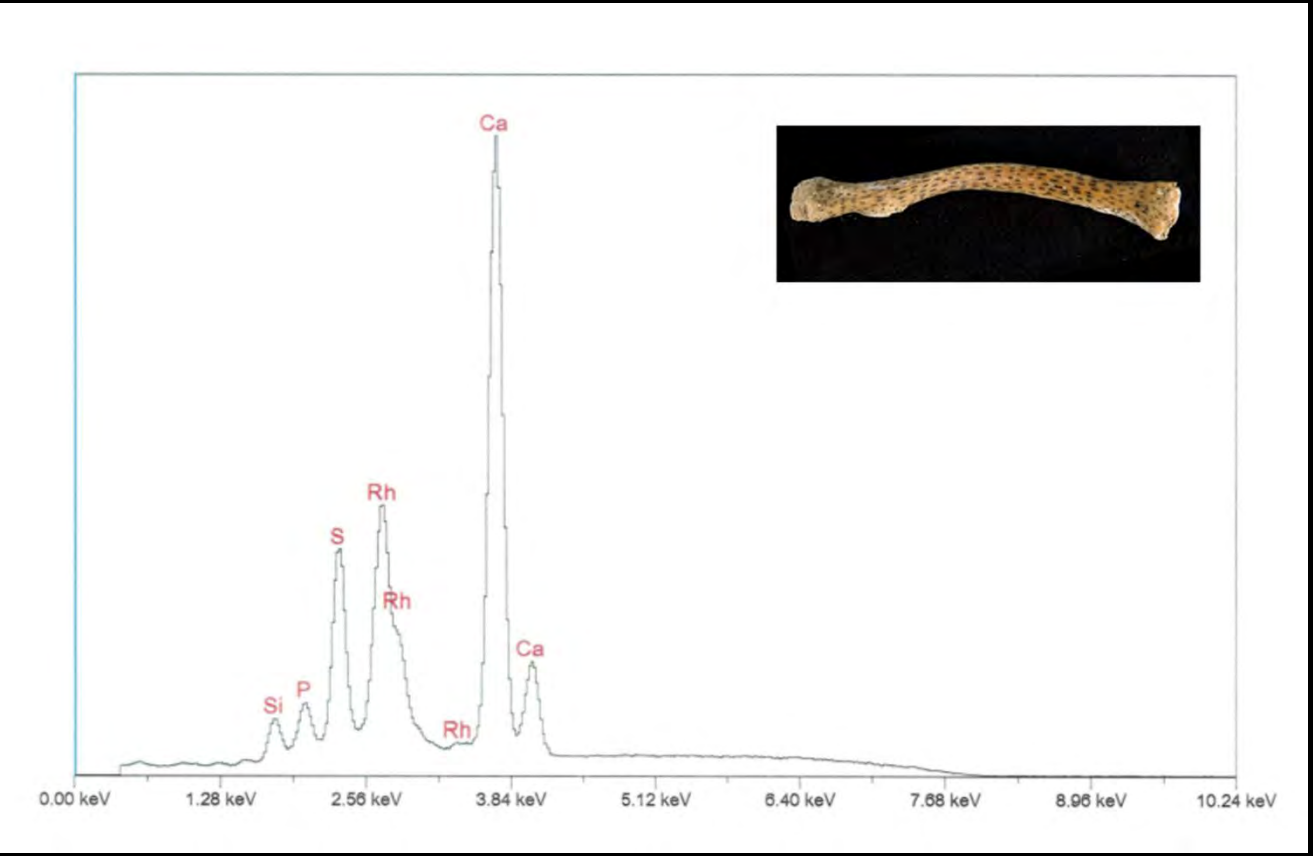

- Forensic anthropologists often receive non-medicolegally significant skeletal material for analysis, including remains from educational, archaeological, and historic contexts
- Receipt of former research specimens appears considerably rarer

- Lax institutional controls on the disposition of remains in medical, museological, and medicolegal contexts can lead to instances of body parts being stolen, deaccessioned, or otherwise removed from the institution and sold or held in “black market” collections

- Original provenience of split-line specimens remains unknown
- Appear to be only incidentally related to the criminal investigation
- As a result of other activities, primary suspect convicted on counts including wire fraud, illegally transporting hazardous material, lying to federal investigators
- Case let to two spin-off cases in Phoenix and Chicago where suspects pled guilty to state and federal charges

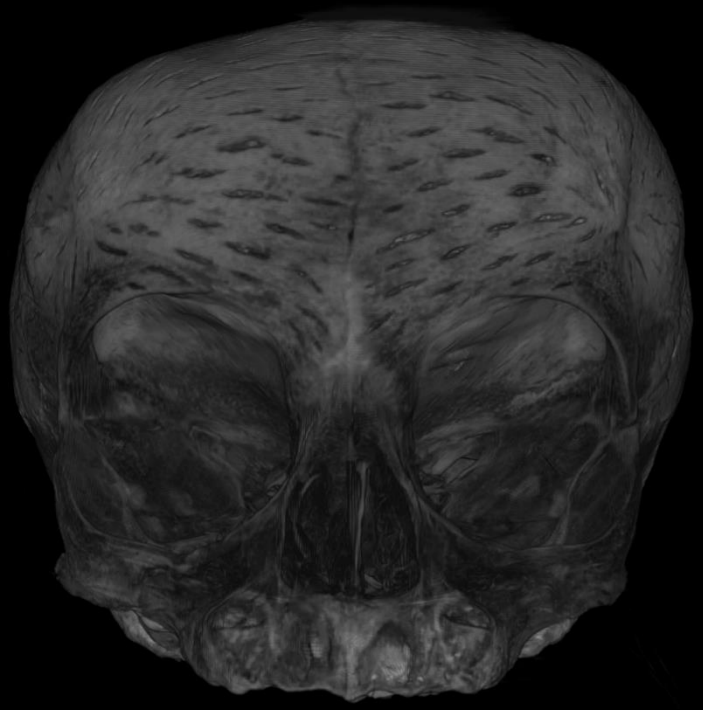

- This is believed to be the only anthropological case involving skeletal research specimens in FBI Laboratory history
- CT imaging significantly complemented photography and other examinations to clarify the likely origin of specimens
- Although rare, the possibility that skeletal remains may be former research specimens should be considered when investigating unusual or novel taphonomic features

References

- Christensen AM, Larsen L, Spatola BF. A case of split-line research specimens submitted for forensic anthropological analysis. *Forensic Anthropology* 2019 2(3):189-192.

Questions and contact

Angi M. Christensen, PhD, D-ABFA

Forensic Anthropologist

FBI Laboratory

2501 Investigation Parkway

Quantico, VA 22135

amchristensen@fbi.gov

Anthropological measurement protocol for post-cranial bones in post-mortem computed tomography using thin slab maximum intensity projection

Laure Spake, Julia Meyers, Soren Blau, Hugo Cardoso, Nicolene Lottering

This poster introduces a **published protocol** for the measurement of post-cranial bones in computed tomography (CT) scans using slab maximum intensity projection (slab MIP) visualization.

The summarized steps of the protocol are described and illustrated using on **page 1**. The full protocol is available through the paper at the DOI below.

Testing of the protocol is reported on **page 2**, and indicates that it yields highly repeatable and accurate measurements, while remaining flexible enough to implement in most DICOM viewers without exporting images to specialized software.

Paper at: doi.org/10.1016/j.fri.2020.200354

Summarized measurement protocol

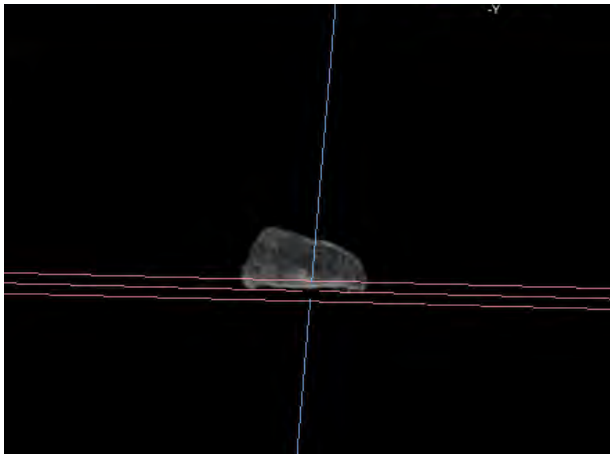

Step 1. Bring transverse slice to one of the ends of the bone. Adjust the measurement plane (middle red line) so that it replicates how the bone would rest on an osteometric board.

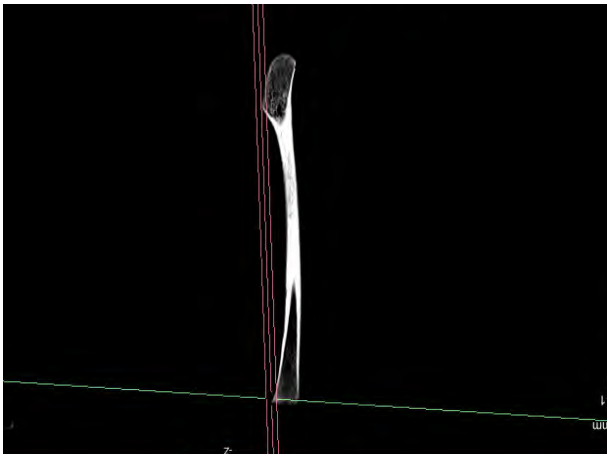

Step 2. Adjust the measurement plane (middle red line) so that it rests on the most posterior/inferior point of the opposite end of the bone.

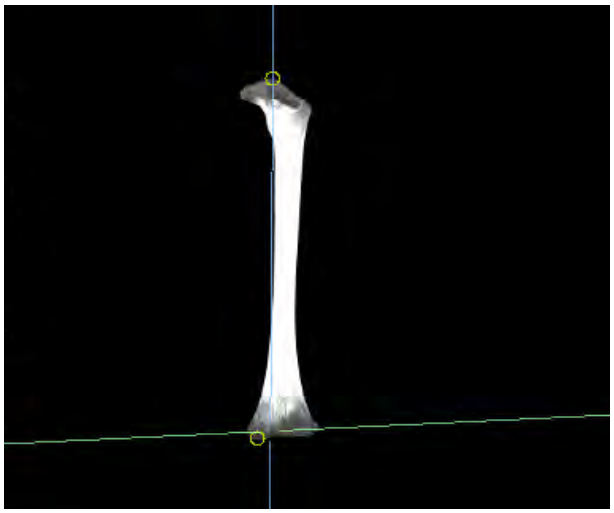

Step 3. Set the measurement slice to slab MIP mode and adjust thickness of the slab so that both maximal points of the bone (yellow circles) are simultaneously observed.

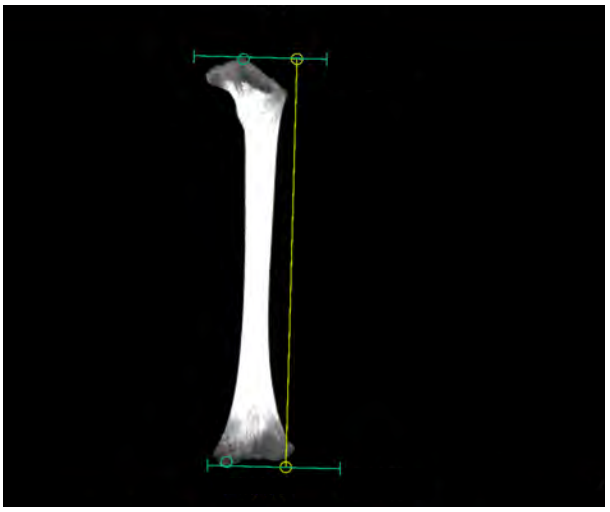

Step 4. Draw a line along the measurement axis. Add lines perpendicular to the axis, and align with the maximal points. Measure between these lines, along the axis of measurement.

Paper at: doi.org/10.1016/j.fri.2020.200354

Comparative testing of protocol

- **Testing repeatability**: Two observers took repeat measurement of four bones in nine juvenile individuals (aged 0-10 years).

	Inter observer error		Intra observer error	
	TEM (mm)	rTEM (%)	TEM (mm)	rTEM (%)
Humerus	1.00	0.66	1.24	0.66
Radius	0.37	0.34	0.28	0.25
Femur	1.51	0.76	1.33	0.67
Tibia	0.96	0.59	0.80	0.49

- **Testing accuracy**: Four dry bones from 10 juvenile individuals (aged 0-11 years) were measured on an osteometric board and in DICOM using the protocol.

	Humerus	Ulna	Femur	Tibia
TEM (mm)	0.45	0.50	0.53	0.45
rTEM (%)	<0.01	<0.01	<0.01	<0.01

- **Comparison to other protocols**: This protocol performs better than DICOM-only protocols [1, 2], but less well than protocols requiring importing images to CAD software [3, 4].

		Inter observer error		Intra observer error	
Study	Bone	TEM (mm)	rTEM (%)	TEM (mm)	rTEM (%)
Robinson [1]	Tibia	1.00	0.66	1.24	0.66
Brough [2]	Clavicle	0.37	0.34	0.28	0.25
Lottering [3]	Cranium	1.51	0.76	1.33	0.67
Reynolds [4]	Femur	0.96	0.59	0.80	0.49

Paper at: doi.org/10.1016/j.fri.2020.200354

References and acknowledgements

- References:

1. Robinson C, Elsma R, Morgan B, Jeffery A, Graham AEM, Black S, Rutty GN. 2008. Anthropological measurement of lower limb and foot bones using multi-detector computed tomography. J Forensic Sci 53:1289-1295.
2. Brough AL, Bennett J, Morgan B, Black S, Rutty GN. 2013. Anthropological measurement of the juvenile clavicle using multi-detector computed tomography – affirming reliability. J Forensic Sci 58:946-951.
3. Lottering N, MacGregor DM, Barry MD, Reynolds MS, Gregory LS. 2014. Introducing standardized protocols for anthropological measurement of virtual subadult crania using computed tomography. J Forensic Radiol Imaging 2:34-38.
4. Reynolds MS, MacGregor DM, Barry MD, Lottering N, Schmultz B, Wilson LJ, Meredith M, Gregory LS. 2017. Standardized anthropological measurement of postcranial bones using three-dimensional models in CAD software. Forensic Sci Int 278:381-387.

- Acknowledgements:

The CT scans used in this study and to illustrate the supplementary file (full protocol) associated with this study are housed at the Victorian Institute of Forensic Medicine (VIFM) in Melbourne, Australia. The PMCT scans used to illustrate Figures 1-4 in this document and the associated paper are house at the Office of the Medical Investigator (OMI) in Albuquerque, UDA. The dry bone scans were taken from individuals house in the Luis Lopes collection at the National Museum of Natural History and Science in Lisbon, Portugal. This study stems from projects approved by the VIFM Ethics Committee (No. 1090) and the SFU Office of Research Ethics (2018s0465 and 2019s0154). Data collection for this study was supported by Mitacs (Globalink Research Award IT13950), the Natural Sciences and Engineering Research Council (NSERC RGPIN-2016-05863), the Social Sciences and Humanities Research Council (SSHRC 752-2019) and the Department of Archaeology at SFU. During the preparation of this poster, LS was supported by the John Templeton Foundation.

- Citation for the published protocol:

Spake L, Meyers J, Blau S, Cardoso HFV, Lottering N. 2020. A simple and software independent protocol for the measurement of post-cranial bones in anthropological contexts using thin slab maximum intensity projection. Forensic Imaging 20:200354.

Paper at: doi.org/10.1016/j.fri.2020.200354

SFU | University of Otago | VIFM | Monash University | Swinburne

ISFRI 2020 Virtual Poster Session

Comparison of attenuation in ascites between antemortem and postmortem computed tomography

Masanori Ishida, Wataru Gonoi, Hiroyuki Abe, Kotaro Fujimoto, Naomasa Okimoto, Tetsuo Ushiku, Osamu Abe

Department of Radiology, The University of Tokyo Hospital, Tokyo, Japan

email address; ishidam-tky@umin.ac.jp (Masanori Ishida, MD,PhD)

Conflict of interest; none

Background

- It is important to understand the postmortem features required for interpreting postmortem computed tomography (PMCT) findings. [1-3]
- In postmortem investigation, increased attenuation of ascites on PMCT is not often pathologically significant.
- Changes in the attenuation of ascites between antemortem computed tomography (AMCT) and PMCT have not been investigated.

Objective

- To investigate the changes in ascites attenuation between antemortem (AMCT) and PMCT analyses of the same subjects.

Methods

- This study was approved by the Ethical Committee of the participating institution.
- Informed consent for the use of the cadavers in our study was obtained from the families of the deceased subjects.
- The potential subjects had been subjected to PMCT and conventional cadaver autopsy after death from non-traumatic causes at our academic tertiary care hospital between April 2009 and December 2018.
- Figure 1 summarizes the subject inclusion and exclusion criteria.

Fig. 1 Flowchart of the study inclusion and exclusion criteria. PMCT, postmortem CT; AMCT, antemortem CT.

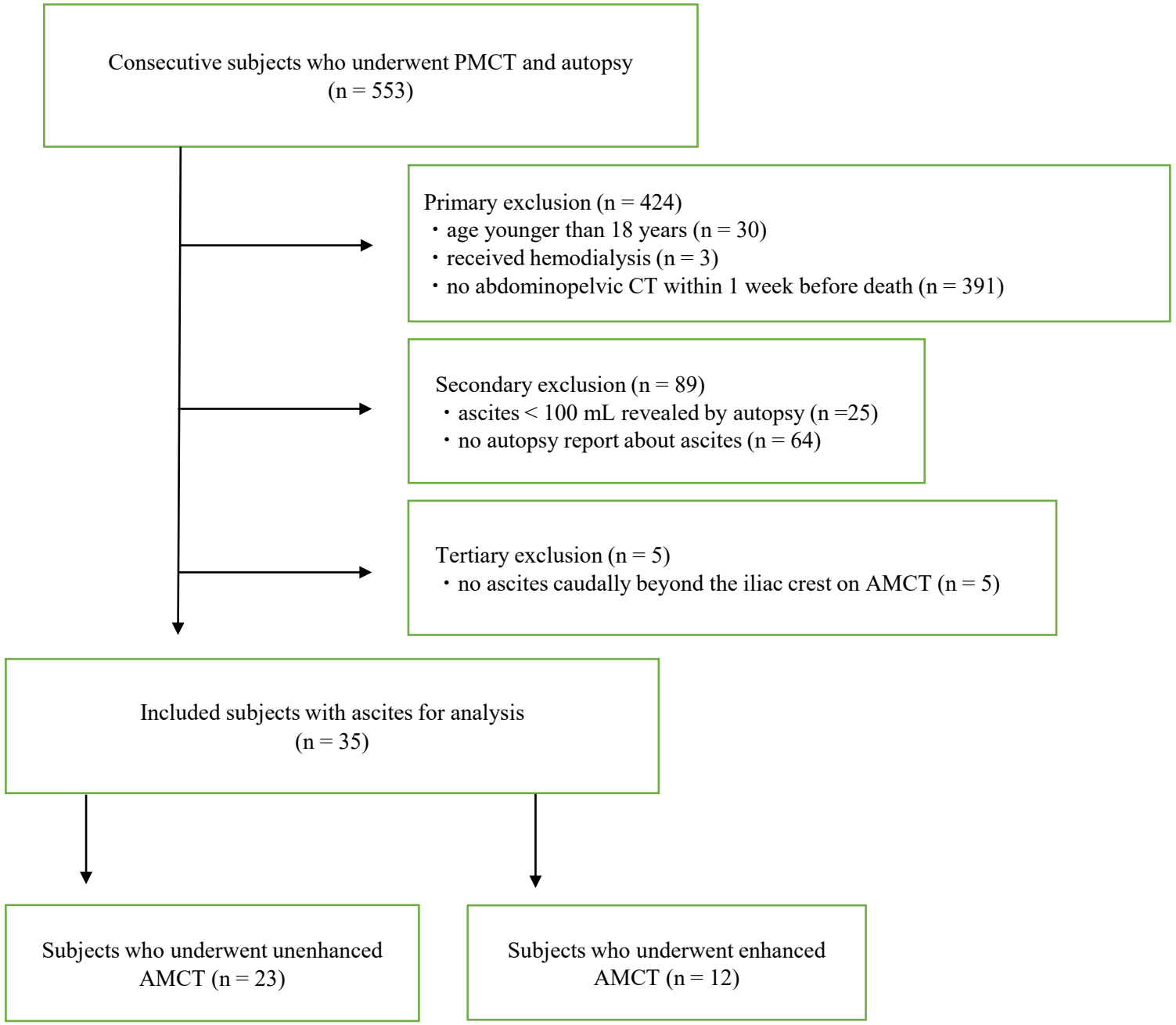

Methods *-CT techniques*

	AMCT (within 7 days before death)	PMCT
CT scanner	64-detector-row (Aquilion 64, Canon Medical Systems Corporation, Ohtawara, Japan; Discovery CT750 HD or LightSpeed VCT, GE Healthcare, Buckinghamshire, UK)	4 or 64-detector-row (Robusto, Hitachi Medical Corporation, Tokyo, Japan; Aquilion 64, Canon Medical Systems Corporation, Ohtawara, Japan)
Contrast medium	unenhanced or enhanced (an intravenous injection of iohexol (Omnipaque; Daiichi-Sankyo Co., Ltd., Tokyo, Japan), iopamidol (Iopamiron; Bayer Yakuhin Ltd., Osaka, Japan, Oypalomin; Fuji Pharma Co., Ltd., Tokyo), or iomeprol contrast medium (Iomeron; Eisai Co., Ltd., Tokyo) at a dose of 300 mgI/kg)	unenhanced
Subjects' upper limbs	raised	lowered

Methods *-Image analysis*

- CT images were reviewed on a two-dimensional workstation (RadiAnt DICOM Viewer, Medixant, Poznan, Poland).
- The attenuation (in Hounsfield units, HU) of ascites was measured manually in 100-mm^2 circular regions of interest (ROIs).
- ROIs were placed at similar sites on pairs of AMCT and PMCT images from each subject (Fig. 2). [4,5]

Fig. 2 Examples of measurement of ascites attenuation on CT. Circular ROIs were set on AMCT (a) and PMCT images (b). CT ascites attenuations was measured on the ventral or dorsal site or both sites.

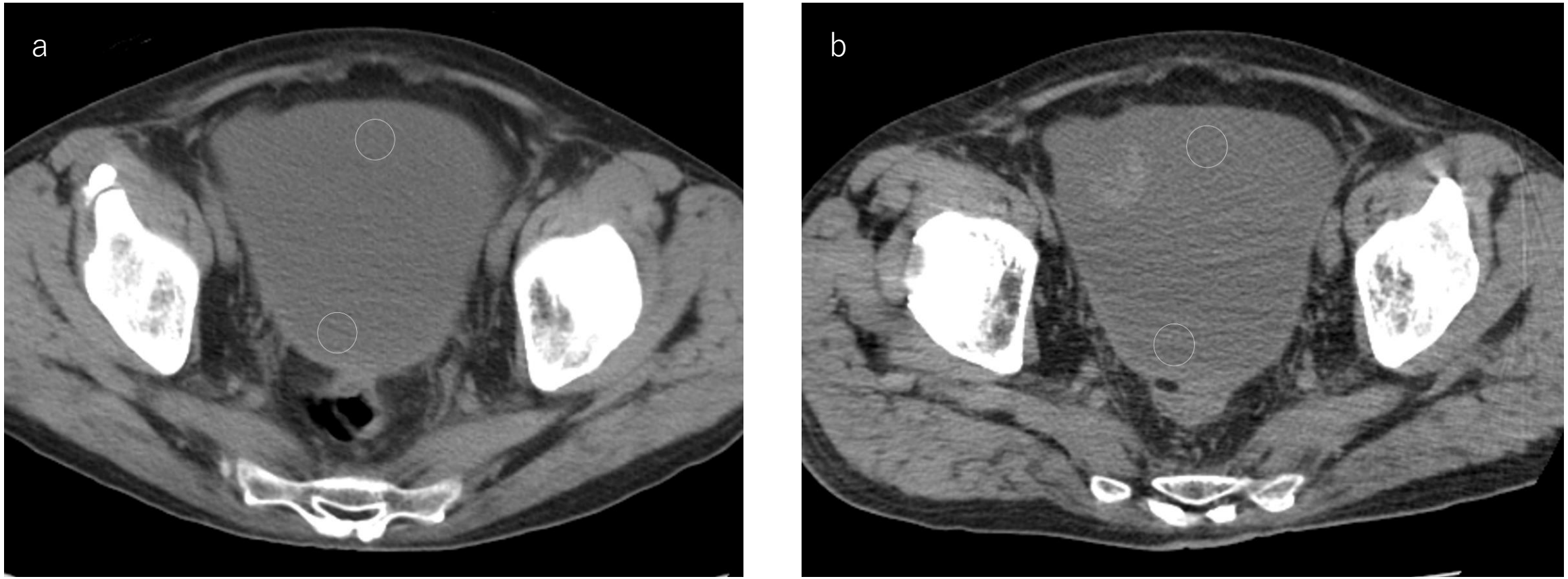

Methods *-Autopsy technique*

- Autopsies using conventional procedures were performed by board-certified pathologists immediately after PMCT.
- The pathologists were informed about the patients' clinical histories and details regarding the circumstances of death and, but they were unaware of the PMCT findings.
- The pathologists noted the findings of ascites, including the volume and appearance (i.e., serous, hemorrhagic, proteinous, chylous, and/or fecal).

Methods -*Clinical and autopsy data*

- The following data were collected:
  - Serum albumin concentration and estimated glomerular filtration rate (eGFR) within 1 day before AMCT
  - History of hemodialysis and cardiopulmonary resuscitation
  - Time intervals between AMCT and PMCT and between death and PMCT
  - Ascites findings (the volume and appearance)
  - Presence of carcinomatous peritonitis

Methods –*Data and statistical analysis*

- Mann–Whitney U test; to compare the demographic, clinical, imaging, and autopsy characteristics between subjects who underwent unenhanced and enhanced AMCT.
- Paired t-test; to evaluate differences in the attenuations of ascites between AMCT and PMCT.
- A multiple regression analysis; to evaluate potential factors contributing to changes in attenuation between AMCT and PMCT in subjects who exhibited significant changes in ascites attenuation.
- Spearman's rank correlation coefficient; to analyze a relationship between the time interval between enhanced AMCT and PMCT and elevated CT attenuation of ascites on PMCT.

Results –*Subject characteristics*

	Unenhanced AMCT (n = 23)	Enhanced AMCT (n = 12)	P value
Demographics			
Age (y), mean ± SD (range)	67.3 ± 11.2 (45–85)	70.6 ± 8.5 (54–84)	0.497
Sex, no. of males (%)	14 (61)	7 (58)	0.902
Clinical data			
Albumin (g/dL), mean ± SD (range)	2.5 ± 0.6 (1.4–3.8)	2.3 ± 0.5 (1.6–3.0)	0.701
eGFR (mL/min/1.73 m^2), mean ± SD (range)	50.5 ± 42.8 (11.6–168.0)	59.4 ± 23.5 (24.2–105.3)	0.086
CPR, no. of performance (%)	5 (22)	5 (42)	0.234
Time between AMCT and PMCT (days), mean ± SD (range)	3.4 ± 1.8 (0.5–7.0)	3.0 ± 2.6 (0.2–7.0)	0.443
Time between death and PMCT (hours), mean ± SD (range)	7.7 ± 5.5 (2.0–18.0)	6.6 ± 3.8 (1.5–14.5)	0.931
Imaging findings			
CT attenuation of ascites (HU), mean ± SD (range)	13.5 ± 8.8 (−4.4–31.8)	12.2 ± 6.2 (−7.9–20.8)	0.964
Autopsy findings			
Volume of ascites (mL), mean ± SD (range)	1676 ± 2369 (100–9700)	1100 ± 1306 (150–4600)	0.508
Appearance of ascites, no. of subjects with serous ascites (%)	11 (48)	7 (58)	0.574
Presence of carcinomatous peritonitis, no. of subjects (%)	1 (4)	1 (8)	0.666

Table 1 Characteristics of subjects who underwent unenhanced and enhanced AMCT
Abbreviations: SD, standard deviation; eGFR, estimated glomerular filtration rate; CPR, cardiopulmonary resuscitation

- Patients who underwent unenhanced and enhanced AMCT did not differ significantly.

Results –*Attenuation differences between AMCT and PMCT*

	Unenhanced AMCT group			Enhanced AMCT group		
Sites of ascites	Ventral (n = 21)	Dorsal (n = 21)	Total (n = 42)	Ventral (n = 10)	Dorsal (n = 10)	Total (n = 20)
CT attenuation (AMCT/PMCT, mean ± SD)	12.3 ± 10.0/12.7 ± 9.3	14.7 ± 7.7/14.0 ± 9.5	13.5 ± 8.9/13.4 ± 9.3	11.4 ± 7.9/20.0 ± 11.8	13.1 ± 4.6/17.4 ± 9.3	12.2 ± 6.3/18.7 ± 10.4
P value	0.380	0.729	0.554	0.024*	0.078	0.006*

Table 2 Comparison of ascites attenuation between AMCT and PMCT

- Significantly higher attenuation was observed with PMCT than with enhanced AMCT in ROIs on the ventral side and in a combined analysis of the ventral and dorsal ROIs.
- No significant differences in ascites attenuation were observed between unenhanced AMCT and PMCT.

Results –*Factors associated with increased ascites attenuation on PMCT*

	Measured site of ascites		
	Ventral	Dorsal	Total
Factors			
AMCT-PMCT interval	0.058	0.303	0.011*
Albumin	0.404	0.397	0.191
eGFR	0.876	0.702	0.785
Volume of ascites	0.676	0.971	0.670

Table 3 Associations of various factors with changes in ascites attenuation in the subjects who underwent enhanced AMCT and PMCT

- Time interval between AMCT and PMCT as a factor contributing to the change in CT ascites attenuation was identified in subjects who underwent enhanced AMCT and PMCT.

Discussion

- An increase in the PMCT attenuation of ascites was observed in subjects who had undergone enhanced AMCT.

- Previous reports described the increased CT attenuation of ascites in a living body at a particular time interval after a previous enhanced CT scan.[4,6] However, the mechanism of the delayed increase in CT attenuation of ascites was not determined.

- Increased vascular permeability may occur once circulation stops after death, leading to the postmortem leakage of plasma components from blood vessels.

- Water-soluble iodinated contrast medium comprises small molecules that diffuse readily through the pores of blood vessels into the extravascular and extracellular spaces.[7-9]

- Therefore, contrast medium may leak from the blood vessels into the ascites near and after death, which would support the observed increase in ascites attenuation on PMCT in the present study.

Discussion

- Significantly higher attenuation was observed with PMCT than with enhanced AMCT in ROIs on the ventral side and in a combined analysis of the ventral and dorsal ROIs.

- We consider that this result may be attributable to the dorsal sedimentation due to high specific gravity of contrast medium or the uneven distribution of leaked contrast medium in the ascites, which is repeatedly produced and absorbed.

- We identified the time interval between enhanced AMCT and PMCT as a factor associated inversely with the change in the CT attenuation of ascites.

- This observation suggests that considerable amounts of the injected contrast medium leaked from the blood vessels into the ascites immediately after injection and during the early postmortem state.

Discussion –*Limitation*

- AMCT and PMCT scans were conducted on different scanners. This is an important but inevitable limitation at institutions where different scanners are used for clinical patients and corpses.
- AMCT was performed with arms raised and PMCT was performed with arms at the sides.
- The number of subjects was small.
- There was a lack of enough consideration of the distribution of ascites.

Conclusions

- We confirmed an elevated level of ascites attenuation on PMCT relative to AMCT in subjects who underwent enhanced AMCT shortly before death.

References

1. Levy AD, Harcke HT, Mallak CT. Postmortem imaging: MDCT features of postmortem change and decomposition. *Am J Forensic Med Pathol.* 2010;31:12–17.
2. Ishida M, Gonoi W, Okuma H, et al. Common postmortem computed tomography findings following atraumatic death: Differentiation between normal postmortem changes and pathologic lesions. *Korean J Radiol.* 2015;16:798–809.
3. Wagensveld IM, Blokker BM, Wielopolski PA, et al. Total-body CT and MR features of postmortem change in in-hospital deaths. *PLoS One.* 2017;12:e0185115.
4. Benedetti N, Aslam R, Wang ZJ, et al. Delayed enhancement of ascites after IV contrast material administration at CT: Time course and clinical correlation. *AJR Am J Roentgenol.* 2009;193:732–737.
5. Seishima R, Okabayashi K, Hasegawa H, et al. Computed tomography attenuation values of ascites are helpful to predict perforation site. *World J Gastroenterol.* 2015;21:1573–1579.
6. Cooper C, Silverman PM, Davros WJ, et al. Delayed contrast enhancement of ascitic fluid on CT: Frequency and significance. *AJR Am J Roentgenol.* 1993;161:787–790.
7. Hammerman AM, Oberle PA, Susman N. Opacification of ascitic fluid on delayed contrast computed tomography scans. *Clin Imaging.* 1990;14:221–224.
8. Wise SW, DeMeo JH, Austin RF. Enhancing ascites: An aid to CT diagnosis. *Abdom Imaging.* 1996;21:67–68.
9. Helbich TH, Roberts TPL, Gossmann A, et al. Quantitative gadopentetate-enhanced MRI of breast tumors: Testing of different analytic methods. *Magn Reson Med.* 2000;44:915–924.

Dating Post Mortem Submersion Interval (PMSI) of mammal bone- initial findings by Micro-CT Scan

Guareschi EE(1), Magni PA(1), Palmesino M(2)

1 Medical, Molecular & Forensic Sciences Cluster; College of Science, Health, Engineering & Education, Murdoch University, Western Australia

2 Servizio di Radiologia, Ente Ospedaliero Cantonale (EOC), Lugano, Switzerland

Introduction

Twelve large mammal bones, associated with underwater archaeological excavations on four shipwrecks on the Western Australia coast, were analysed by Micro-CT Scan (Skyscan 1176). They all belong to the collections of the Shipwrecks Museum, a section of the Western Australian Museum in Fremantle, Western Australia.

The aim is the investigation of any physical modifications linked to underwater taphonomy and diagenesis of bone.

The shipwrecks are Batavia (sunk in 1629), Vergulde Draak (Draeck) (Gilt Dragon) (sunk in 1656), Zeewijk (sunk in 1727) and Rapid (sunk in 1811).

The underwater archaeological excavations were conducted between 1968 and 1980.

Western Australian Shipwrecks Museum

Batavia (1629)

Courtesy of WA Shipwrecks Museum, 45 Cliff St, Fremantle 6160, Western Australia

Batavia (1629)

Courtesy of WA Shipwrecks Museum, 45 Cliff St, Fremantle 6160, Western Australia

Micro-CT Scan

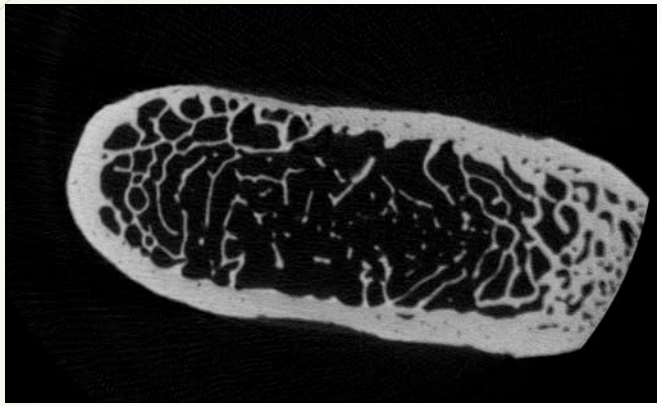

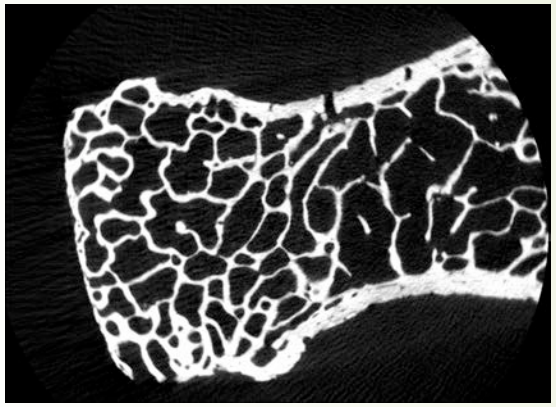

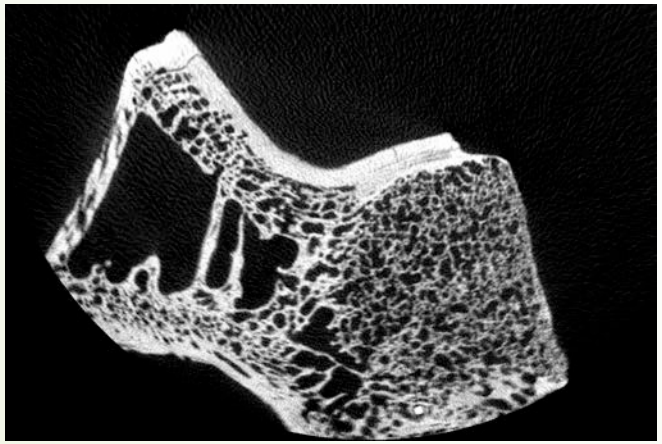

Upper Left
Cortical bone: NO INTERRUPTIONS, DENSE
Trabecular bone: SPARSE HOMOGENEOUS RAREFACTION

Upper Right
Cortical bone: MOSTLY DENSE, INTERRUPTED ON THE UPPER SIDE
Trabecular bone : SPARSE REGULAR MODERATE RAREFACTION

Lower Left
Cortical bone: DENSE WHERE PRESERVED, HAIRLINE FRACTURE INTERRUPTIONS ON THE UPPER SIDE
Trabecular bone: HETEROGENOUS WITH AREAS OF COMPLETE DESTRUCTION IN CONTACT WITH NORMAL TRABECULAR BONE STRUCTURE

MicroCT Scans have been acquired, reconstructed and analysed at the Centre for Microscopy, Characterisation and Analysis (CMCA), The University of Western Australia

Vergulde Draeck (1656)

Courtesy of WA Shipwrecks Museum, 45 Cliff St, Fremantle 6160, Western Australia

Vergulde Draeck (1656)

Courtesy of WA Shipwrecks Museum, 45 Cliff St, Fremantle 6160, Western Australia

Micro-CT Scan

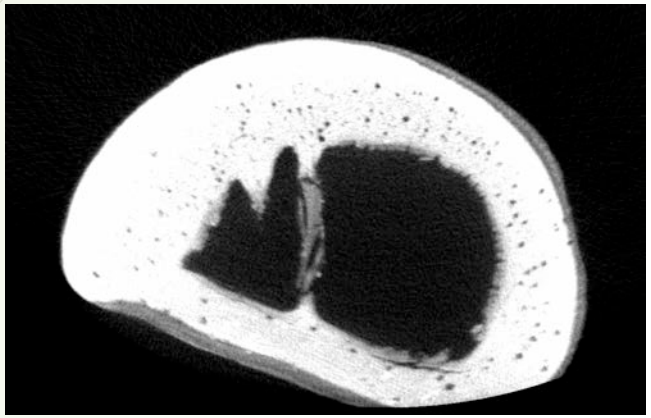

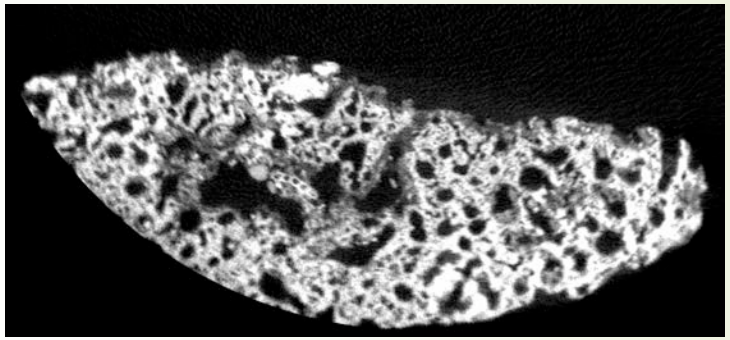

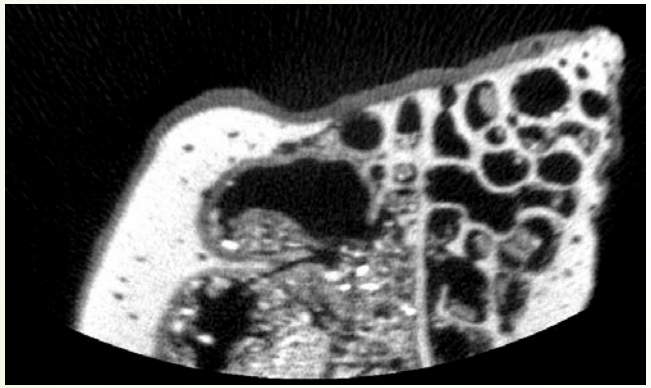

Upper Left
Cortical bone: DENSE AND HOMOGENOUS
Trabecular bone: ALMOST COMPLETELY DISAPPEARED, EXCEPT FOR ONE REMAINING "SEPTUM"

Upper Right
Cortical bone: ABSENT
Trabecular bone: SPARSE RAREFACTION AREAS WITH ENCLOSED FOREIGN BODIES

Lower Left
Cortical bone: HETEROGENEOUS DENSITY, PARTLY PRESERVED AND PARTLY ABSENT
Trabecular bone: LARGE DESTRUCTION MIXED WITH RAREFACTION AREAS ENCLOSING FOREIGN BODIES, ESPECIALLY CLOSE TO THE MID-LINE

MicroCT Scans have been acquired, reconstructed and analysed at the Centre for Microscopy, Characterisation and Analysis (CMCA), The University of Western Australia

Zeewijk (1727)

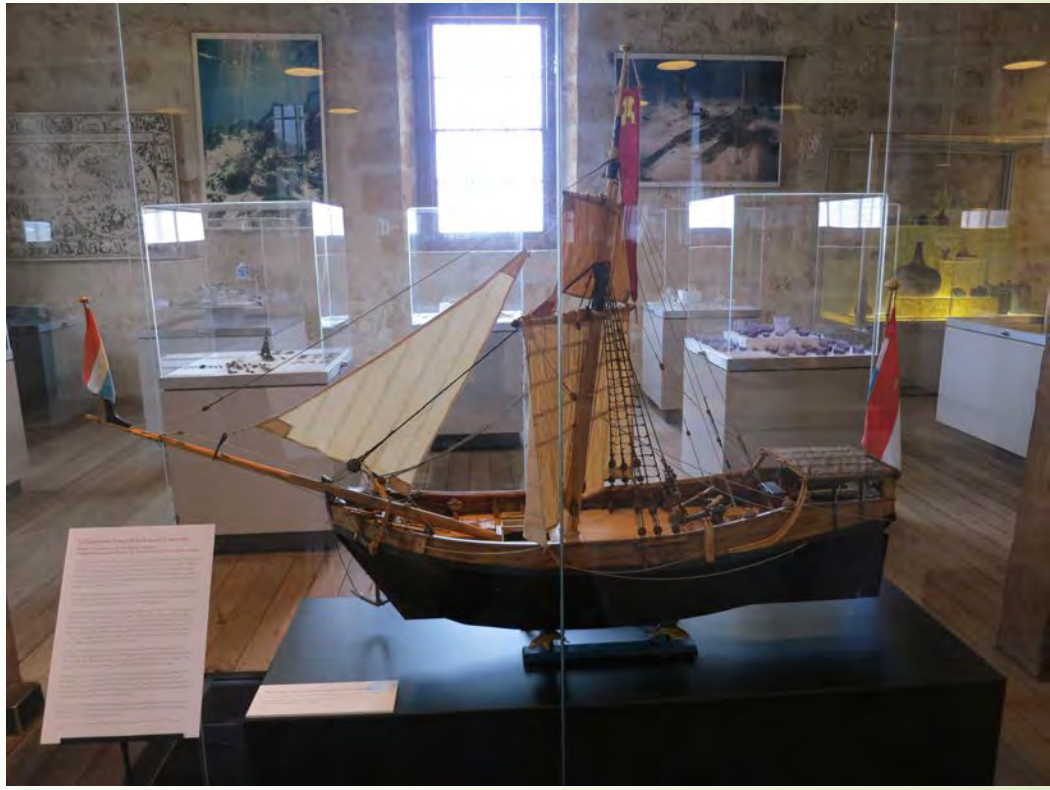

Courtesy of WA Shipwrecks Museum, 45 Cliff St, Fremantle 6160, Western Australia

Zeewijk (1727)

Courtesy of WA Shipwrecks Museum, 45 Cliff St, Fremantle 6160, Western Australia

Micro-CT Scan

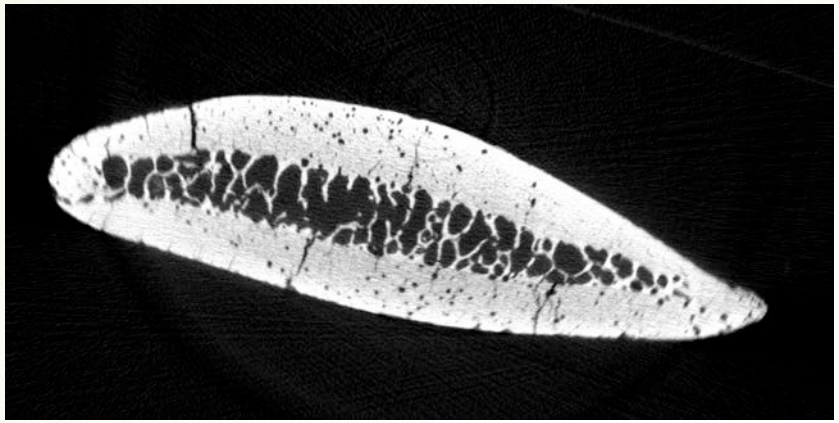

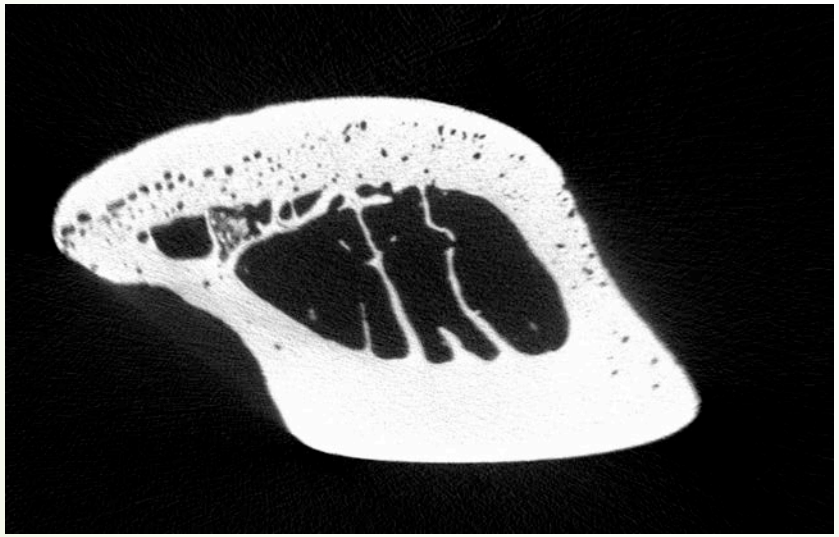

Upper Left
Cortical bone: INTERRUPTED BY FULL-THICKNESS CRACKS, POROUS
Trabecular bone: DIFFUSELY RAREFIED

Upper Right
Cortical bone: MOSTLY DENSE WITH FOCAL SPARSE POROSITY
Trabecular bone: DIFFUSELY RAREFIED WITH REMAINING "SEPTA"

Lower Left
Cortical bone: MOSTLY DENSE WITH AREAS OF INCREASED POROSITY
Trabecular bone: ALMOST COMPLETELY ABSENT, TWO FULLY PRESERVED "SEPTA"

MicroCT Scans have been acquired, reconstructed and analysed at the Centre for Microscopy, Characterisation and Analysis (CMCA), The University of Western Australia

Rapid (1811)

Courtesy of WA Shipwrecks Museum, 45 Cliff St, Fremantle 6160, Western Australia

Rapid (1811)

Courtesy of WA Shipwrecks Museum, 45 Cliff St, Fremantle 6160, Western Australia

Micro-CT Scan

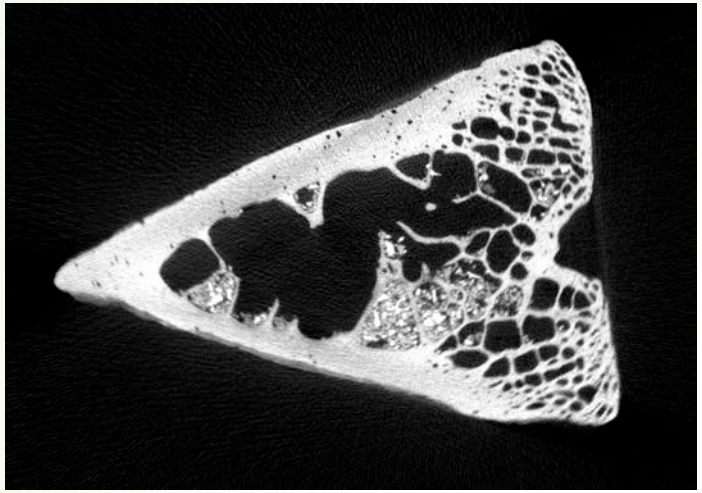

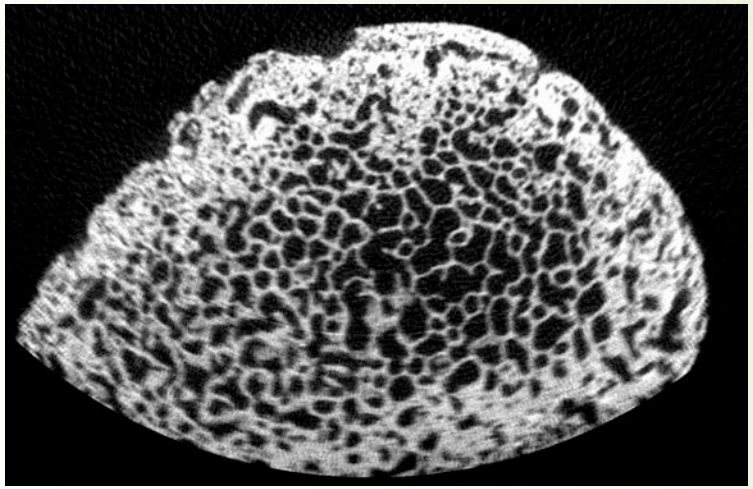

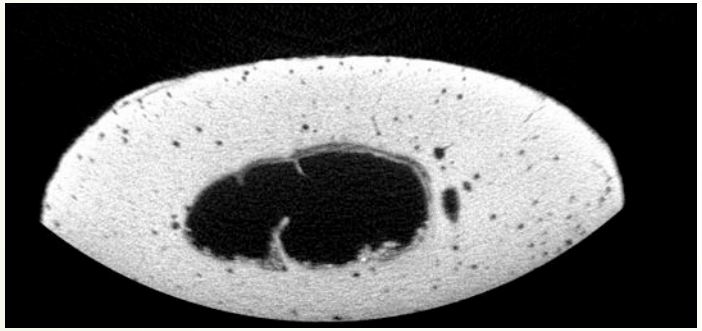

Upper Left
Cortical bone: COMPLETELY ABSENT ON ONE SIDE, SPARSELY POROUS ON THE REMAINING TWO SIDES
Trabecular bone: AREAS OF ALMOST COMPLETE DESTRUCTION IN CONTACT WITH DENSER TRABECULAE AND ENCLOSED FOREIGN-BODIES
Upper Right
Cortical bone: ABSENT IN MOST OF THE SECTION
Trabecular bone: MINIMAL DESTRUCTION IN CENTRAL AREAS OF THE SECTION. OTHERWISE HOMOGENEOUSLY MODERATELY RAREFIED
Lower Left
Cortical bone: PRESENT ON THE WHOLE SECTION, WITH PARTLY POROUS CONFIGURATION

MicroCT Scans have been acquired, reconstructed and analysed at the Centre for Microscopy, Characterisation and Analysis (CMCA), The University of Western Australia

Conclusions

- Large mammal bones aboard historical ships were contained in barrels, as part of preserved meat.
- The time of uninterrupted submersion of the analysed bones in saltwater and sediment spans between 169 years (Rapid) and 347 years (Batavia).

Taphonomy (macroscopic)	Absence of soft tissues (dry bone), longitudinal and network cracks, artefacts of sample preparation (glue prints), metal concretions, perimortem and postmortem fractures, rodent teeth marks, cutting and chopping marks
Diagenesis (macroscopic)	Abrasion with fragmentation and extensive damages to the cortical bone, stains of different colors
Micro-CT Scan	-Increase in total porosity due to full-thickness cracks and holes in the cortical bone, rarefaction of trabecular bone, areas of complete destruction -Foreign bodies enclosed among septa of the trabecular bone
Ongoing research	-Microscopic investigation of collagen degradation and of bioerosion -Elemental analysis

References

Palacio-Mancheno, P. E., Larriera, A. I., Doty, S. B., Cardoso, L., & Fritton, S. P. (2014). 3D Assessment of Cortical Bone Porosity and Tissue Mineral Density Using High-Resolution Micro-CT: Effects of Resolution and Threshold Method. J Bone Miner Res., 29(1).

Booth, T. J., Redfern, R. C., & Gowland, R. L. (2016). Immaculate conceptions: Micro-CT analysis of diagenesis in Romano-British infant skeletons. Journal of Archaeological Science, 74, 124-134. doi:10.1016/j.jas.2016.08.007

Tripp, J. A., Squire, M. E., Hedges, R. E. M., & Stevens, R. E. (2018). Use of micro-computed tomography imaging and porosity measurements as indicators of collagen preservation in archaeological bone. Palaeogeography, Palaeoclimatology, Palaeoecology, 511, 462-471. doi:10.1016/j.palaeo.2018.09.012

Corresponding author: Edda.Guareschi@murdoch.edu.au

Developing a jMRUI Software-based Method to Quantify and Analyze Brain Metabolites in Post-Mortem ^{1}H Magnetic Resonance Spectroscopy for Assessing Acute Fatal Intoxication

[1]Sarah R. Dallo, [1,2]Natalie L. Adolphi Ph.D.

[1]Department of Biochemistry and Molecular Biology,
[2]Center for Forensic Imaging, Office of the Medical Investigator,
School of Medicine, University of New Mexico

SCHOOL OF MEDICINE
CENTER FOR FORENSIC IMAGING

McNAIR SCHOLARS PROGRAM & RESEARCH OPPORTUNITY PROGRAM

HEALTH SCIENCES
SCHOOL OF MEDICINE

Introduction

- Drug overdoses have surpassed motor vehicle fatalities as a leading cause of death in the U.S. (CDC)
  - 2017 United States: 70,237 deaths
  - 2017 New Mexico: 547 deaths
- The “Opioid Crisis” is driving this trend
- Drug overdose deaths require investigation by a medical examiner or coroner

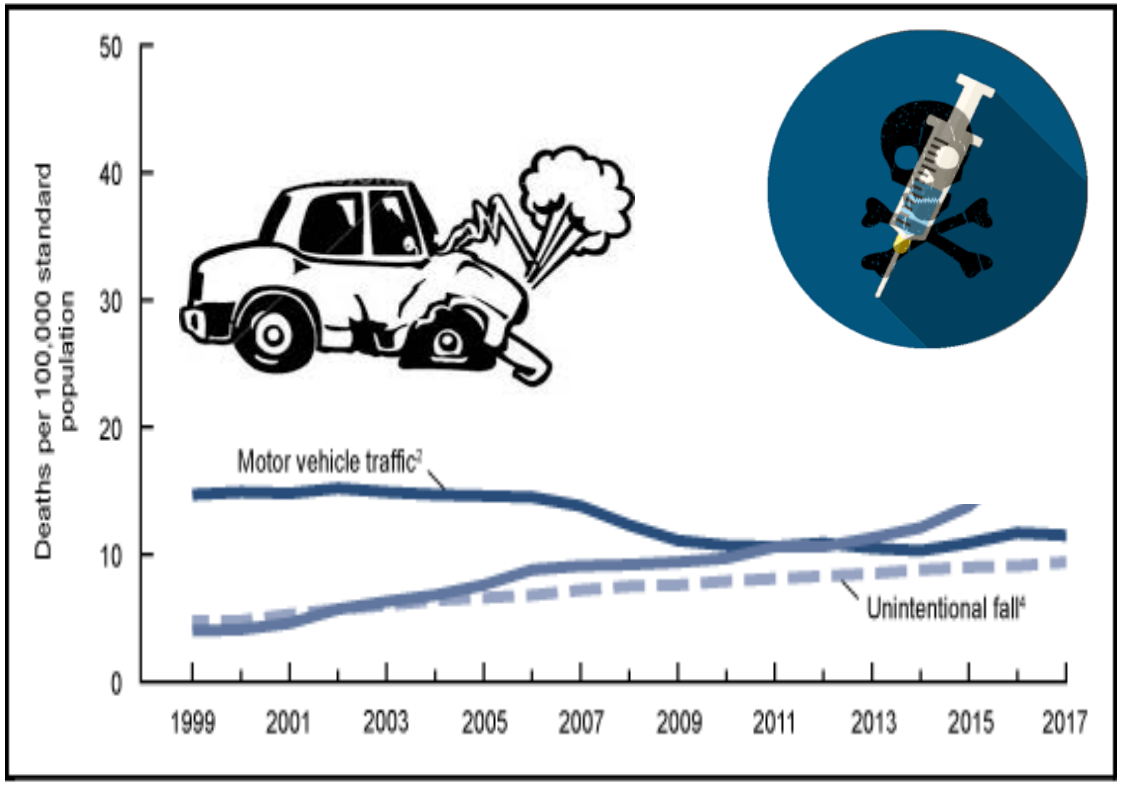

Graph from: https://www.cdc.gov/nchs/products/databriefs/db343.htm

MRI and ^{1}H MRS

- Magnetic Resonance Imaging (MRI)
  - Anatomical information
  - Used to detect injury or disease
- Magnetic Resonance Spectroscopy (MRS)
  - Chemical information
  - Used to detect metabolites in tissue or fluid
- Can MRI, combined with MRS, be used to investigate drug deaths?

Whole body MRI

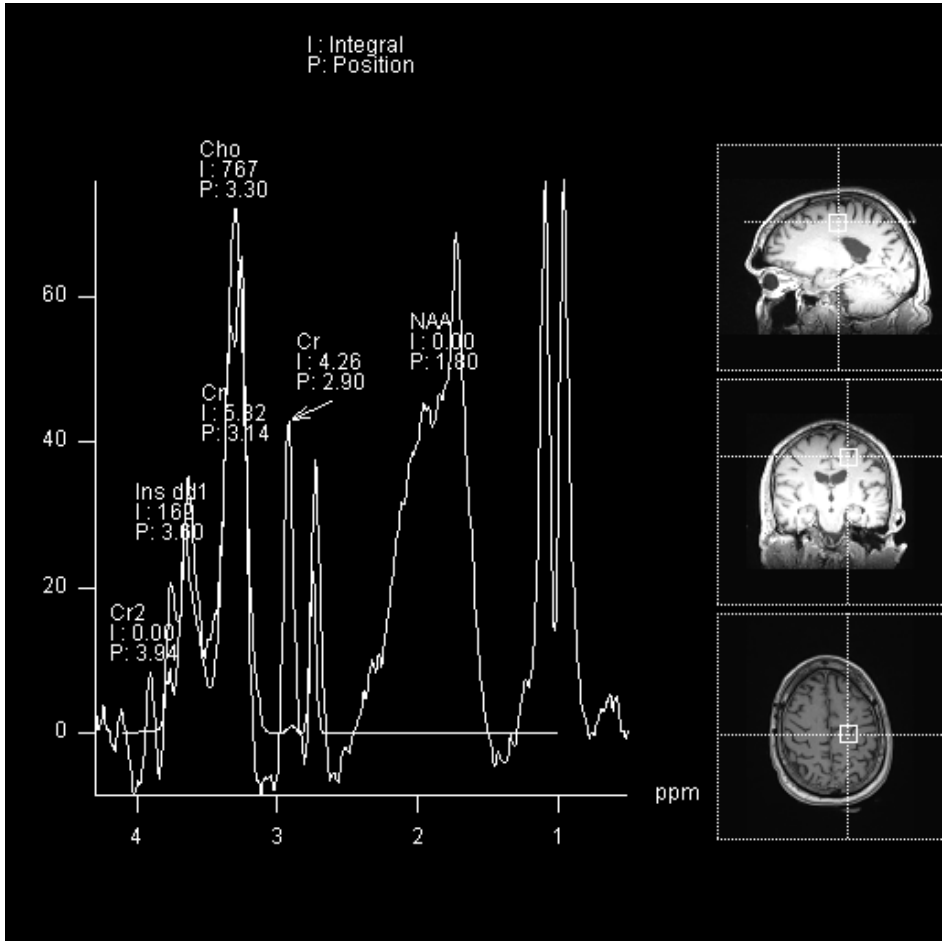

^{1}H MRS of a human brain

Background

- Previous researchers have used ^{1}H MRS to demonstrate changes in brain metabolites after exposure to drugs or alcohol:
  - Living subjects, chronic drug or alcohol use
  - Living subjects, prescription drug use
  - Post-mortem subjects, chronic drug or alcohol exposure
- No one has measured brain metabolites in the context of acute, fatal intoxication (i.e., drug overdose)
  - Ethical problems in living subjects

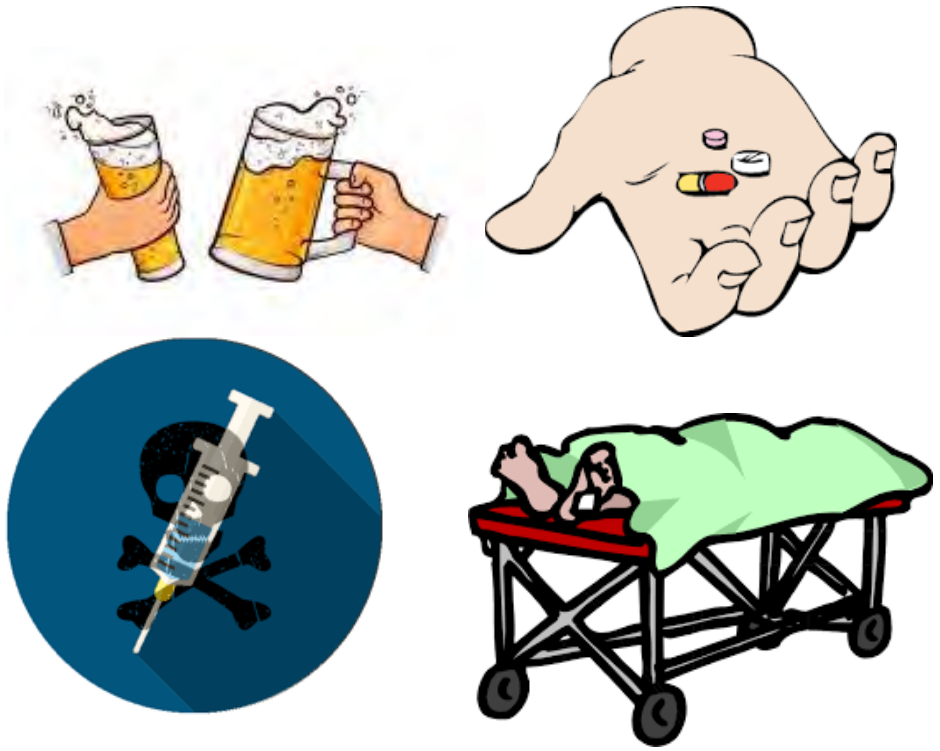

Research Questions

- Can ^{1}H MRS be used as a novel, rapid means of determining acute drug intoxication in post-mortem individuals?
- Can one or more brain metabolites be identified that can serve as a biomarker of acute fatal intoxication?
- We hypothesize that glutamate and glutamine levels will be significantly decreased, relative to those of unintoxicated subjects, in cases of fatal acute intoxication by opioids.

Data Collection Methods

Data Collection:

- 1.5 T Siemens Symphony TIM MR scanner
- Obtain ^{1}H MRS data
  - Single-voxel spectroscopy (SVS) with TE=30 ms
  - 20 mm^3 voxel of anterior cingulate cortex
- Post-mortem animal (antelope) and human subjects

1.5 T Siemens Sonata MR scanner

Sagittal MRI slice locating the voxel volume with the blue square over the anterior cingulate cortex region of the brain

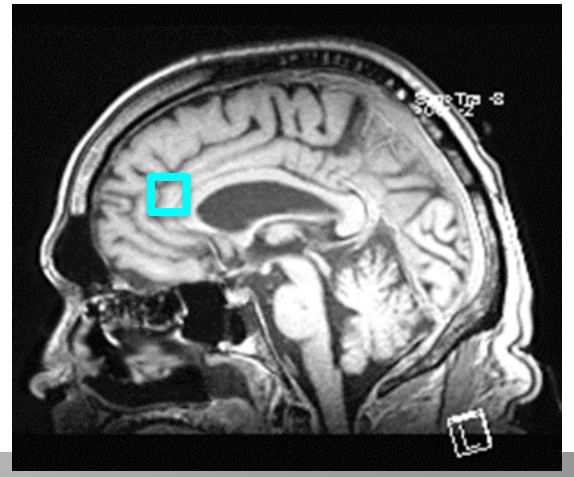

Data Analysis Methods

Spectral Data Analysis:

- jMRUI software
  1. Processing (frequency shift, truncate, zero-fill, apodize, phase adjust, and suppress unwanted peaks)
  2. Quantification
     - i. Each peak and corresponding line width initialized individually
     - ii. Appropriate constraints are applied
     - iii. Peak amplitudes and positions quantified by the AMARES algorithm

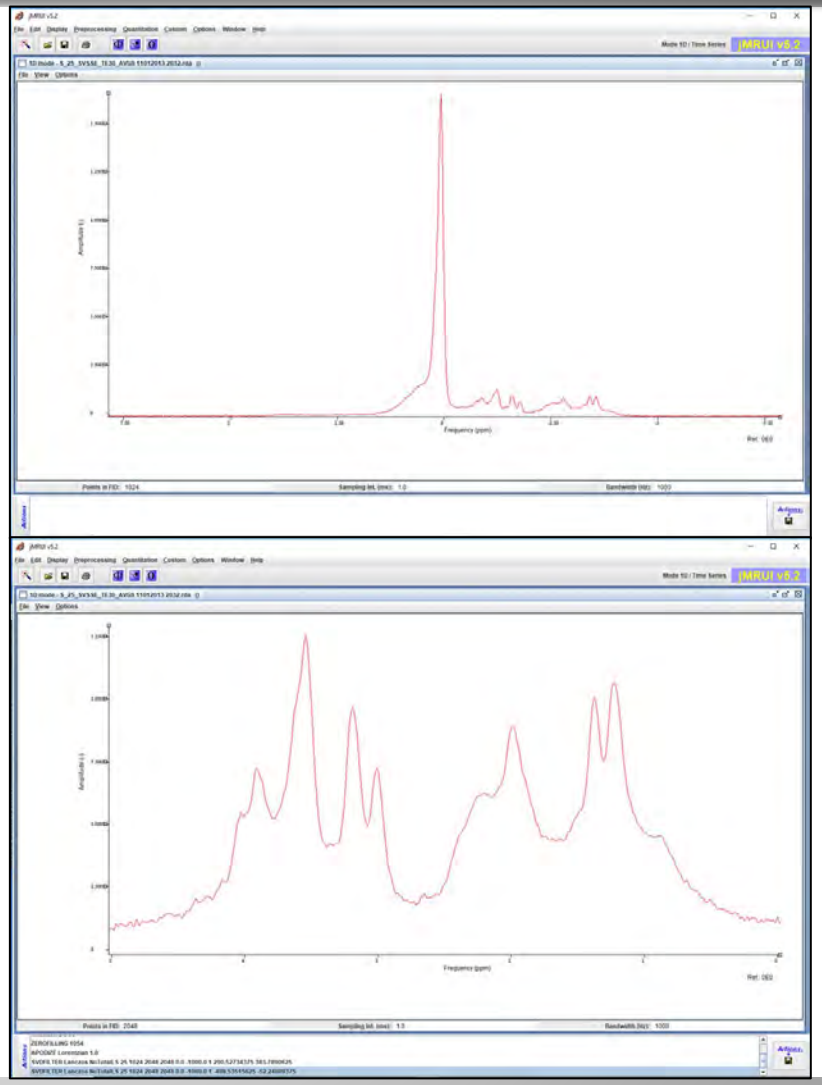

The spectrum before (up) and after (down) the water peak has been removed.

Peak Fitting Results (example)

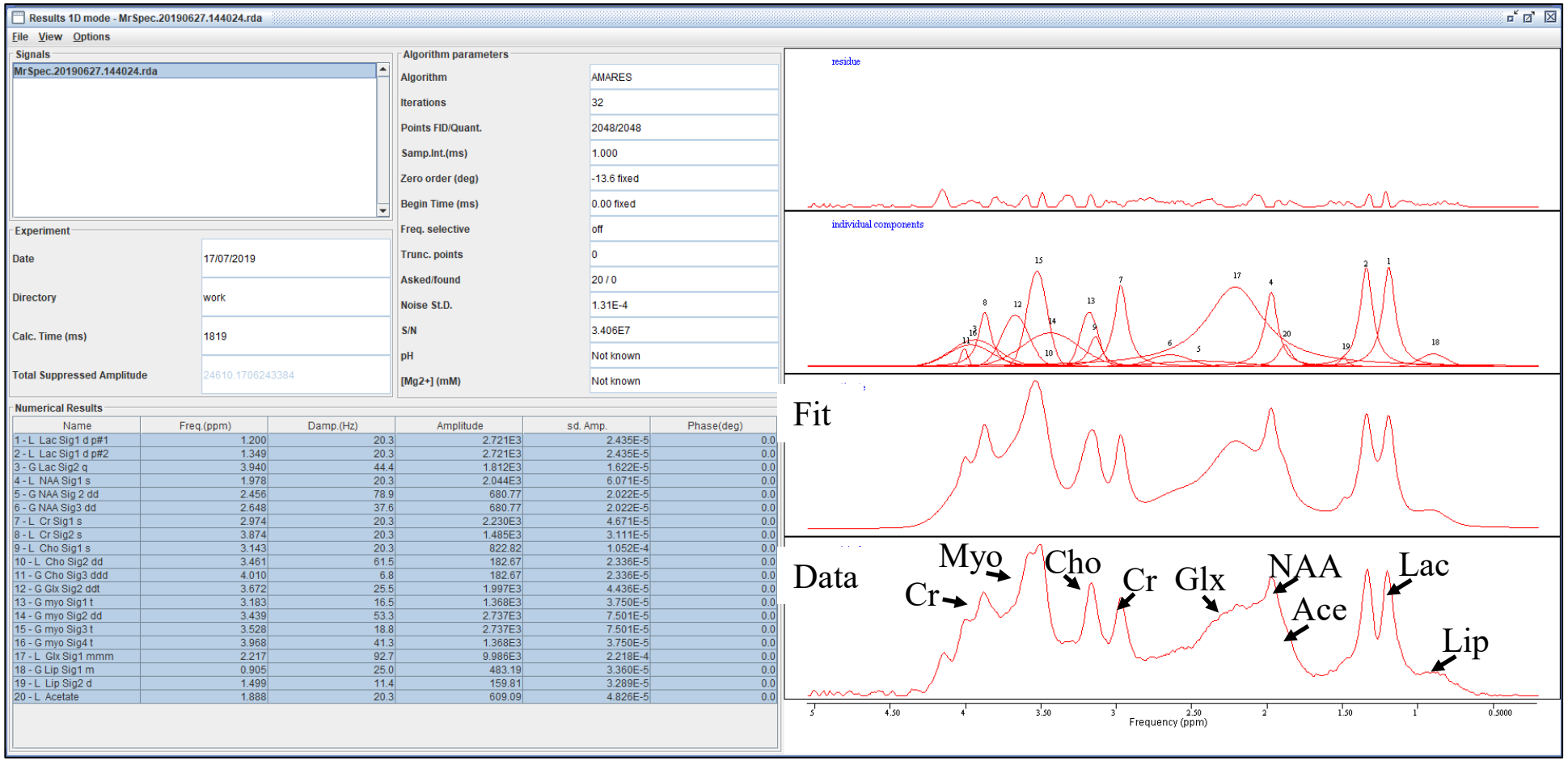

Abbreviations used: Lip, Lipid; Lac, Lactate; Ace, Acetate; NAA, N-acetylaspartate; Glx, Glutamate + Glutamine; Cr, Creatine; Cho, Choline; Myo, Myo-Inositol

View of the spectrum after quantification by the AMARES algorithm

Metabolite Amplitudes (example) – Antelope

Metabolite	Amplitude	Relative Amplitude
Lip	36	0.056
Lac	85	0.130
Ace	20	0.031
NAA	137	0.209
Glx	118	0.180
Cr	41	0.062
Cho	89	0.135
Myo	130	0.198
Total	656	1.000

The amplitude of each metabolite is proportional to the metabolite concentration and the number of hydrogen atoms per molecule. The relative amplitude is the ratio of the metabolite amplitude to the total spectral amplitude.

Dependence of Amplitudes on Prior Knowledge Constraints - Antelope

Avg Values for Metabolites When jMRUI Prior Knowledge Parameters Change								
	Lac	Cho	Cr	NAA	Glx	Myo	Lip	Ace
No Ace, No Lip2, Glx(G)	0.201	0.109	0.096	0.026	0.333	0.132	0.102	N/A
Ace, Lip2, Glx(G)	0.203	0.116	0.093	0.018	0.290	0.135	0.124	0.020
No Ace, No Lip2, Glx(L)	0.214	0.116	0.087	0.045	0.332	0.117	0.089	N/A
Ace, Lip2 Glx(L)	0.200	0.106	0.082	0.113	0.149	0.160	0.155	0.036

The average relative amplitudes of each metabolite with varying prior knowledge conditions:

1) inclusion or exclusion of Acetate (Ace) and Lipid2 (Lip2)
2) specifying the Glx1 (glutamate+glutamine) line shape as Lorentzian (L) or Gaussian (G).

Dependence of Fitting Stability on Prior Knowledge Constraints – Antelope

Stdev/Avg Values for Metabolites When jMRUI Prior Knowledge Parameters Change								
	Lac	Cho	Cr	NAA	Glx	Myo	Lip	Ace
No Ace, No Lip2, Glx(G)	2.98%	4.28%	4.19%	91.29%	5.33%	6.12%	0.63%	N/A
Ace, Lip2, Glx(G)	0.07%	1.33%	1.67%	136.9%	3.52%	1.35%	2.81%	48.72%
No Ace, No Lip2, Glx(L)	0.06%	0.11%	0.24%	0.40%	0.16%	0.06%	0.21%	N/A
Ace, Lip2 Glx(L)	0.25%	1.60%	0.76%	0.68%	1.37%	1.95%	0.58%	0.23%

The error of the averages for each metabolite with varying prior knowledge conditions.

For each prior knowledge condition, fitting was repeated 5 times on the same spectrum, using a slightly upper bound for the water peak removal during each run, as shown in the next panel. Ideally small changes in the specification of the water peak removal range should result in small variations in the fitted amplitudes. However, specifying a Gaussian line shape for Glx resulted in greater instability, as particularly large variations in the fitted amplitude of NAA occurred with small variations in the water peak removal range under this condition. Specifying the Glx line shape as Lorentzian stabilized the fitted amplitudes against small variations in the water peak removal range.

Glx Amplitude – Antelope

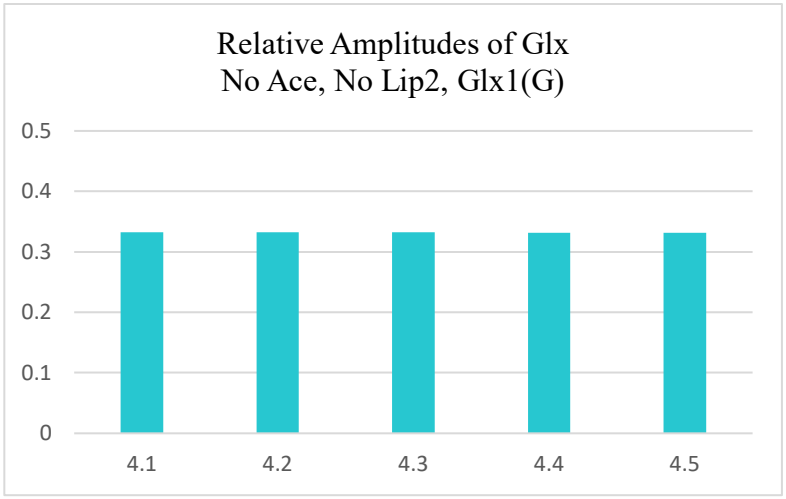

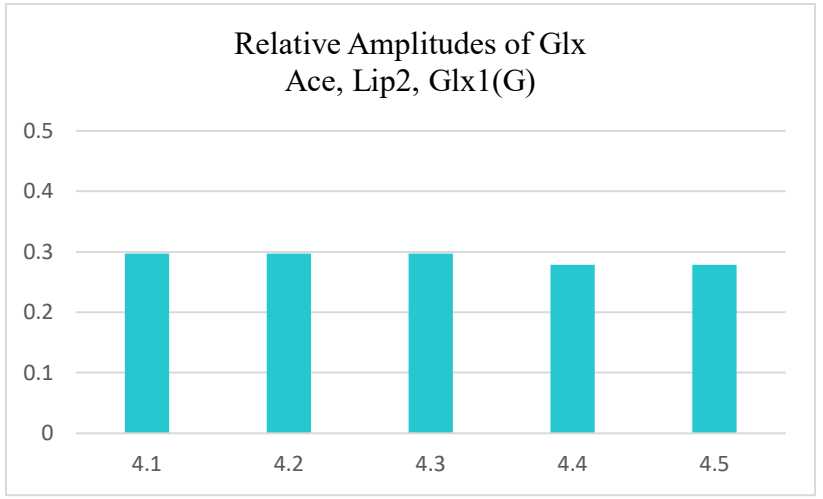

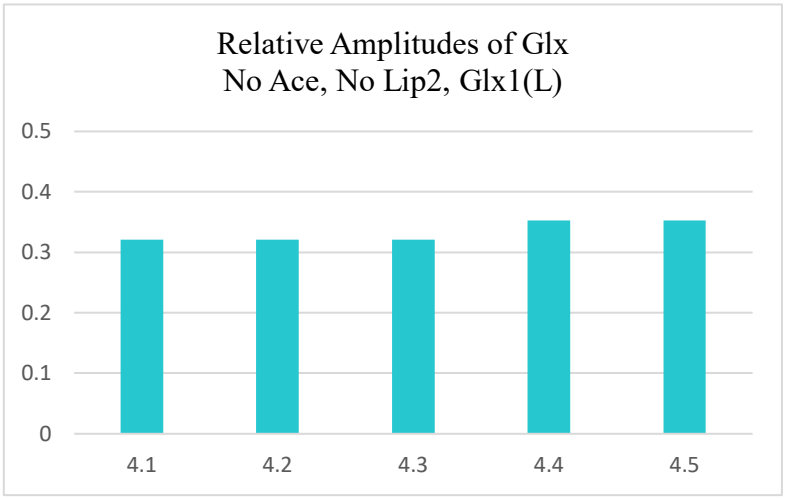

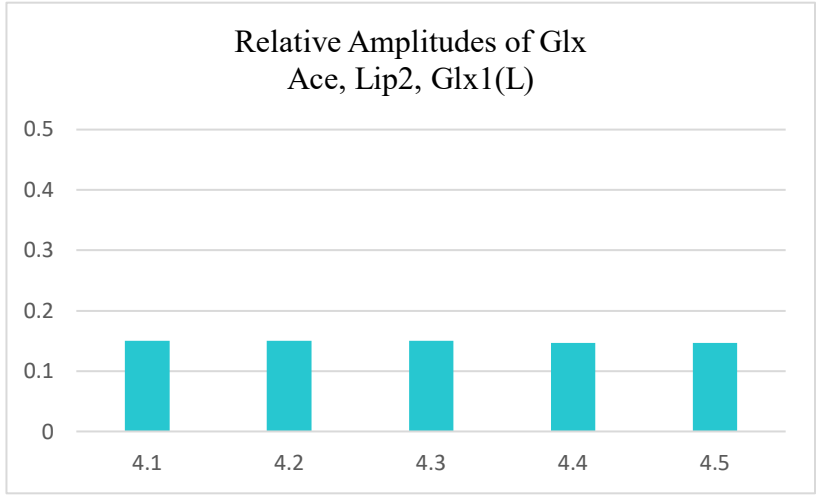

The relative amplitude of the metabolite Glx as a function of water peak suppression range (6.5 ppm to 4.1-4.5 ppm), inclusion or exclusion of Ace and Lip2, and Glx line shape (Gaussian or Lorentzian). The Glx fitted amplitude is relatively stable under all conditions, although the amplitude of some other metabolites showed greater variations. (See previous panel.)

Goodness of Fit – Antelope

Sum of Squares to Test Goodness of Fit Dependence on jMRUI Prior Knowledge Parameters	
	Sum of the Squares of the Difference Between Fitted and True Spectra
No Ace, No Lip2, Glx(G)	2.53×10^8
Ace, Lip2, Glx(G)	2.24×10^8
No Ace, No Lip2, Glx(L)	3.40×10^8
Ace, Lip2, Glx(L)	2.38×10^8

Data from the sum of squares analysis of all four jMRUI Prior Knowledge conditions (antelope brain spectrum). The residue spectra, which are the true data minus the fitted data, were taken directly from the AMARES results as a .mrui file, then converted to a .txt file. These .txt files contained data points of the residue spectra. These data points were squared and summed to achieve the sum of squares for each condition.

The inclusion of Ace and Lip2 decreases the sum of squared differences.

Goodness of Fit – Human

Human Sum of Squares to Test Goodness of Fit on jMRUI Prior Knowledge Parameters	
	Sum of Squares of the Difference Between the Fitted and True Spectra
No Ace, No Lip2, Glx(L)	8.07×10^9
Ace, Lip2, Glx(L)	7.63×10^9

Data from the sum of squares analysis of two jMRUI Prior Knowledge conditions in post-mortem human spectra. The residue spectra, which are the true data minus the fitted data, were taken directly from the AMARES results as a .mrui file, then converted to a .txt file. These .txt files contained data points of the residue spectra. These data points were squared and summed to achieve the sum of squares for each varying condition.

The inclusion of Ace and Lip2 resulted in a better fit (i.e., smaller sum of squared differences), consistent with our results in the antelope data.

Metabolite Amplitudes – Human

Metabolite	Amplitude	Relative Amplitude
Lac	4055	0.135
NAA	1716	0.057
Cr	2684	0.089
Cho	2240	0.075
Glx	7290	0.243
Myo	6890	0.229
Lip	1604	0.053
Ace	3543	0.118
Total	30022	1

Results from fitting the post-mortem human subject, using the prior knowledge constraints that produced the most stable fit in the antelope data (Lorentzian line shape for Glx, and inclusion of Ace and Lip2). The amplitude of each metabolite is proportional to the metabolite concentration and the number of hydrogen atoms per molecule. The relative amplitude is the ratio of the metabolite amplitude to the total spectral amplitude.

Conclusions

- Analysis of post-mortem ^{1}H brain spectra (Siemens 1.5 T) from an antelope and a human were demonstrated using jMRUI.
- With appropriate prior knowledge constraints, the AMARES algorithm can be used to fit spectra and quantify the relative amplitudes of metabolites of interest.
- Attributing the peak of primary interest (Glx) with a Lorentzian line shape appears to yield a more stable quantification of the Glx amplitude, while the inclusion of Acetate and a 2^{nd} Lipid peak improves the overall goodness of fit.
- In the future, we will test the method on human subjects to determine whether the Glx amplitude correlates with opioid intoxication

References

- Scholl L, Seth P, Kariisa M, Wilson N, Baldwin G. Drug and Opioid-Involved Overdose Deaths — United States, 2013–2017. MMWR Morb Mortal Wkly Rep 2019;67:1419–1427. DOI: http://dx.doi.org/10.15585/mmwr.mm675152e1
- New Mexico Office of the Medical Investigator. Annual Report. Albuquerque: State of New Mexico; 2017: 55. Available at: https://omi.unm.edu/common/reports/ar2017.pdf. Accessed June 3, 2019.
- Centers for Disease Control and Prevention. All injuries. https://www.cdc.gov/nchs/fastats/injury.htm. Accessed July 16, 2019.
- Centers for Disease Control and Prevention. Unintentional Injury Death Rates in Rural and Urban Areas: United States, 1999–2017. https://www.cdc.gov/nchs/products/databriefs/db343.htm. Accessed July 16, 2019.
- Hansen TM, Olesen AE, Simonsen CW, Fischer IW, Lelic D, Drewes AM, Frøkjaer JB. Acute Metabolic Changes Associated With Analgesic Drugs: An MR Spectroscopy Study. J Neuroimaging. 2016 Sep;26(5):545-51. doi: 10.1111/jon.12345. Epub 2016 Mar 30. PubMed PMID: 27028269.
- Hansen TM, Olesen AE, Simonsen CW, Drewes AM, Frokjaer JB. Cingulate metabolites during pain and morphine treatment as assessed by magnetic resonance spectroscopy. Journal of Pain Research. 2014:269. doi:10.2147/JPR.S61193.
- Gao H, Xiang Y, Sun N, et al. Metabolic changes in rat prefrontal cortex and hippocampus induced by chronic morphine treatment studied ex vivo by high resolution 1H NMR spectroscopy. *Neurochemistry International*. 2007;50(2):386-394. doi:10.1016/j.neuint.2006.09.012.
- Liu XL, Li L, Li JN, Tang JH, Rong JH, Liu B, Hu ZX. Quantifying absolute glutamate concentrations in nucleus accumbens of prescription opioid addicts by using (1)H MRS. Brain Behav. 2017 Jul 14;7(8):e00769. doi: 10.1002/brb3.769. eCollection 2017 Aug. PubMed PMID: 28828225; PubMed Central PMCID: PMC5561325.
- Zahr NM, Pfefferbaum A. Alcohol's Effects on the Brain: Neuroimaging Results in Humans and Animal Models. Alcohol Res. 2017;38(2):183-206. Review. PubMed PMID: 28988573; PubMed Central PMCID: PMC5513685.

Acknowledgements

The authors acknowledge support from Awards 2012-DN-BX-K019 and 2016-DN-BX-0173 from the National Institute of Justice, Office of Justice Programs, and the University of New Mexico Ronald E. McNair Scholars Program. The opinions, findings, and conclusions or recommendations expressed in this presentation are those of the authors and do not necessarily reflect those of the Department of Justice.

Development of a 3D-Printed Brain Holder for Post-Mortem Pediatric Brain MRI at 7T

Mark D Ehrhart[1], Colin M Wilson[1], Reed G Selwyn[1], Heather S Jarrell[2]

1. Department of Radiology, University of New Mexico School of Medicine, Albuquerque, New Mexico
2. Department of Pathology, University of New Mexico School of Medicine, Albuquerque, New Mexico

INTRODUCTION

- The purpose of this project was to design, prototype, and test a holder to house a gross pathology brain for post-mortem MRI of pediatric brain specimens.
- This project is part of a larger project correlating post-mortem ex vivo MRI imaging findings with pathology of pediatric non-accidental trauma victims.
- In order to correlate neuroimaging and neuropathology data, we designed a novel brain holder for ex-vivo MR imaging.
- The holder was designed to be MRI-compatible and to facilitate reproducible positioning of the pediatric brain specimen in a 7T preclinical scanner.
- A literature search revealed ex-vivo imaging methods have been developed for clinical scanners at 3-Tesla[1,2], but no reported prototypes for ex-vivo 3D-printed pediatric brain holders at higher magnet strength.
- Therefore, our holder was designed de-novo to fit on a Bruker guinea pig bed and within a 15-cm volume coil (Figure 1).

METHODS

- Prototypes were designed using Mimics Research software version 21.0 (Materialise, Leuven, Belgium) and saved as stereolithography (STL) files.
- Designs were printed in polylactide (PLA) with a Replicator Z18 fused deposition modelling (FDM) 3D printer (MakerBot, New York City, NY) (Figure 2).
- Post-mortem imaging was performed using sheep and human brain specimens submerged in fomblin.
  - T2, susceptibility, and diffusion-weighted imaging sequences were acquired on a BioSpec 70/30 USR (Bruker, Billerica, MA) 7-Tesla pre-clinical magnet (Figure 3).
    - MRI Acquisition Parameters:
      - T2-weighted image had a matrix size of 220x170, field of view of 110 mm x 85 mm, slice thickness of 0.5 mm, with isotropic 0.5 mm voxels, TE/TR = 33/23525 ms, an echo-train length of 8, echo-spacing 11ms, and scan time 17 mins.
      - SWI scans were acquired using FLASH based T2* phase-enhanced sequence with the same geometry as T2, TE/TR = 14/7880 ms, and scan time 23 mins.
      - DTI scans were acquired using a four-shot EPI sequence with the same geometry as T2, TE/TR = 46/40000, 2 averages and scan time was 4 h 14 min. The diffusion preparation consisted of 30 diffusion directions with b = 2,000, 1000, 500 and five b = 0 images, with d/delta = 4/18 ms.

Figure 1. Bruker guinea pig bed (left) and bed inserted into 15-cm volume coil (right).

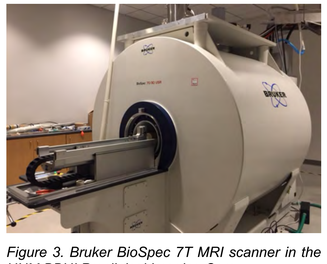

Figure 3. Bruker BioSpec 7T MRI scanner in the UNM BBHI Preclinical Imaging Core.

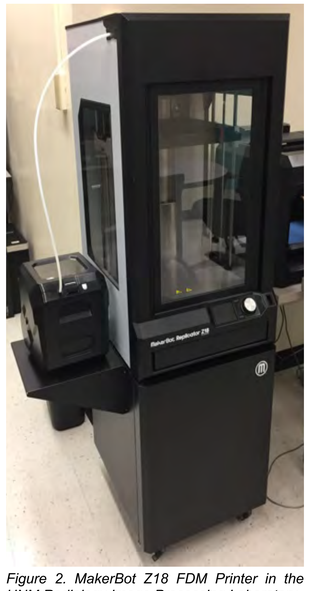

Figure 2. MakerBot Z18 FDM Printer in the UNM Radiology Image Processing Laboratory.

RESULTS

3D-printed Brain Holder Prototypes

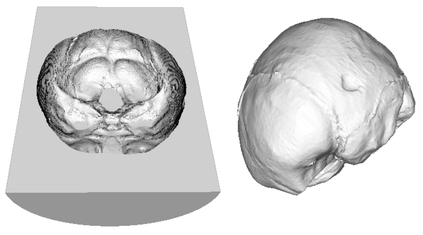

Prototype 1

- New features: solid piece with cut out for each brain using 3D rendering of brain specimen from post-mortem in vivo CT scan
- Problems: weight; stability of specimen; reprinting holder for each brain; changes in specimen volume with preservation of the specimen

Prototype 2

- New features: hollow cylinder
- Problems: field of view too large for scanner with larger brain specimens; floating brain within fomblin made rendered brain cut out useless; Floating brain limited quality of images when brain partly out of Fomblin

Prototype 3

- New features: smaller overall (brain would be sectioned), rendered brain cut out removed; bag removed, and container directly filled with fomblin; lid added, with modelled rods to keep brain submerged
- Problems: container leaked fomblin; lid rods long and narrow, difficult to print (lots of errors); rods did not provide sufficient rotational stability of the brain specimen

Prototype 4

- New Features: added tracks to the base with moveable stanchions to provide stability of the brain from below as well as from the lid; coated base in Coat-It GOOP, a graphite-based epoxy; lid design changed, with two angled wedges to provide stability
- Problems: low friction within the Fomblin limited usefulness of stanchions; two lid wedges not sufficient for stability

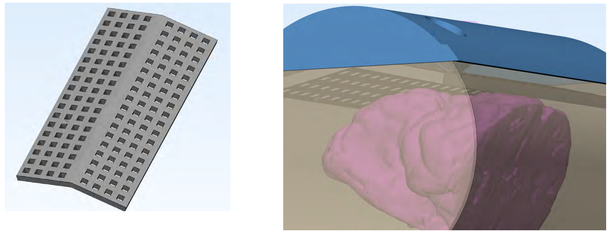

Prototype 5 (Final)

- New features: tracks/stanchions removed; wedges removed from lid; angled fenestrated plate attached to lid (left), allowed brain to float to stable position while keeping entire specimen submerged (right)

Preliminary Imaging Results

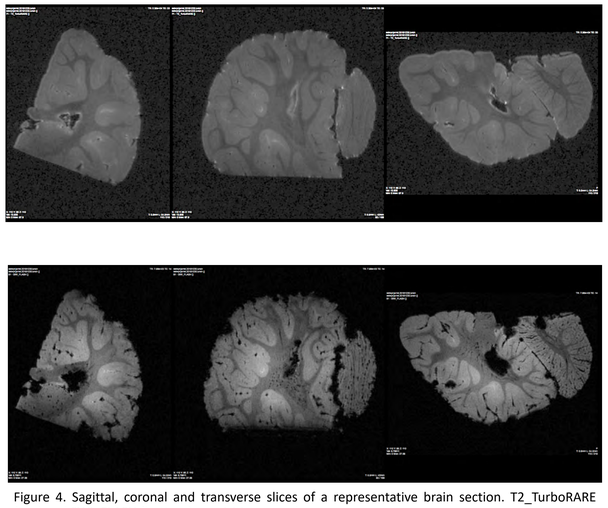

Figure 4. Sagittal, coronal and transverse slices of a representative brain section. T2_TurboRARE (top) and SWI_FLASH (bottom) acquisitions are shown.

DISCUSSION & CONCLUSION

- 3D printing allows for inexpensive rapid prototyping, where designs can be refined quickly with relatively short printing times (usually can be completed overnight).
  - Additionally, given the non-metallic nature of the 3D printing plastic, it also makes a great material for the final product.
- The University of New Mexico Brain and Behavioral Health Institute (BBHI) houses a preclinical scanner with higher magnet strength than the 3T scanners used for clinical applications.
  - Acquisition of images in higher magnet strength requires more time, and is therefore more sensitive to patient movement. This limitation is not present in post-mortem imaging.
- Our successful design and testing resulted in a brain holder that was MRI safe, and allows for increased stability of the brain specimen, easier repeatability, and overall better aesthetic of scanning brain specimens.
- Future work will focus on optimization of advanced acquisition methods, including diffusion and Gadolinium-enhanced imaging.

REFERENCES

1. Shatil, AS. et al. A Method for Whole Brain Ex Vivo Magnetic Resonance Imaging with Minimal Susceptibility Artifacts. Frontiers in Neurology 7, 208 (2016).
2. Shatil, AS. et al. Quantitative Ex Vivo MRI Changes due to Progressive Formalin Fixation in Whole Human Brain Specimens: Longitudinal Characterization of Diffusion, Relaxometry, and Myelin Water Fraction Measurements at 3T. Frontiers in Medicine 5, 31 (2018).

ACKNOWLEDGEMENTS

Study funding was provided by the National Institute of Justice (NIJ-2017-11080). The authors are grateful to RuthAnne Bump for support with 3D-printing and Chandra Gerrard for many many helpful suggestions during the design process. We would also like to thank Kevin Townsend of Materialise for providing software expertise and assistance with the design, as well as Yirong Yang of UNM BBHI for his help with acquiring the ex-vivo MRI data.

Physical and structural obstacles for post-mortem computed tomography quality

Pernille A Nielsen[1], Dina M Bech[1], Julie B Nielsen[1]
Pernille L Hansen[1], Dennis L Hansen[2, 3]
Svea D Mørup[1], Helle Precht[1,4], Peter M Leth[5]

[1] CONRAD Research Program, UCL University College, Odense, Denmark
[2] Department of Hematology, Odense University Hospital, Odense, Denmark
[3] Department of Clinical Research, University of Southern Denmark, Odense, Denmark
[4] Cardiology Research department, Odense University Hospital, Svendborg, Denmark
[5] Institute of Forensic Medicine, University of Southern Denmark, Odense, Denmark

Contact info: Pernille Lund Hansen, peha@ucl.dk

SDU University of Southern Denmark

UCL University College

Introduction

- Post Mortem CT (PMCT) image quality is affected by the same factors as *in vivo* CT image quality, as well as new factors such as decay and incineration
- Impaired image quality can lead to ambiguous or erroneous conclusions
- Of relevant factors are:
  - Correct centering, so that the scanner can calculate dosage correctly, for optimal image quality.
  - Positioning of the body, so anatomy does not overshadow other anatomy and the entire region of interest is within the scan field of view
  - Metal artefacts, hereunder localization and amount
- Knowledge of the distribution and nature of the factors that reduces the image quality, is important to be able to address them
- The aim of this study was to retrospectively explore the types and frequencies of factors leading to reduced diagnostic quality of PMCT scans, at a facility where PMCT's were performed by non-technologists

Materials and methods

- One hundred PMCT scans, 2018–2019, were examined retrospectively.
- Inclusion criteria were: over 15 years of age at death and Full Display Field Of View scan
- All scans were performed on a GE Healthcare Lightspeed VCT 64 slice scanner
- For each scan, anatomy outside of scan field of view, localization of metal objects, centering, body type and state of decay was registered.
- The observations were made on a high-quality screen and evaluated by two observers.
- The data was analyzed in Stata 15.1

ACQUISITION PARAMETERS	
TUBE VOLTAGE (KV)	120
AUTO MA RANGE	150-700
SLICE THICKNESS (MM)	1.25
HELICAL PITCH	0.516
ROTATION TIME (S)	0.60
NOISE INDEX	21

Results – centering

- The deceased was off-center in 77% of the scans
- Off-centering was correlated with the condition of the deceased at the time of scanning
- Weight status also correlate with centering. One hundred percent of underweight, 76% of normal weight and 70% of the overweight deceased were off-center

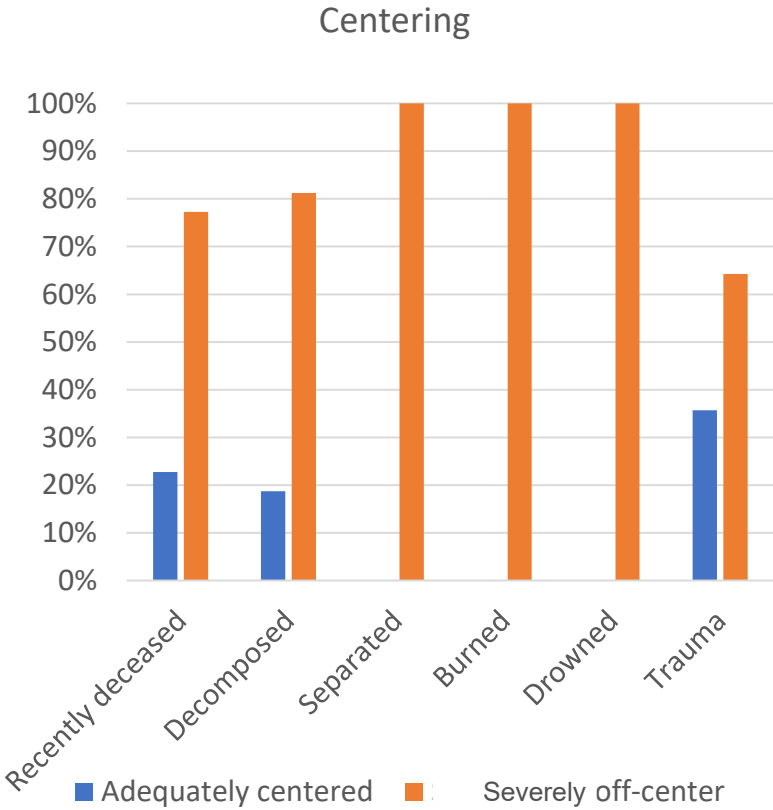

Table 1.
Ratio of deceased that are adequately centered, or severely off-center, categorized on status of the deceased

Results – missing anatomy and positioning

- One hundred percent of scans had some anatomy out of Field Of View, resulting in out of field of view artefacts. Missing anatomy was predominantly vertex and elbows
- Part of the anatomy was also missing in the truncal area; thorax area was affected in 21%, abdomen in 19% and pelvis 26% of scans
- In 53% of the scans, the head was not centered correctly
- Arms were placed next to, or on the trunk, and often asymmetrically

Figure 1. Example of scan with anatomy outside scan field of view.
Besides missing information, the incomplete projection also results in streak artifacts, causing sub-optimal imaging of the thoracic cavity

Results – metal artefacts

- More than 90% of the scans had metal artifacts that affected the imaging
- Metal objects were found both internally and externally of the deceased
- Loose metal (keys, coins, phones), were often placed on top of the body, or next to the head

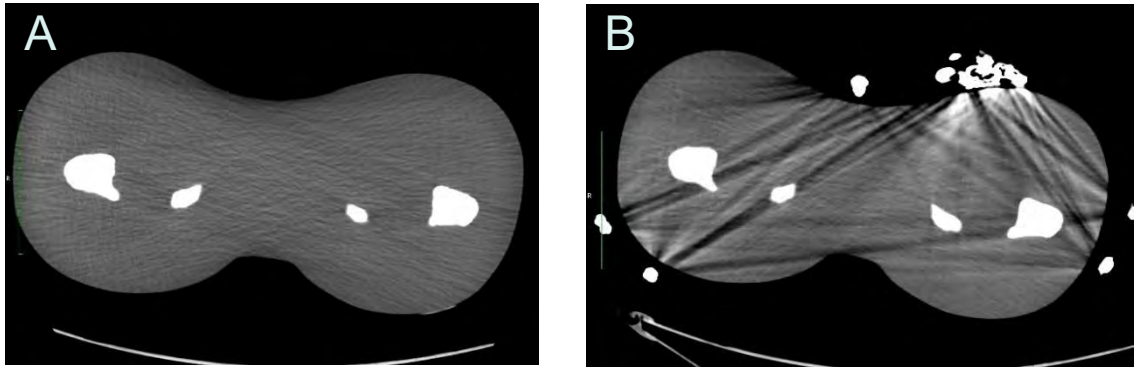

Figure 3. External metal in the pelvic area.
A represents deceased where no metal is present.
B represents deceased with metal objects present; keys, zipper, buttons and studs.
The metal interacts, even over large distances, and causes streak artifacts and shadows that can mask anatomy

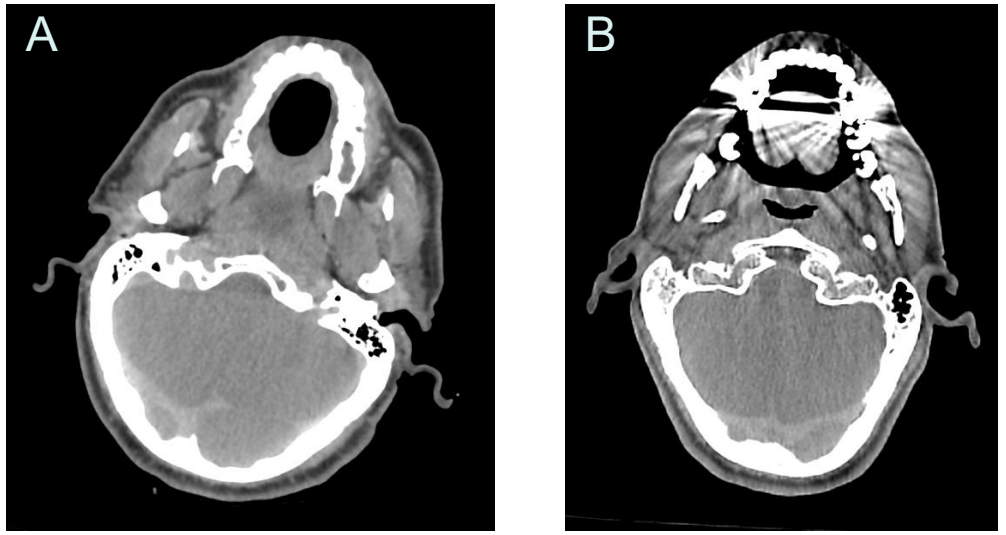

Figure 2. Metal artefacts from dental implants.
A represents deceased without dental implants.
B represents deceased with dental implants. Notice how metal interacts and cause streak artifacts in the scan.

Conclusions part 1

- PMCT pose a set of challenges, partially overlapping with *in vivo* CT
- Image quality is directly linked to diagnostic potential of the images
- Most of the factors that reduced image quality can be avoided
- Correct positioning of the deceased is complicated both by legal and practical challenges

Conclusions part 2

- External metal should be removed whenever possible. Belt buckets, rings, coins, keys, phones, chains and metal buttons can interact substantially with image quality
- If the deceased must be scanned with all objects, loose metal is preferably located near the feet, rather than near the head
- Overall, when PMCT is performed by non-technologists, education in image quality is essential
- We suggest: Place a poster in the scanner room, to remind scan personnel of factors that increase image quality

Suggested poster

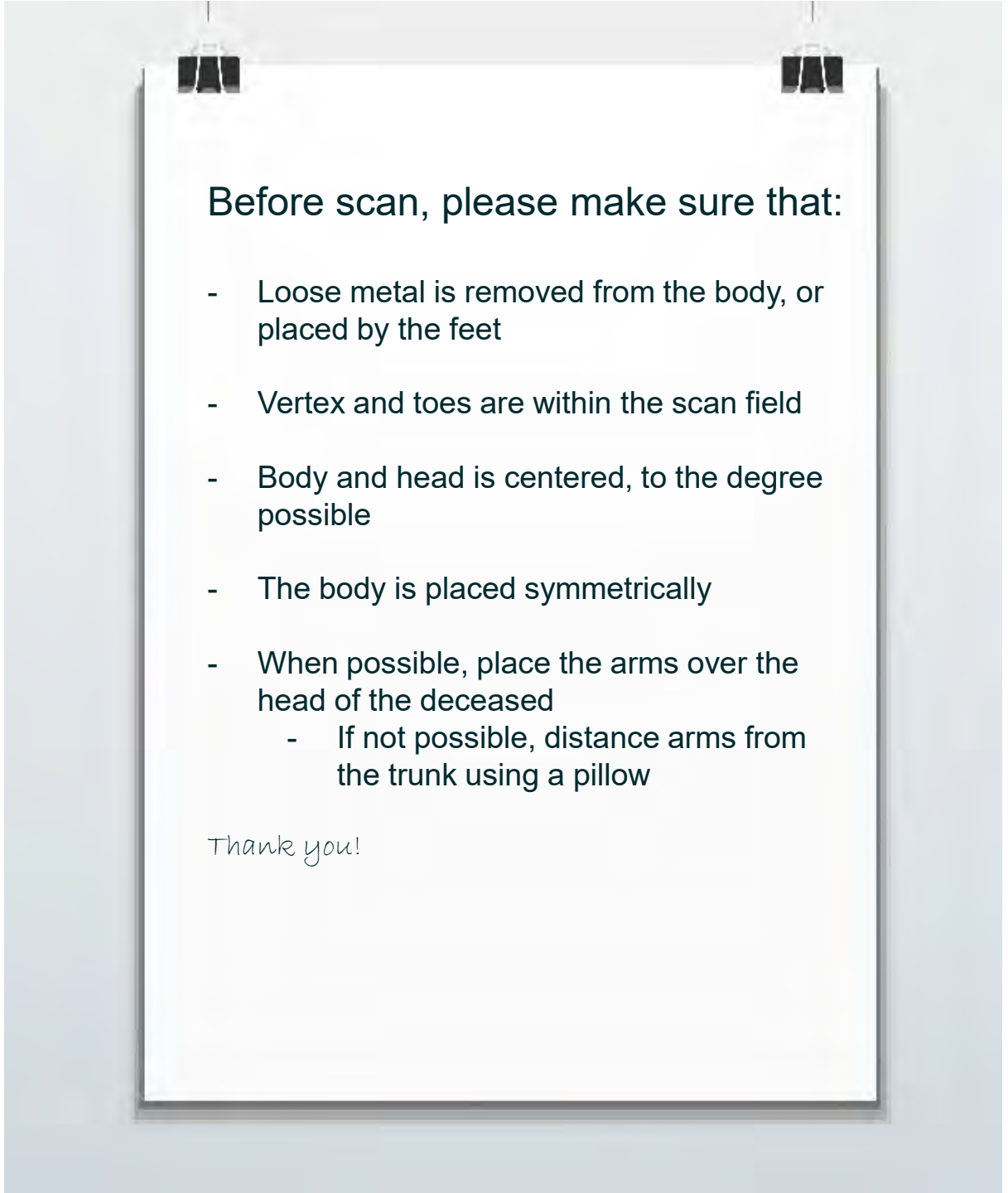

University College

Limitations

- The study was performed at only one institution
- Study population was limited to one hundred scans, with a low number of burned, drowned and severed deceased present

Ethics committee approval / Funding

- This study was a quality improvement study and did as such not require ethics committee approval under Danish law
- There has not been applied for funding for this study

SDU
University of Southern Denmark

The Invisible Killer - does carbon monoxide leave traces on PMCT?

Authors: K.Kahr, P.Leth, J.Kunkel
Institution: Department of Forensic Medicine - University of Southern Denmark

Postmortem computed tomography for identifying carbon monoxide related lesions in Globus Pallidus

Introduction

The aim of this study was to investigate whether acute and lethal exposure to carbon monoxide is associated with subsequent changes in globus pallidus, as can be visualized and measured with post mortem computed tomography (PMCT). The literature describes varying prevalences in vivo of globus pallidus specific radiological changes associated with carbon monoxide exposure, but this has never been investigated in a forensic setting.

Materials and Methods

All forensic cases handled by the Institute during a specified time period were screened. A number of inclusion and exclusion criteria were applied. Autopsy reports and routine PMCT images were retrieved for 10 individuals whom had died following acute carbon monoxide poisoning as confirmed by blood chemistry test. In addition, material from 10 cases without any exposure or confounding pathology was retrieved. All images subsequently underwent analysis of globus pallidus radio attenuation parameters (HU) in transverse sections by a board certified radiologist, randomized and blinded for all details except for sex and age. Group measurements were compared using two-sample t-test and the Mann-Whitney U test.

Results

In the group of exposed individuals, we found a significantly lower maximum attenuation of globus pallidus, right-sided. (t-test: Δ-5,2, CI = -8,995;-1,405, p=0,01, two-tailed) Left side maximum and bilateral average attenuation were consistently lower, but did not reach statistical significance.

Conclusion - More pictures, please

The exposed group showed a significant lower maximal attenuation right sided in globus pallidus; however, a bilateral response was to be expected. We reason that naturally occurring post mortem changes together with components of bias such as time alive after the exposure and the design and power of the current study add to the conclusion that further studies may be proposed. These may include a larger population and/or one with another modality such as magnetic resonance imaging.

Fig 1: PACS-Software: Analysis of globus pallidus - control

Fig 2: PACS-SoftAnalysis of globus pallidus - carbon monoxide posisoning

Key References

J.Lapresle, M. Fardeau. The central nervous system and carbon monoxide poisoning II. Anatomical study of brain lesions following intoxication with carbon monoxide (22 cases). 1967. Volume 24, Pages 31-74

Jones JS., Lagasse J., Zimmerman G. Computed tomographic findings after acute carbon monoxide poisoning. The american journal of emergency medicine, July 1994, volume 12, issue 4, pages 448-451

Silver DA., Cross M., Fox B., Paxton RM. Computes tomography of the brain in acute carbon monoxide poisoning. Clinical radiologi, July 1996, Volume 51, Issue 7, Pages 480-483

O'Donnel P., Buxton PJ., Pitkin A., Jarvis LJ. (2000). The magnetic resonance imaging appearances of the brain in acute carbon monoxide poisoning. Clinical radiology, April 2000;55(4):273-80

QSM-MRI exceeds CT for discrimination of small calcifications and microbleeds

Masatoshi Kojima[1,2)]

Radiographer

E-mail: m.kojima1982@gmail.com

Yohsuke Makino[1,3)], Maiko Yoshida[1)], Hirotaro Iwase[1,3)]

1) Department of legal medicine, Graduate school of medicine, Chiba university
2) Department of radiology, Chiba medical center
3) Department of forensic medicine, Graduate school of medicine, The university of Tokyo

Introduction

Importance of microbleeds

Lesion with small bleeding (microbleeds) such as axonal injuries, or cerebral amyloid angiopathy, are sometimes important for forensic medicine. These lesions are difficult to detect macroscopically and tomographic imaging is expected to be good guide for microbleeds. MRI is the best for detecting this entity due to ability for emphasizing susceptibility. T2*WI can emphasize susceptibility but it cannot distinguish micro bleeds from small calcification.

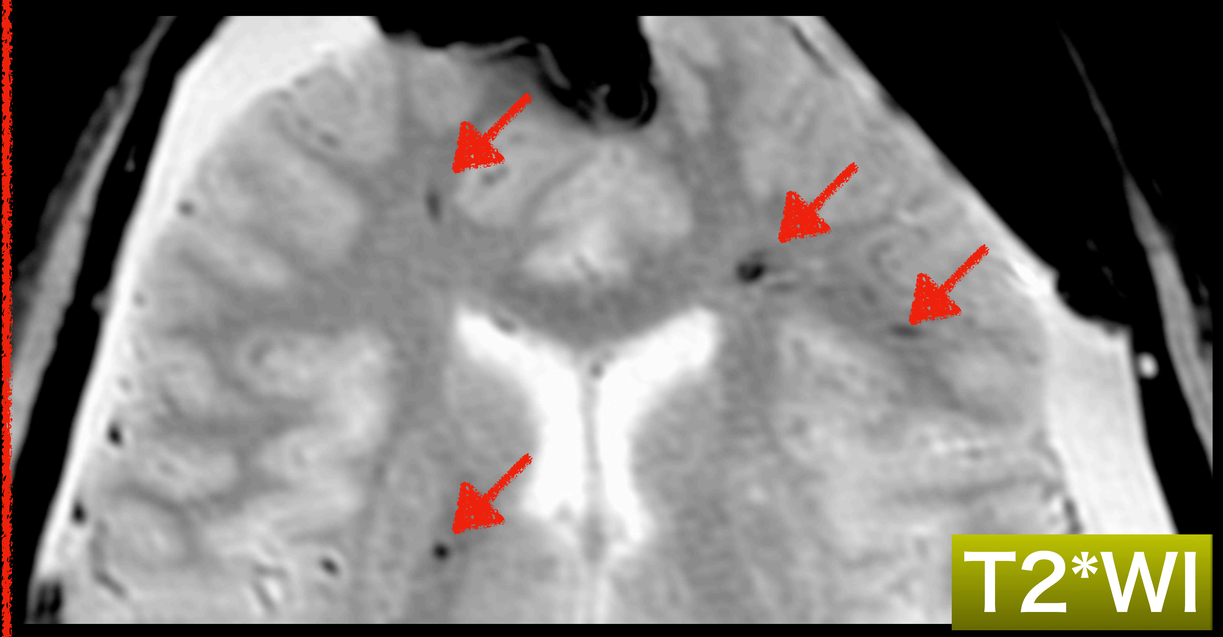

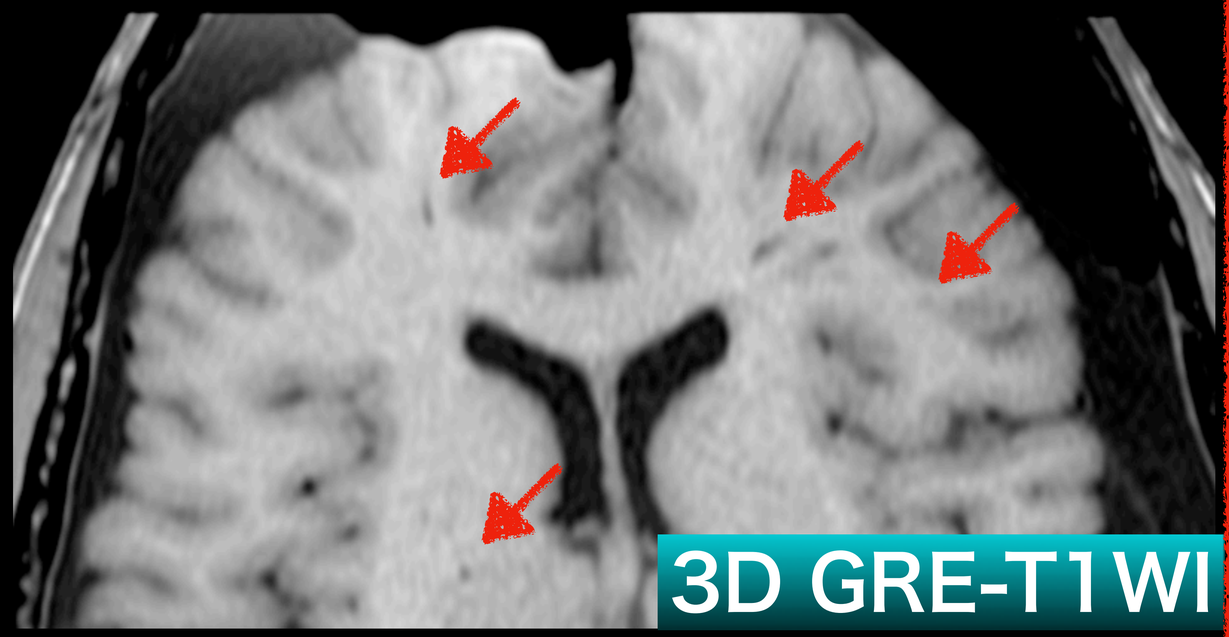

T2*WI is more detectable than GRE-T1WI.

Introduction

Quantitative susceptibility mapping (QSM)

Generally, T2*WI or Susceptibility Weighted Image (SWI) is used detect bleeding.

QSM is recently developed imaging methods for quantifying tissue's magnetic property. QSM is calculated by magnitude image and phase image.

Hemorrhage and calcification differ in phase shift.
QSM can quantify this phase shift difference and produce images that include the information.

The aim of this study is to evaluate the ability to detect small calcifications and microbleeds using QSM-MRI.

QSM analysis flow chart

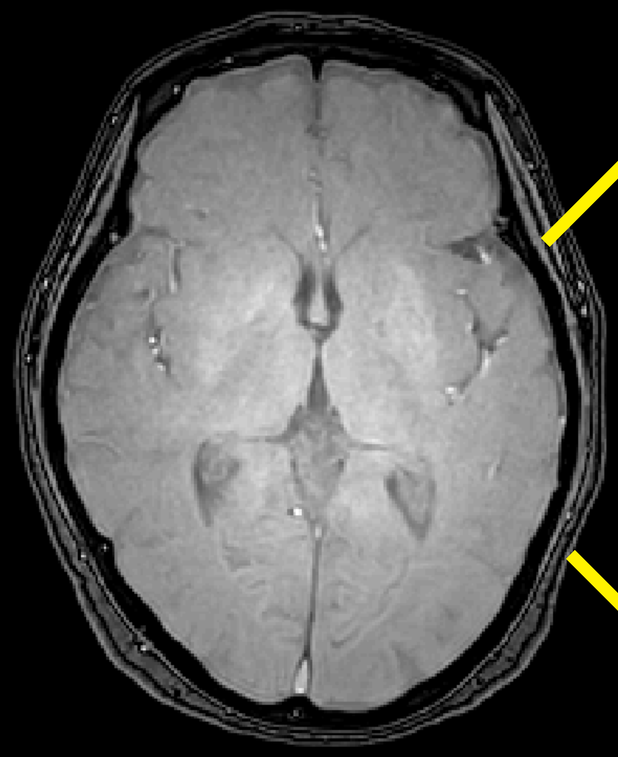

T2*WI
(multi echo GRE)
or
SWI
(Susceptibility
weighted
image)

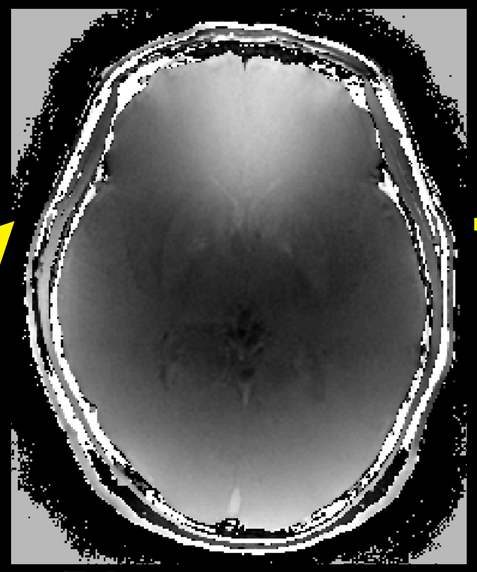

Phase map
(rad)

Musk

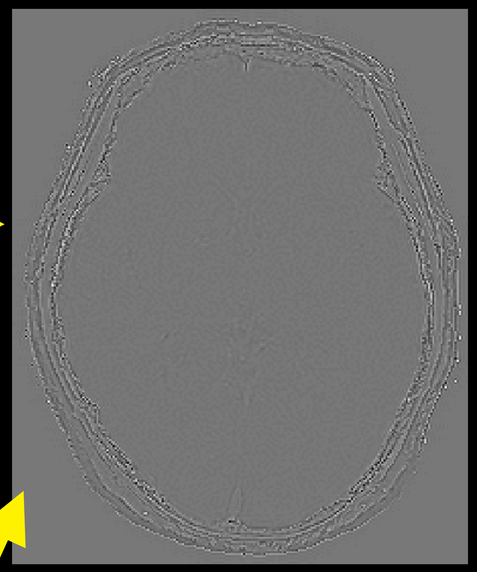

Laplacian

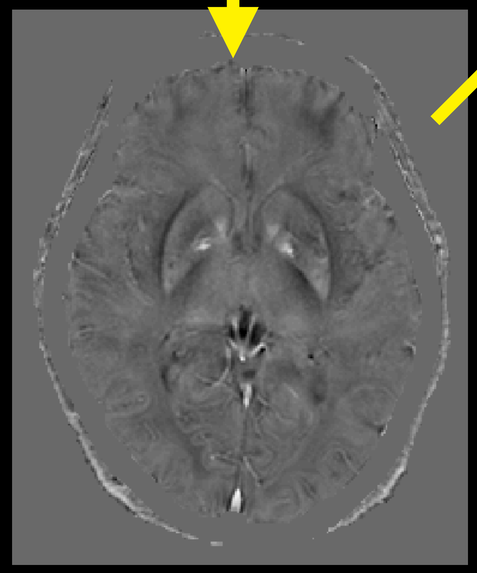

Frequency
(Hz)

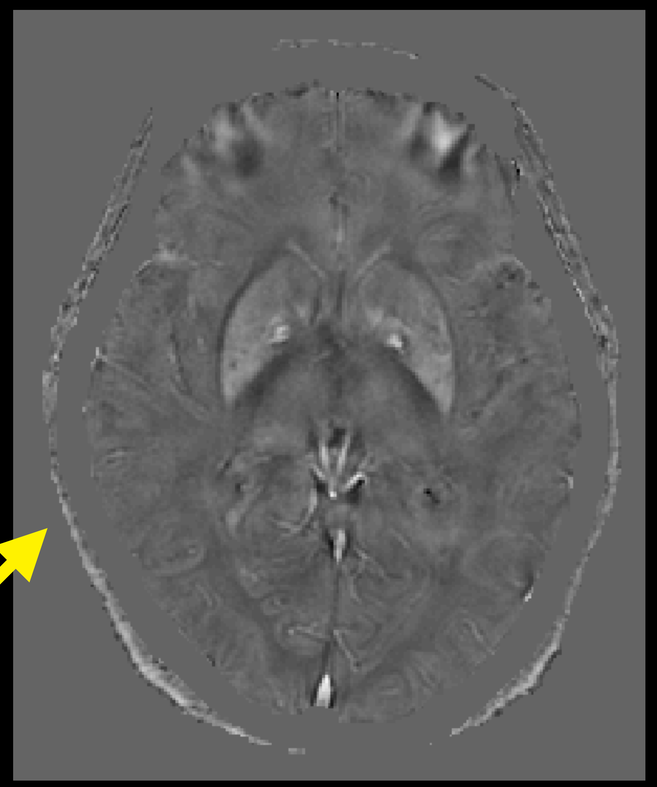

QSM
(ppm)

Materials

Phantom design

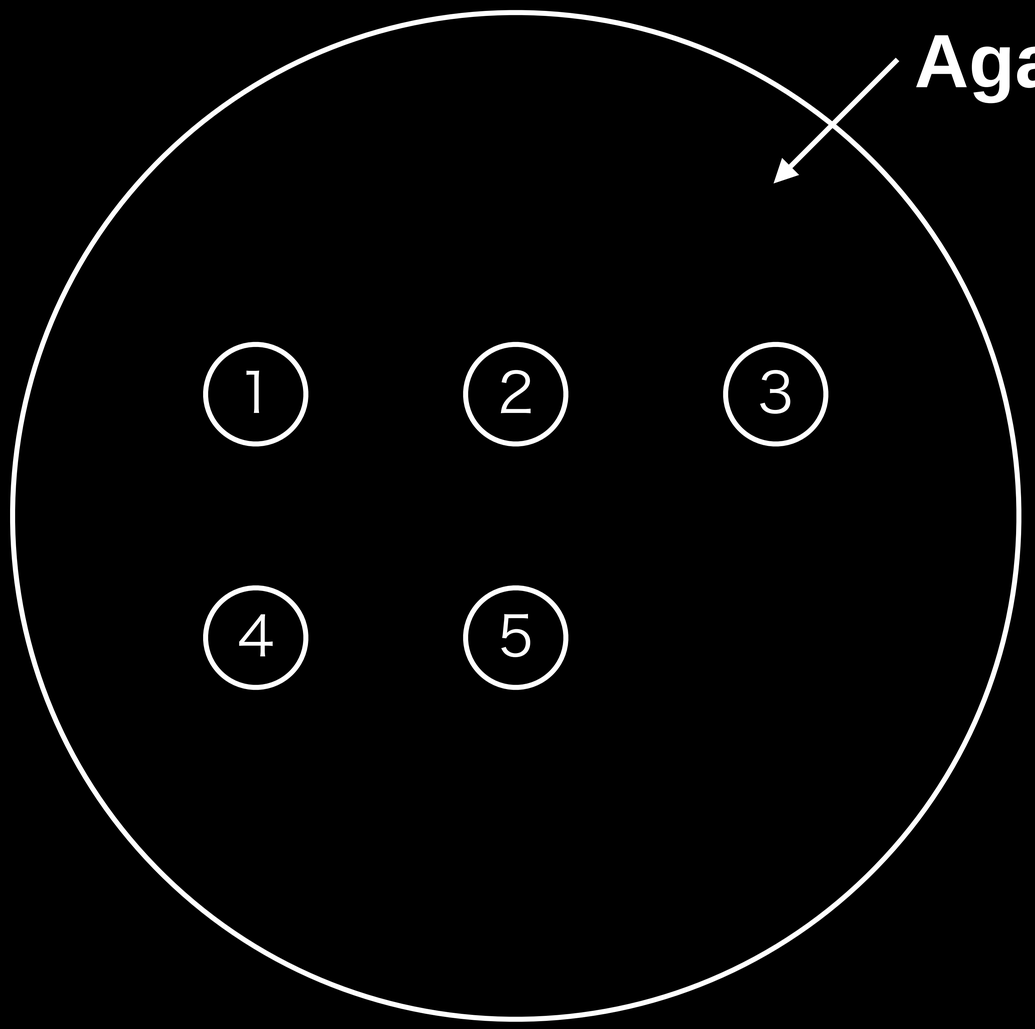

① 0.1~0.3mm
② 0.5~1.0mm
③ 1.0~1.5mm
④ ＞2.0mm
⑤ SPIO

We placed agarose (2%) solutions in a circular PVC container. When the agarose had hardened, we used a straw to poke 30mm holes in it.
Lime stone crushed to different sizes was placed ① - ⑤ holes.

And SPIO (superparamagnetic iron oxide) had placed in ⑥ as hemorrhage.

Methods

Scan conditions

CT

SOMATOM Definition Flash (Siemens)

64 row multi-detector

Slice Thickness [mm]	kV	mAs	Pitch	Rotation Time [sec]
1 mm	100	200	0.8	1.0

MRI

Ingenia 3.0T (Philips) 32ch torso coil

	Slice Thickness [mm]	Matrix (Freq)	Matrix (Phase)	TE [ms]	TR [ms]
SWI	1	0.89	0.72	24	38
multi echo GRE	1	0.94	0.92	3.1 (delta 2.8)	32

Methods① Area measurement

Phantom was scanned by CT and MRI.
Imaging parameters are listed slide No 6.

The area of calcification were measured from CT, T2*WI and SWI.
CT and MRI were scanned 1 mm slice thickness.
All images were binarized using ImageJ.
The area of calcifications were measured 10 consecutive slices, and average area were calculated.

Regions of interests (ROIs) were put on low density area in each images.

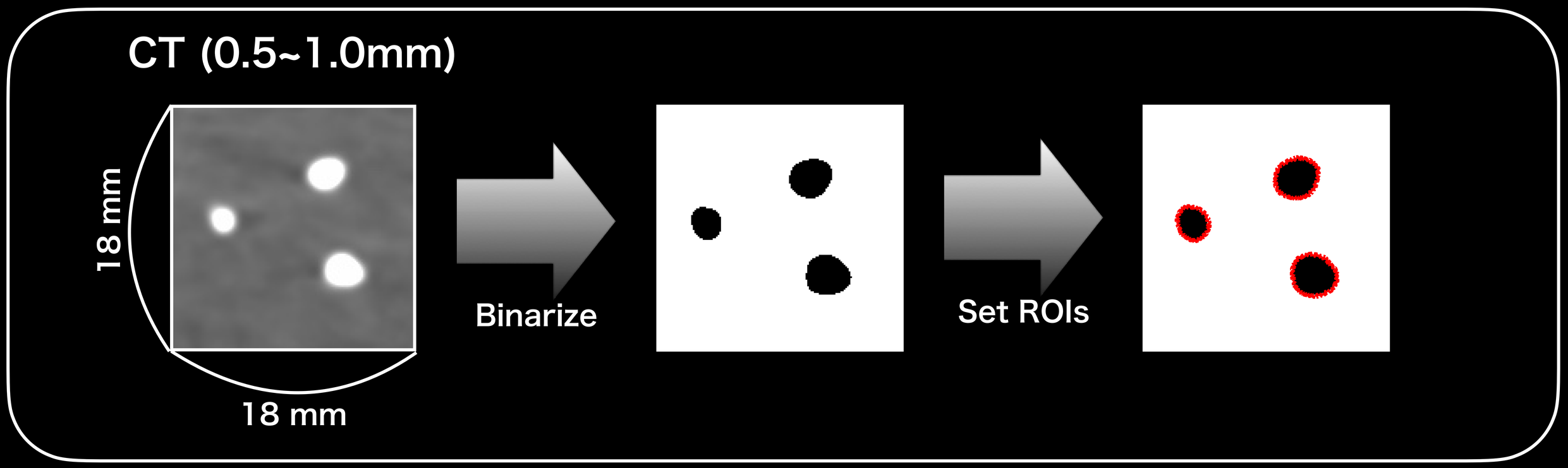

Methods②

Distinguish between calcification and iron

QSM were generated from T2*WI (multi echo GRE) and SWI, using “STI suite” on Matlab. (http://people.duke.edu/~c1160/)

Phase shift were measured with same ROIs on QSM.
Phase shift of calcification and SPIO were compared.

SWI is overestimated compared to T2*WI, so QSM was performed using T2*WI.

Statistics: Student’s t-test was used for all statistical analysis.

$P<0.05$ was considered to be statically significant.

Results ①

Area measurement

	0.1 ~ 0.3 (mm)	0.5 ~ 1.0 (mm)	1.0 ~ 1.5 (mm)	>2.0 mm	SPIO
CT	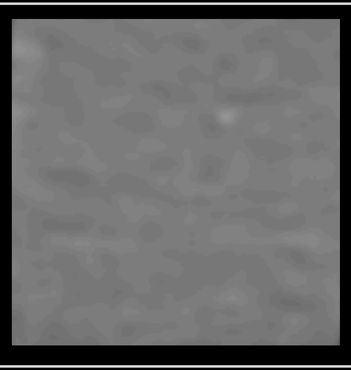	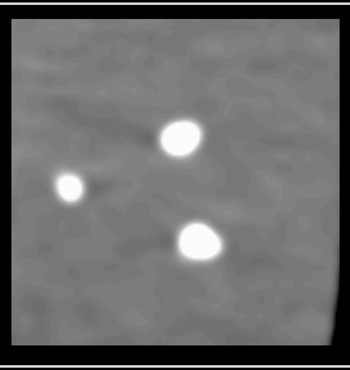	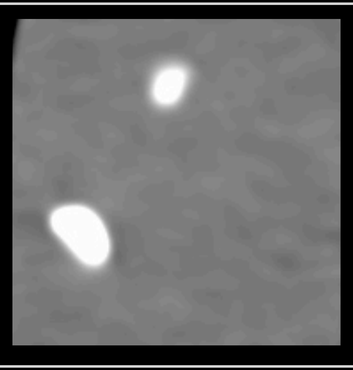	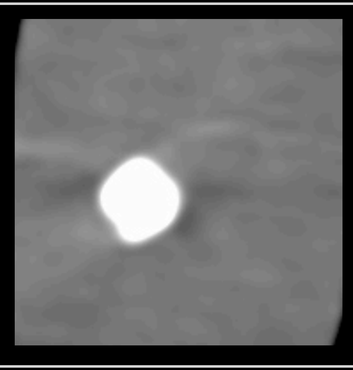	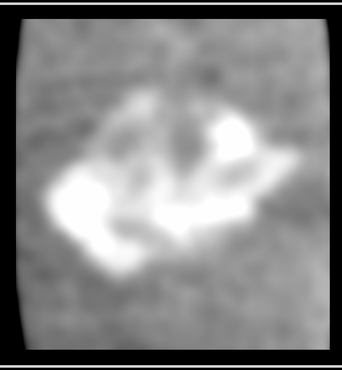
[mm^2]	0.08	58.76	72.16	79.12	647.5
MRI (T2*WI)	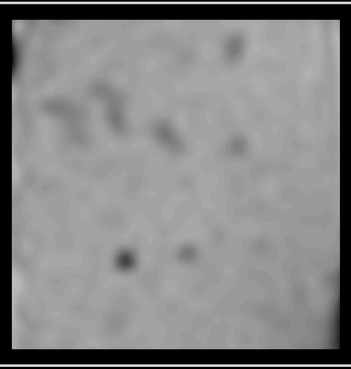	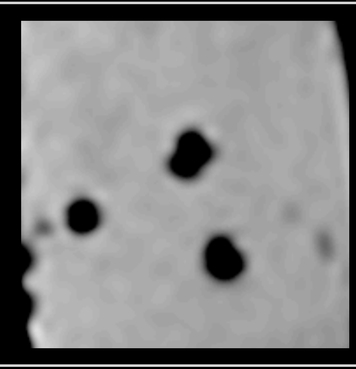	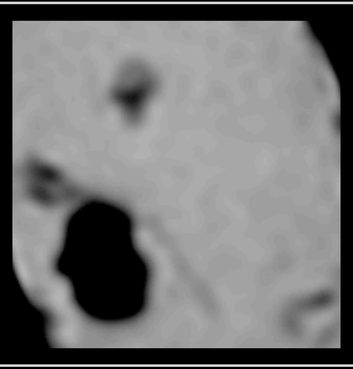	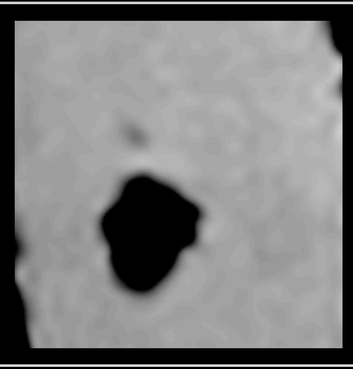	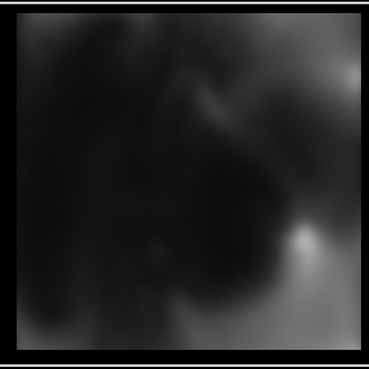
[mm^2]	2.56	76.08	199.8	130.44	1622.5
MRI (SWI)	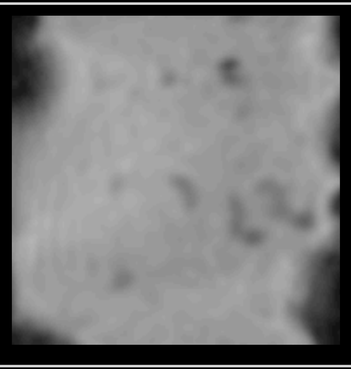	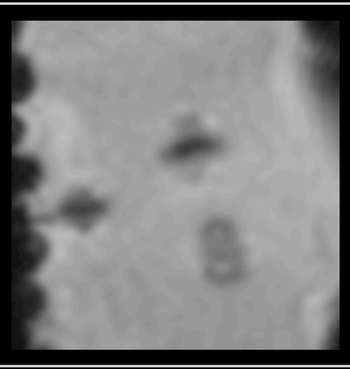	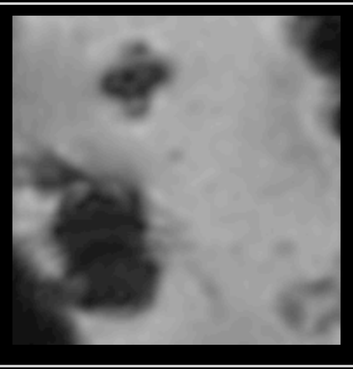	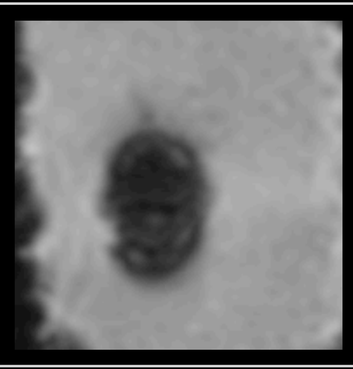	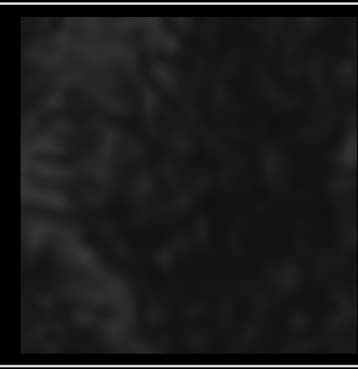
[mm^2]	17.34	72.32	278.76	212.28	2068.1

Results ①

Area measurement

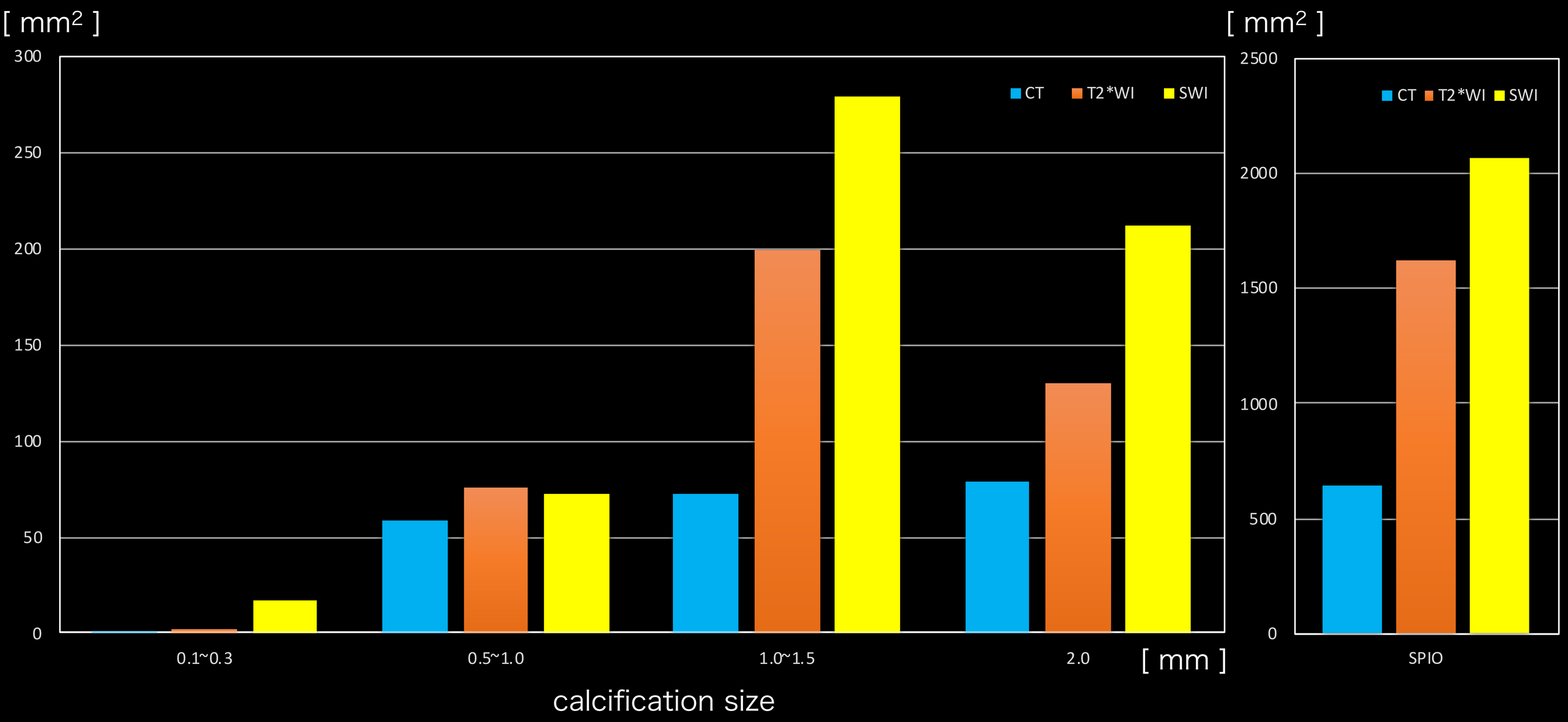

Results ②

Distinguish between calcification and iron

	0.1 ~ 0.3 (mm)	0.5 ~ 1.0 (mm)	1.0 ~ 1.5 (mm)	>2.0 mm	SPIO
CT	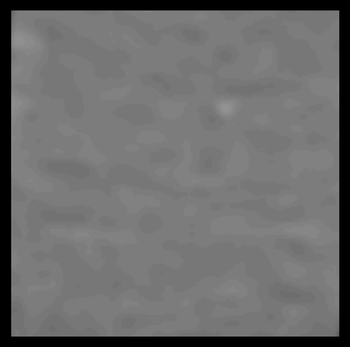	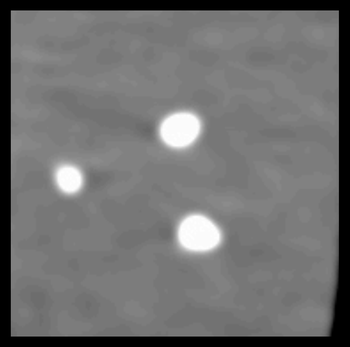	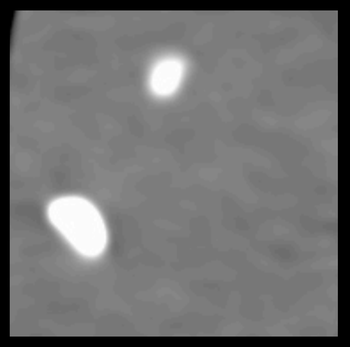	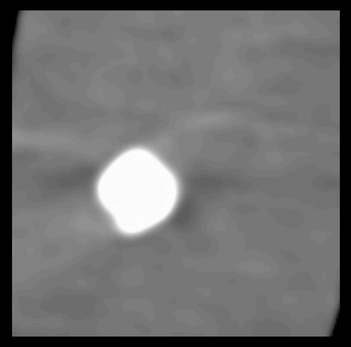	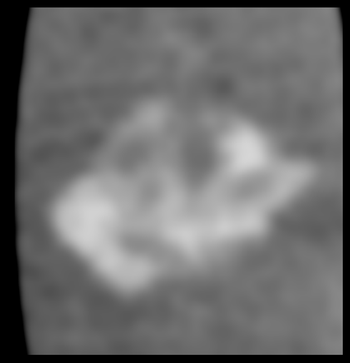
(HU: Hounsfield Unit)	-	404	452	1201	49.56
MRI (T2*WI)	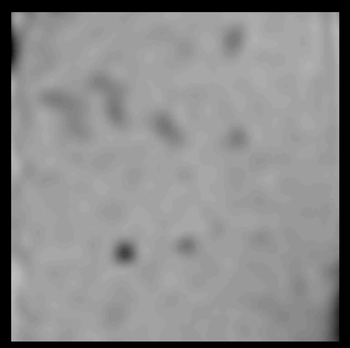	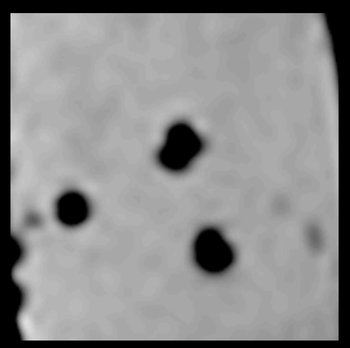	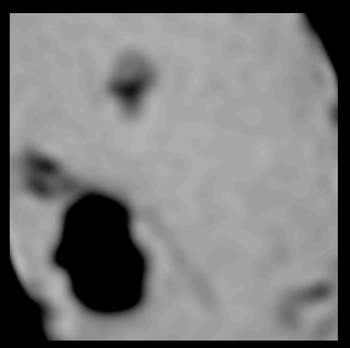	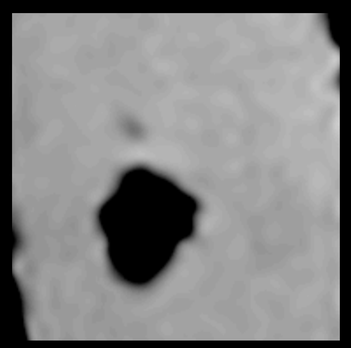	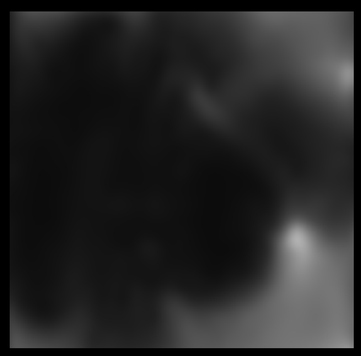
(ppm)	-0.189	-0.280	-0.199	-0.265	-0.588

Results ②

Distinguish between calcification and iron

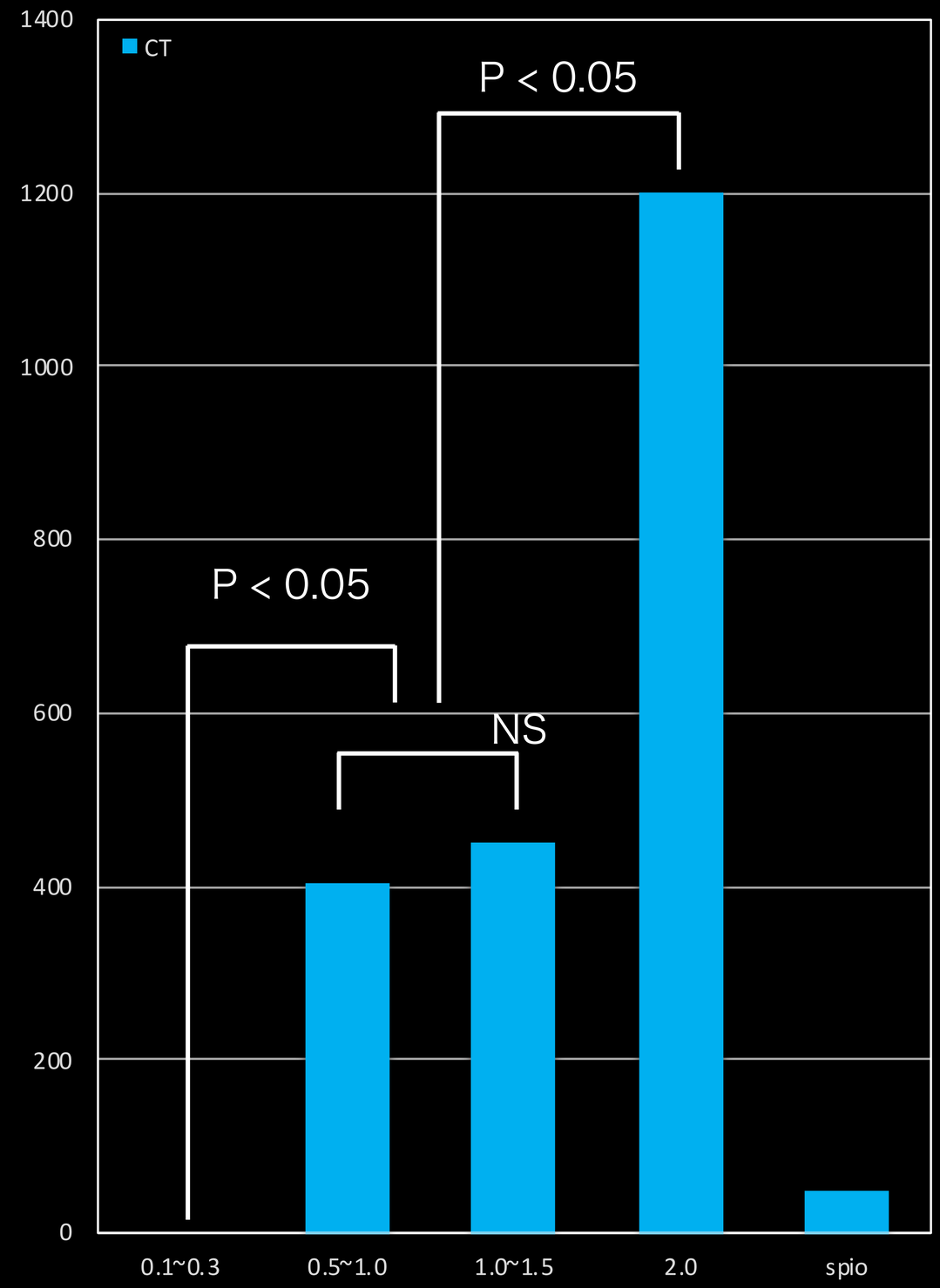

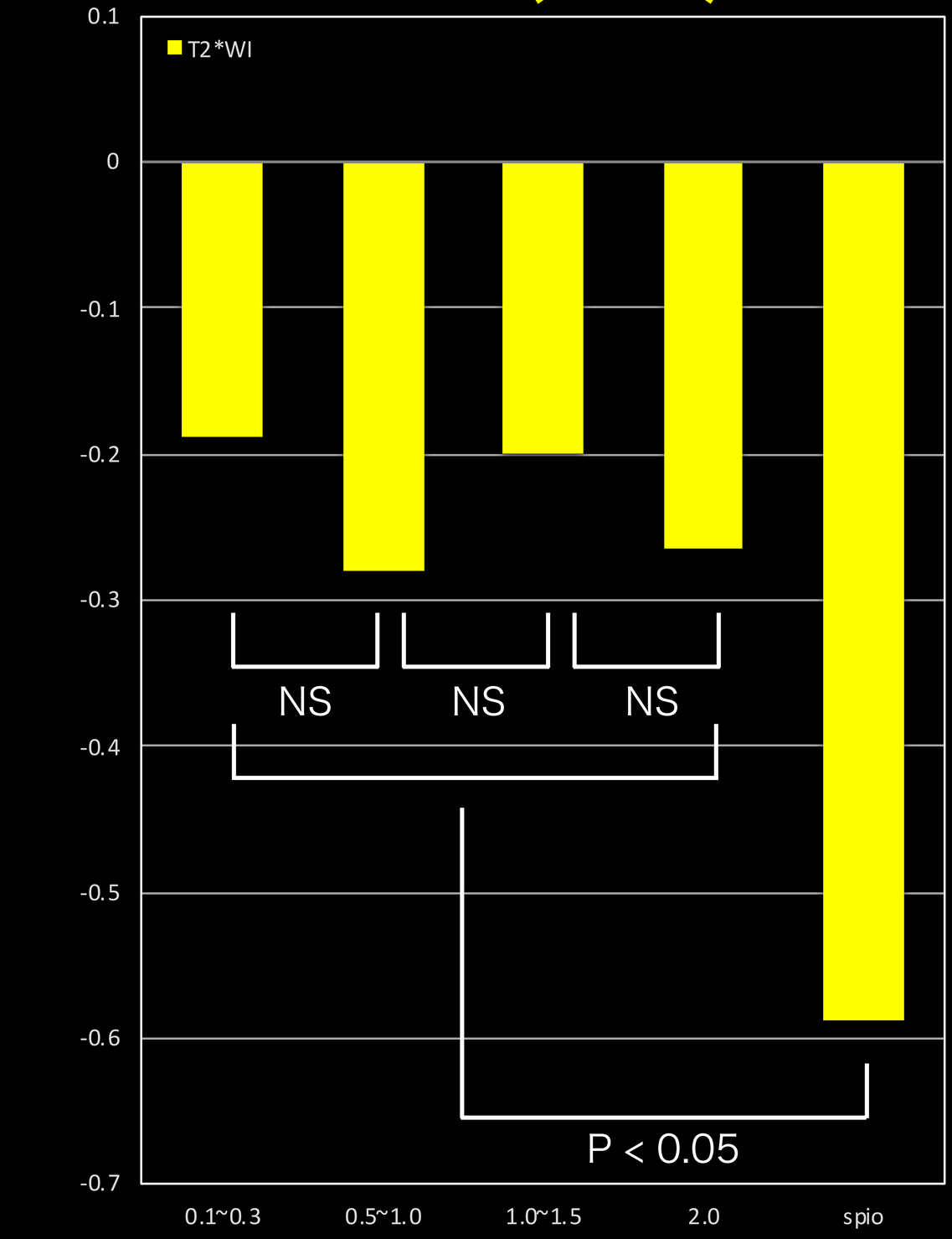

Discussion①

Area measurement

A comparison of detection areas showed that MRI detected a predominantly larger average area at all sizes.
In generally, the resolution limit of CT is 0.35 mm.
Calcification particles in the size range of 0.1 - 0.3 mm were not detected by CT, but were detected by MRI.
We think that MRI was able to detect small particles by shortening the T2* value due to the effect of magnetic susceptibility.

However, MRI overestimates the area due to the effect of magnetic susceptibility. It should be noted that although the detection rate is high, the size of the particles is not accurate.

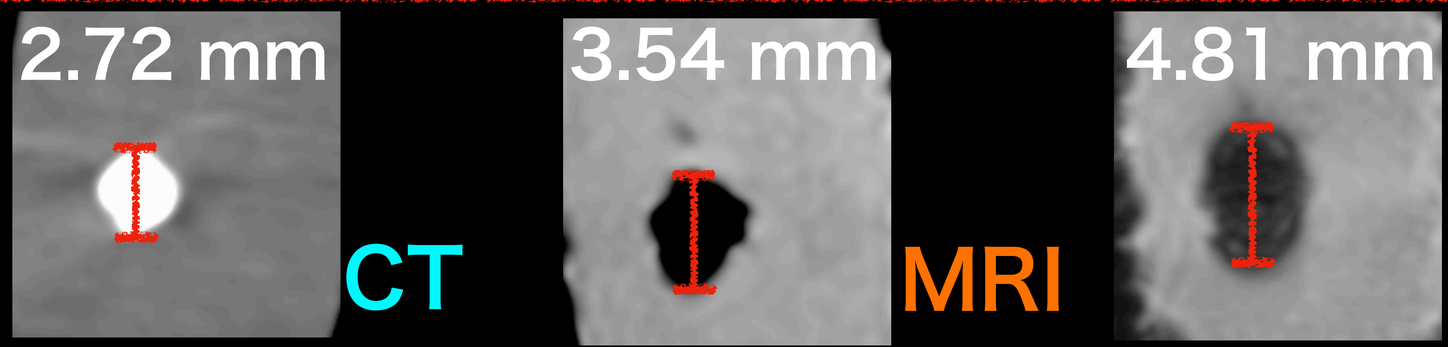

Measured values of calcified particles (> 2.0 mm)

Discussion②

Distinguish between calcification and iron

Different sizes of calcified particles in CT caused differences in CT values. We think that this is due to the partial volume effect. It is not suitable for discriminating between different compositions because of the size difference.

In MRI, both images showed a low signal on the magnitude images and could not be discriminated from each other.

The hemorrhage component has a lager phase shift than the calcified particles due to the magnetic susceptibility of the hemosiderin.

Using QSM, the phase shifts were predominantly different and could be discriminated between the two.

Conclusion

- MRI showed higher detectability than CT.
- 0.1~0.3 mm calcification was not detected by CT, but MRI can it.
- QSM can discriminate calcification and microbleeds.

The usefulness of QSM-MRI for the detection and differentiation of microbleeds leading to the cause of death unknown by CT was suggested.
The present study is a phantom study and needs to be validated on the body in the future.

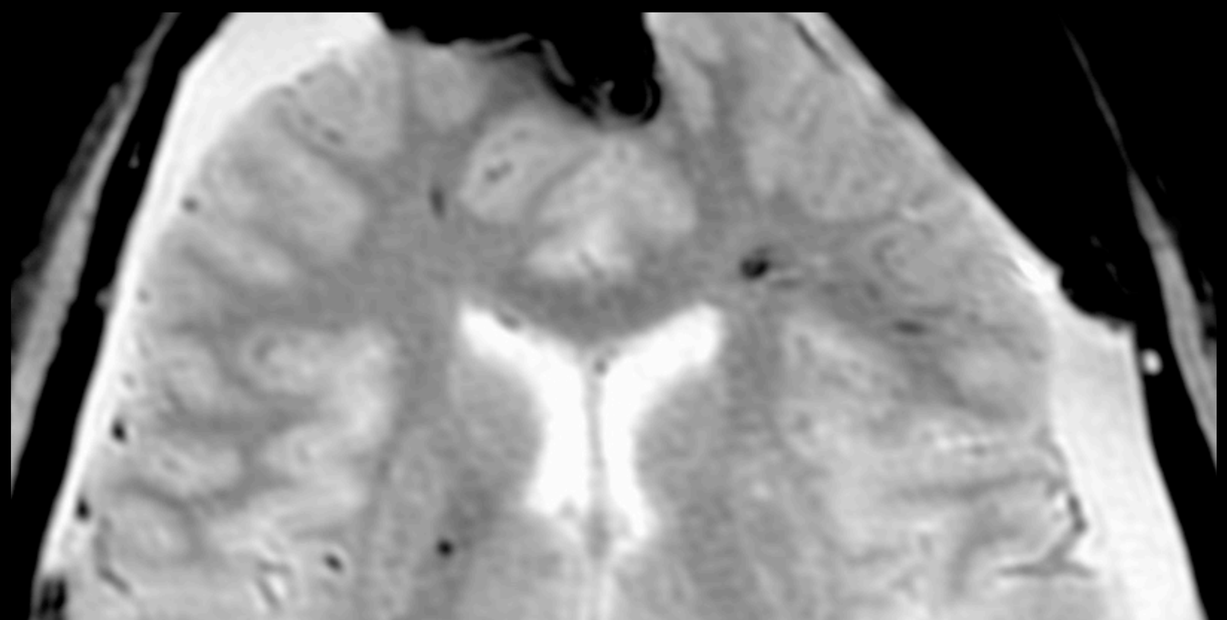

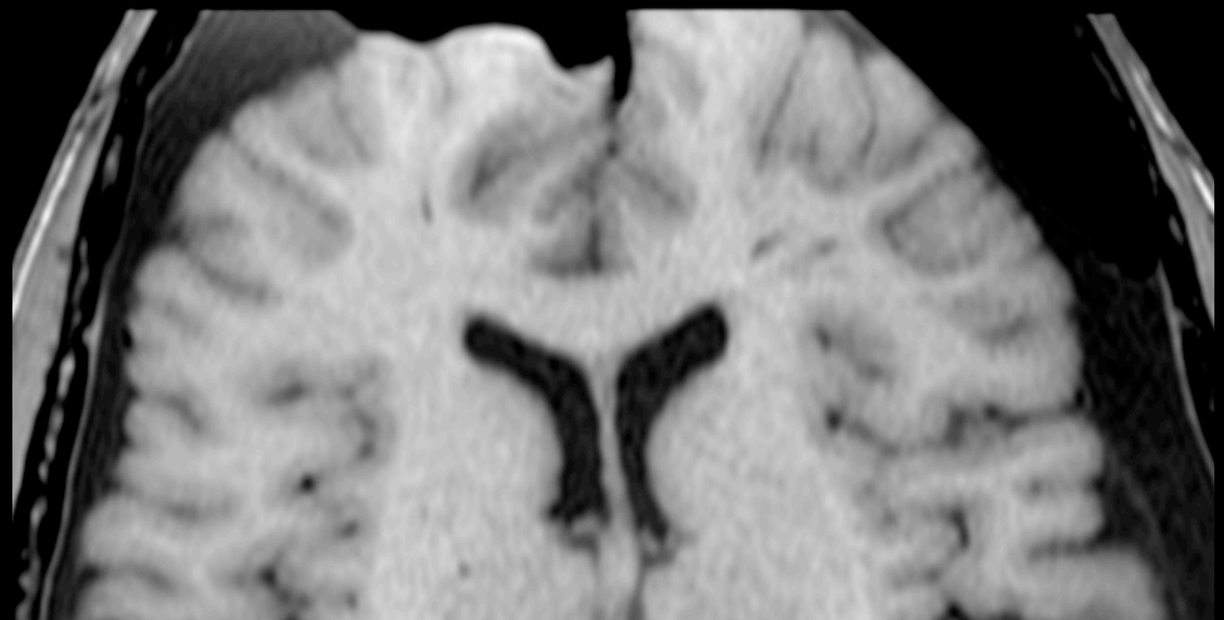

Referense

STI Suite: Software Package for Quantitative Susceptibility Imaging. Wei Li, Magn Reson Med, 22, 2014.

Multiple sclerosis lesion geometry in quantitative susceptibility mapping (QSM) and phase imaging. Eskreis-Winkler S, Deh K, et al. Journal of Magnetic Resonance Imaging 42 (1) pp. 224-229, 2015.

On the role of physiological fluctuations in quantitative gradient echo MRI: implications for GEPCI, QSM, and SWI. Magn Reson Med 2015;73:195-203.

Quantitative susceptibility mapping (QSM) as a means to measure brain iron? A post mortem validation study. Langkammer C, Schweser F, et al. Neuro Image, 62 (3) pp. 1593-1599, 2012.

Quantitative MR imaging of brain iron: a postmortem validation study. Langkammer C, Krebs N, Radiology 257, 455-462, 2010.

Ruptured Distal Anterior Cerebral Artery Aneurysm shows like a traumatic intracranial hemorrhage; case report.

Ayumi Motomura[1)2)3)], Go Inokuchi[2)3)], Maiko Yoshida[2)], Yohsuke Makino[2)3)], Hirotaro Iwase[2)3)], Daisuke Yajima[1)2)]

1) Department of Legal Medicine, School of Medicine, International University of Health and Welfare 2) Department of Legal Medicine, Graduate School of Medicine, Chiba University

3) Department of Legal Medicine, Graduate School of Medicine, University of Tokyo

Introduction

A ruptured cerebral aneurysm in the base of the brain is highly likely to cause a subarachnoid hemorrhage (SAH). Therefore, endogenous SAH is suspected when a computed tomography (CT) scan shows high density in the basal cistern. On the other hand, exogenous intracranial hemorrhage is likely suspected when subdural hematoma (SDH) is accompanied with SAH. However, endogenous SDH due to raptured aneurysms of the distal branch is rare, and the origin of the bleeding is difficult to detect on postmortem plain CT or autopsy. Here, we report a case of suspected traumatic death due to SAH, in which intraventricular hemorrhage and SDH revealed an aneurysm rupture at the distal part of the anterior cerebral artery (ACA) on selective head contrast-enhanced CT.

Case Information

A 72-year-old woman was found dead on the floor of her house in December 2018. She had lived alone and worked 4 days a week in a nursing home. She was found dead by her colleague who visited her because she did not report for work and respond to calls. No evidence of mobile phone use was found for the 2 days before she was reported to dead.

She underwent a surgery for breast cancer in July 2014, which was followed by an anticancer treatment. No cancer recurrencewas observed since September 2018. In addition, she had high blood pressure, cystitis, and central retinal vein occlusion.

Materials and Methods

We performed a selective cerebral CT angiography by injecting contrast medium through a catheter inserted in the left internal carotid artery to perfuse the anterior brain and right vertebral artery in the posterior brain. On autopsy, prior to opening the skull, a 6-Fr catheter was inserted in the left internal carotid artery. The other catheter was inserted in the right vertebral artery on the contralateral side, and both were tightly ligated. Water was then injected in each artery to confirm that the catheters were correctly inserted in the target arteries and to expel any air in the vasculature before the contralateral end was clamped. After preparation in the autopsy room, the body was moved to the CT room. CT scans were performed using a 16-slice multi-ditectore CT scanner (ECLOS, Hitachi Medical Systems, Tokyo, Japan). Raw data acquisition was performed at 120 kV, 200 mAs, and a collimation of 1.25 x 16 mm, and image reconstruction was performed at a 1.25-mm slice thickness. The scanning range was set to 275 mm to cover the entry site of the vertebral artery into the vertebral column and the blood vessels at the top of the skull. Non-contrast angiography was performed.. Then, a total of five scans were performed at 2, 25, 48, 71, and 117 s during contrast medium injection. By using two injectors, 25 ml of the same contrast medium was injected in the catheter of the internal carotid artery at a rate of 0.2 ml/s, and 12.5 ml of contrast medium was injected into the catheter of the vertebral artery at a rate of 0.1 ml/s. Therefore, the amounts of contrast medium injected in the body at the aforementioned scan times were 0.6, 7.5, 14.4, 21.3, and 35.1 mL, respectively. The nonionic water-soluble contrast medium iohexol (Omnipaque 300; Daiichi Sankyo Co., Tokyo, Japan) was prepared by dilution in water and polyethylene glycol (contrast medium-to-water-to-polyethylene glycol ratio, 1:5:10). Immediately after scanning, planar and volume-rendering images, which were generated by the CT workstation software, were interpreted by the operator. Image findings were then compared with the corresponding autopsy findings by the dissector. After autopsy, volume renderings were generated again using imaging analysis software (SYNAPSE VINCENT 3D image analysis system; Fujifilm Medical, Tokyo, Japan). The subtraction method was used to visualize blood vessels. In this method, only blood vessels are presented by subtracting the bone information by performing pre- and post-contrast imaging in the same position. The bleeding sites were determined on autopsy, and the brain was removed while injecting milk through the catheters used in the angiography to identify the site of the milk leakage as the bleeding site.

Results

The pre-autopsy CT revealed a high density area throughout the basal cistern. A small hematoma was found in the fourth ventricle, with an intrathecal hemorrhage combined with SAH. It also showed a left-dominant bilateral SDH (Fig. 1). Selective cerebral CT angiography revealed anextravasation from a small aneurysm of the distal ACA (Fig. 2).

Fig. 1 Pre-autopsy computed tomography image. a) Bilateral subdural hematoma (arrow). b) Subarachtoid hemorrhage throughout the basal cistern. c) A small hematoma in the fourth ventricle (arrow head).

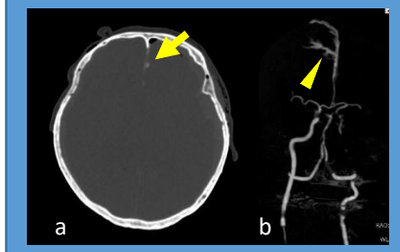

Fig. 2 Selective cerebral computed tomography angiography image. a) Extravasation at the longituidinal cerebral fissure between the frontal lobes (arrow). b) Reconstructed angiography image showing an extravasation from the small aneurysm of the left distalanteriar cerebral artery (arrow head).

In the anatomy, a vascular bulge was found at the peripheral bifurcation of the left ACA, corresponding to the leakage of the contrast medium confirmed using CT. The apex of the ACA aneurysm ruptured, and the milk injected into the blood vessel leaked from that point (Fig. 3). Approximately 83.8 g of hematoma attached under the dura, centering on the surface of the left cerebral hemisphere (Fig. 4a). The brain was slightly swollen, but no obvious cerebral hernia was observed. The patient was thought to have died relatively rapidly on the basis of the autopsy findings of cardiac blood fluidity, mild congestion in various organs, and patechiae. In addition, the findings showed no evidence of external force being applied to the head (Fig. 4b,c). Therefore, the cause of death was considered to be internal SAH due to left ACA aneurysm rupture.

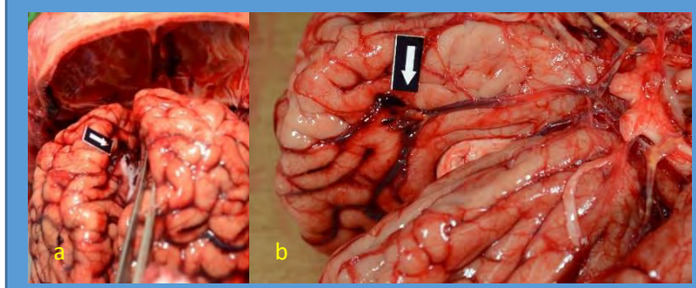

Fig. 3 Autopsy findings of aneurysm. a) Milk leakage from the ruptured distal branch of the anterior cerebral artery (ACA; black arrow). b) Small aneurysm of the ACA (black arrow).

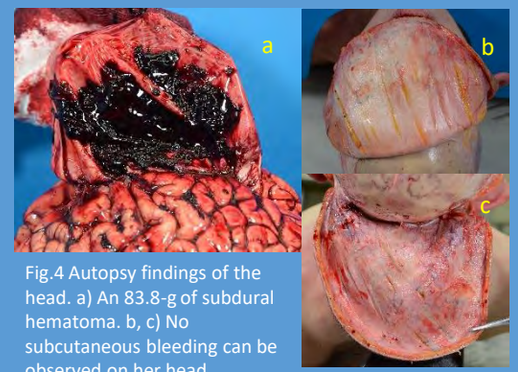

Fig.4 Autopsy findings of the head. a) An 83.8-g of subdural hematoma. b, c) No subcutaneous bleeding can be observed on her head.

Discussion

In general, traumatic causes are considered in cases of SDH on the surface of the hemisphere ditected on CT. Especially in Japan, the cause of death may be clinically investigated using non-contrast CT before or after death in the emergency department. Therefore, in such cases, traumatic SDH can be diagnosed on the basis of such findings. However, SAH due to an intrinsic aneurysm rupture may be missed, as the clinical incidence of SDH complications is reported to be only 0.5-7.9%.[*1]

Even in autopsy, forensic pathologists may miss microaneurysms on the distal side of arteries without pre-autopsy information from CT images for bleeding from the subdural cavity and small fissure of the vessel and make a wrong diagnosis of traumatic SDH or SAH.

Therefore, selective cerebral CT angiography is useful detecting the causative lesion of intracranial hemorrhage and easier investigation of the origin of bleeding in cases of small distal aneurysm rupture.

*1. Kamiya K, Inagawa T, Yamamoto M, Monden S. Subdural hematoma due to ruptured intracranial aneurysm. Neurol Med Chir (Tokyo). 1991 Feb;31(2):82-6.

The sensitivities of various imaging modalities in detecting skeletal trauma in simulated cases of child abuse

A.J. SPIES[a,*], M. STEYN[a], E. BUSSY[b], D. BRITS[a]
*Amy.Spies@students.wits.ac.za

[a]Human Variation and Identification Research Unit (HVIRU), School of Anatomical Sciences, Faculty of Health Sciences, University of the Witwatersrand, South Africa
[b]Department of Radiology, Wits Donald Gordon Medical Centre, South Africa

INTRODUCTION

- Physical abuse is a leading cause of child homicides worldwide.
- In 2018/2019, 18 644 assaults, 1 184 attempted murders and 1 014 murders, all involving children, were reported to the South African police [1].
- Skeletal trauma is common in victims of abuse but is often missed during autopsy.
- Various imaging modalities are used to aid in the identification of fractures.
- The aim was to compare the sensitivities of CT, X-ray and Lodox® scans, which are commonly used in South Africa, in detecting fractures in simulated cases of child abuse using a piglet model. The skeletonized remains were used as the gold standard for comparison.

MATERIALS & METHODS

- Ten piglets were, post-mortem, blindly subjected to blunt force trauma on the skull, thorax, fore- and hindlimbs (Fig. 1).
- Full body helical CT scans, X-rays of each body region, and full body Lodox® scans were taken.
- The number of fractures visible in each body region using each modality was recorded.
- Piglets were macerated, and the number of fractures present in each body region on the dry bone was recorded.
- The percentage of fractures detected by each radiological method with respect to the number of fractures detected on the dry bones was calculated.
- A two-way ANOVA was used to determine if any imaging modality differed significantly from dry bone for any body region.

Figure 1. Piglets were blindly struck on the skull, thorax, forelimbs and hindlimbs.

RESULTS & DISCUSSION

A total of 817 fractures were present on the dry bones, of which CT scans detected 531 (65%), X-rays detected 338 (41%) and Lodox® detected 291 (36%). The sensitivity of each modality for each body region is shown in Figure 2.

Most skull fractures missed were of the face and skull base (Fig. 3). The low sensitivity of all modalities is alarming since skull fractures are extremely common in victims of abuse [2].

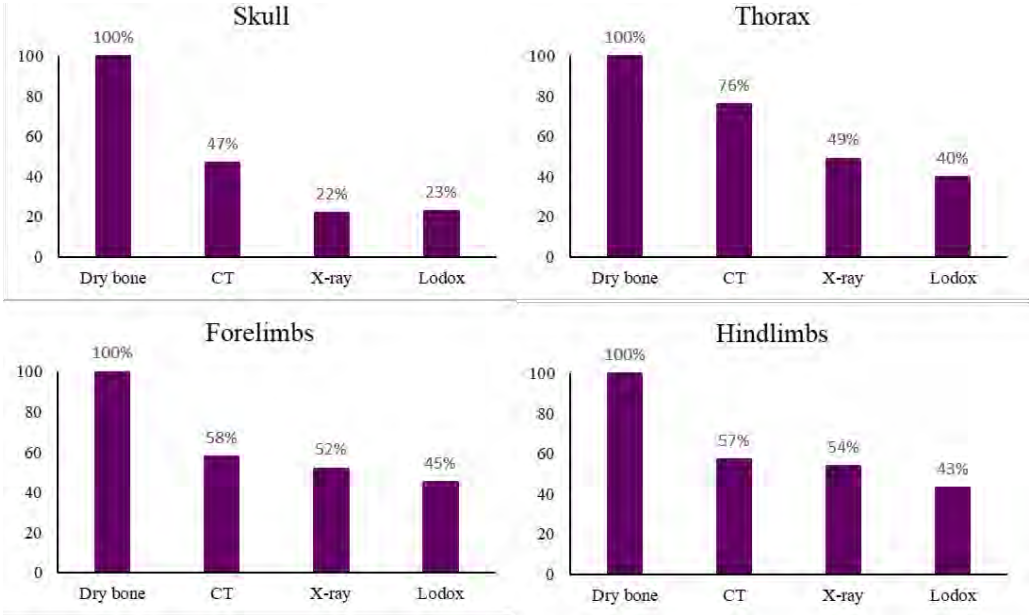

Figure 2. Comparison of percentage of fractures detected by dry bone, CTs, X-rays and Lodox® scans in each body region.

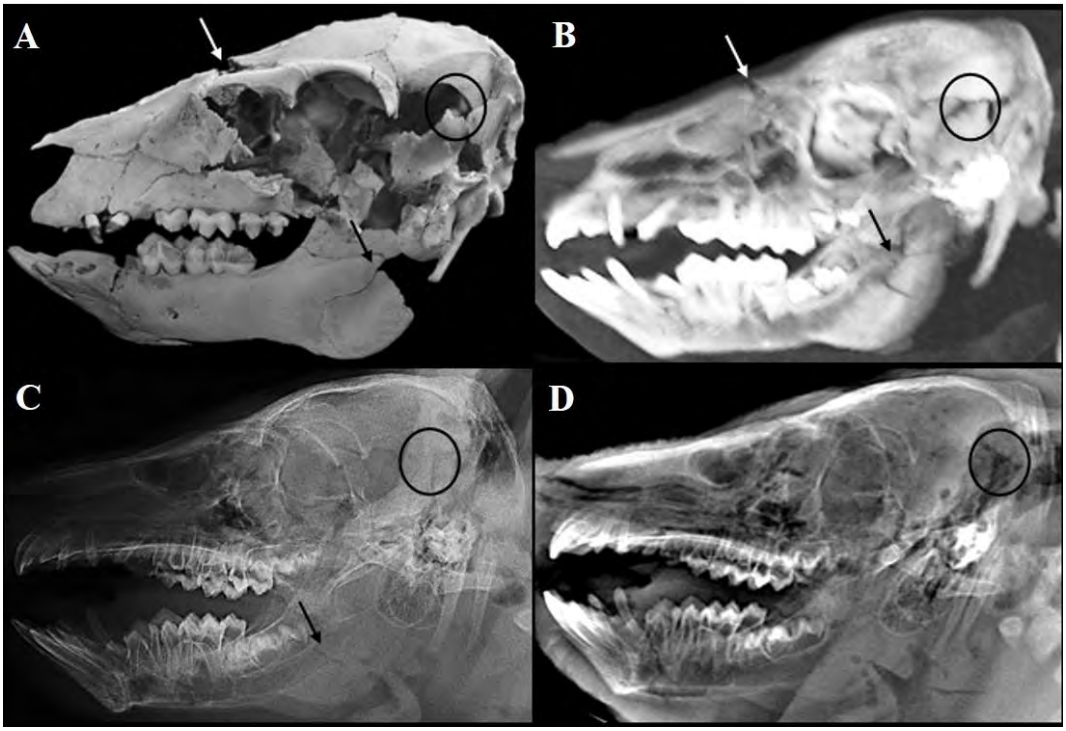

Figure 3. Parietal fracture (black circle) as seen on dry bone (A), CT (B), X-ray (C) and Lodox® (D). A fronto-nasal diastatic fracture (white arrow) is seen on dry bone (A) and CT (B), but not on X-ray (C) and Lodox® (D). A mandibular ramus fracture (black arrow) is also seen on dry bone (A), CT (B) and X-ray (C), but is not visible on Lodox® (D).

RESULTS & DISCUSSION (Cont.)

CTs mainly missed fractures of the sternal rib end, while X-rays and Lodox® scans missed most rib head and sternal end fractures (Fig. 4). These are some of the most common fractures seen in child abuse [2], and the low sensitivities of each method may mean that victims of abuse are not identified.

Most fore- and hindlimb fractures missed were those of the proximal and distal metaphyses of the long bones (Fig. 5). This is concerning since long bone metaphyseal fractures are highly specific for physical child abuse [3].

The two-way ANOVA showed that only CT fracture counts for the hindlimbs did not differ significantly from dry bone ($p>0.05$).

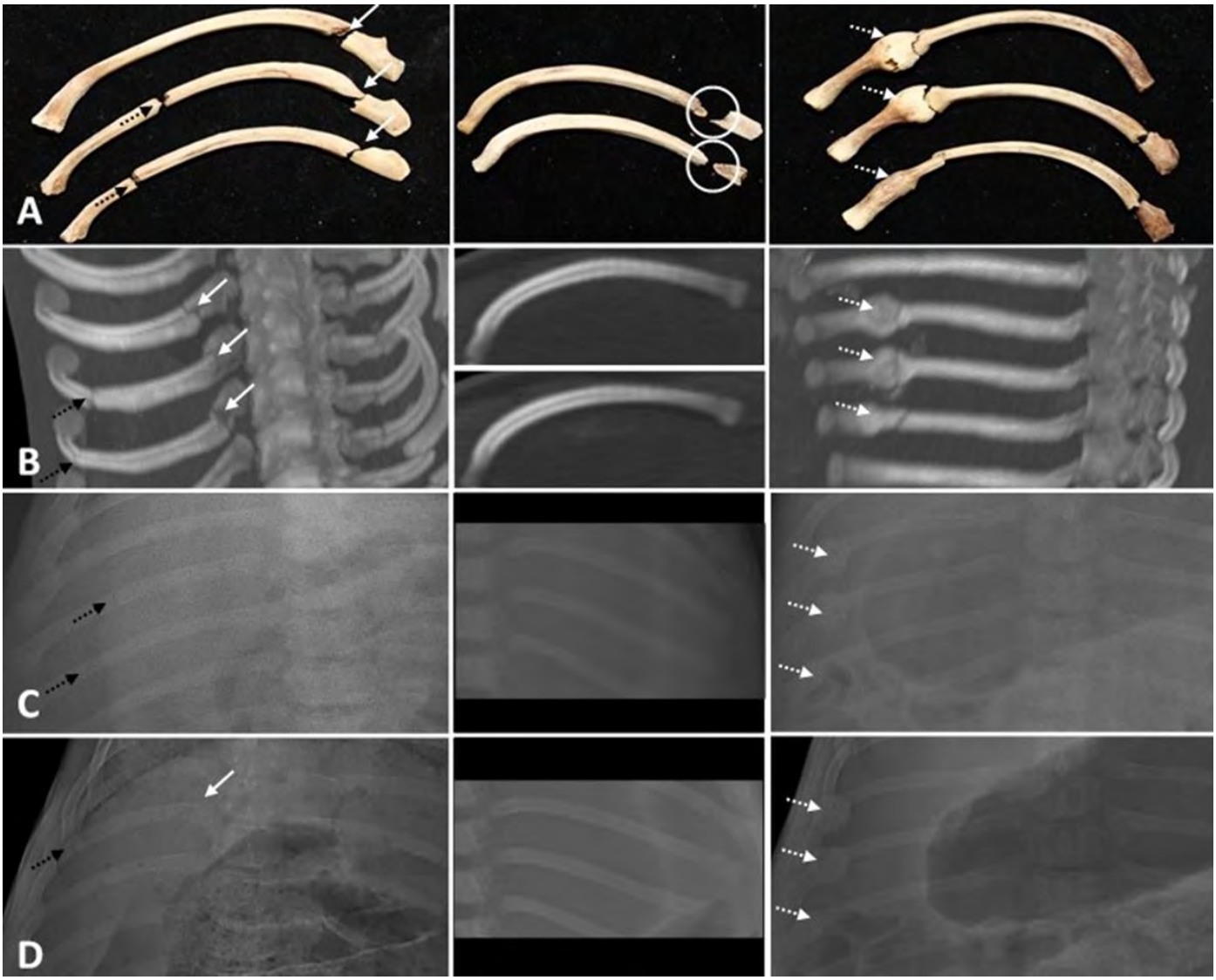

Figure 4. Posterior, sternal end and healed rib fractures (columns 1 – 3) of the same piglets as seen on dry bone (A), CT (B), X-ray (C) and Lodox® (D). White arrows indicate posterior rib fractures, most of which were not observed on X-ray and Lodox® scans. Fractures of the shaft (dashed black arrows) are detected but fractures of the sternal end (white circle) are often missed by CTs, X-rays and Lodox®. Almost all healed fractures (dashed white arrows) are identified by all modalities. The absence of any arrows or circles indicates no fracture detected.

Figure 5. Metaphyseal fractures (black arrows) of the distal ulna (top) and distal tibia (bottom) as seen on dry bone (A), but missed by CT (B), X-ray (C) and Lodox® scans (D). The absence of any arrows indicates no fracture detected.

CONCLUSION

Osteological analysis, when practical, should remain the method of choice when assessing suspected cases of child abuse. When not possible, such as in cases of the living, CT scans should be used. X-ray and Lodox® scans are not recommended for detecting fractures in suspected cases of physical child abuse.

REFERENCES

1. South African Police Services. Crime statistics: April 2018-March 2019. Pretoria: SAPS, 2019.
2. A.M. Kemp, F. Dunstan, S. Harrison, S. Morris, M. Mann, K. Rolfe, S. Datta, D.P. Thomas, J.R. Sibert, S. Maguire, Patterns of skeletal fractures in child abuse: systematic review, BMJ 337 (2008) 859-862. https://doi.org/10.1136/bmj.a1518
3. P.K. Kleinman, J.M. Perez-Rossello, A.W. Newton, H.A. Feldman, P.L. Kleinman, Prevalence of the classic metaphyseal lesion in infants at low versus high risk for abuse, Am. J. Roentgenol. 197 (2011) 1005-1008. https://doi.org/10.2214/AJR.11.6540

ACKNOWLEDGEMENTS

Thanks to Mr du Plessis and Mr Fouche from GHB Farms Pty (Ltd) for the donation of the piglets; the Central Animal Services (CAS) at the University of the Witwatersrand for the use of their facilities to inflict the trauma; Mr Meyer for helping to inflict the trauma; Ms Khoza and Ms Rammekwa from CAS for assisting with X-rays; Dr Haagensen from the Department of Radiology at Wits Donald Gordon Medical Centre for assisting with CT scans; Ms Reindorp from Johannesburg Forensic Pathology Services, and Ms Nkosi from Lodox® Systems (Pty) Ltd, for assisting with the Lodox® scans; Mr Mekwa and the School of Anatomical Sciences at the University of the Witwatersrand for the facilities for the storage and maceration of the piglets; Mr Matjila, Ms Joubert, Ms Swiegers and Ms Mamabolo for assisting with maceration; Ms Joubert, Ms Mamabolo, Ms Lottering and Ms Fredericks for assisting with skull reconstructions.

This work is based on the research supported in part by the National Research Foundation (NRF) of South Africa (Grant number: 118149) and The NRF/Deutscher AkademischerAustausch Dienst (DAAD) (Grant number: 117943). Opinions, findings and conclusions or recommendations expressed are those of the authors and are not necessarily to be attributed to the NRF or DAAD.

This is how misinterpretation of postmortem imaging occurred

～5 error patterns revealed by autopsy results～

Maiko Yoshida[1)2)]、
Yohsuke Makino[1)3)]、Takahiko Mine[2)]、Go Inokuchi[1)]、
Hirotaro Iwase[1)3)]

1) Department of Radiology, Kyorin University Graduate School of Medicine
2) Department of Legal Medicine, Chiba University
3) Department of Forensic Medicine, The University of Tokyo

☑ The author has no conflict of interest to disclose with respect to this presentation.

Introduction

In recent years, image acquisition of cadavers has become more and more common in both the clinical and forensic fields due to a combination of factors such as a decrease in the autopsy rate, widespread availability of imaging devices, and the development of diagnostic imaging.

Importantly, the fundamental law of death investigation was enacted last year and will be enforced from this April, 2020. On the basis of this law, the image acquisition of cadavers of people who died outside hospital will possibly increase.

Consequently, the chances for clinical radiologists to challenge the interpretation of postmortem imaging of those cadavers will increase.

Introduction

Currently, the assignment of responsibility for these images remains a vaguely answered question. Consequently, considerable images are not even interpreted. Other problems should be mentioned here; misinterpretation of postmortem (PMCT) images, particularly by doctors who are neither forensic pathologists nor radiologists, occurs frequently.

Since the chances to verify validity of interpretation are limited under the extremely low rate of autopsy, comparing between PMCT interpretation and autopsy results and sharing the results is crucial for better interpreting postmortem imaging.

Introduction

Here, we present five cases in which apparent misdiagnosis of PMCT was revealed by autopsy results. In all cases, PMCT image acquisition and interpretation was performed at clinical hospitals or clinics other than our institution in order to determine the cause of death. An autopsy was performed together with PMCT as a preliminary examination at our institution. We checked and analyzed the results and extracted five major error patterns of interpretation.

We would like to report those patterns.

Case 1

・A male in his 40’s found dead in a cabin of a boat being moored at a liver.

・A police doctor (not a radiologist, not a forensic pathologist) who examined the body took PMCT and interpreted the images as follows; endogenous subarachnoid hemorrhage （SAH) as the cause of death.

・Thereafter, the blood concentration of carbon monoxide (CO)-Hb was turned out to be 20% and judicial autopsy was performed.

PMCT（about 3 days after death）

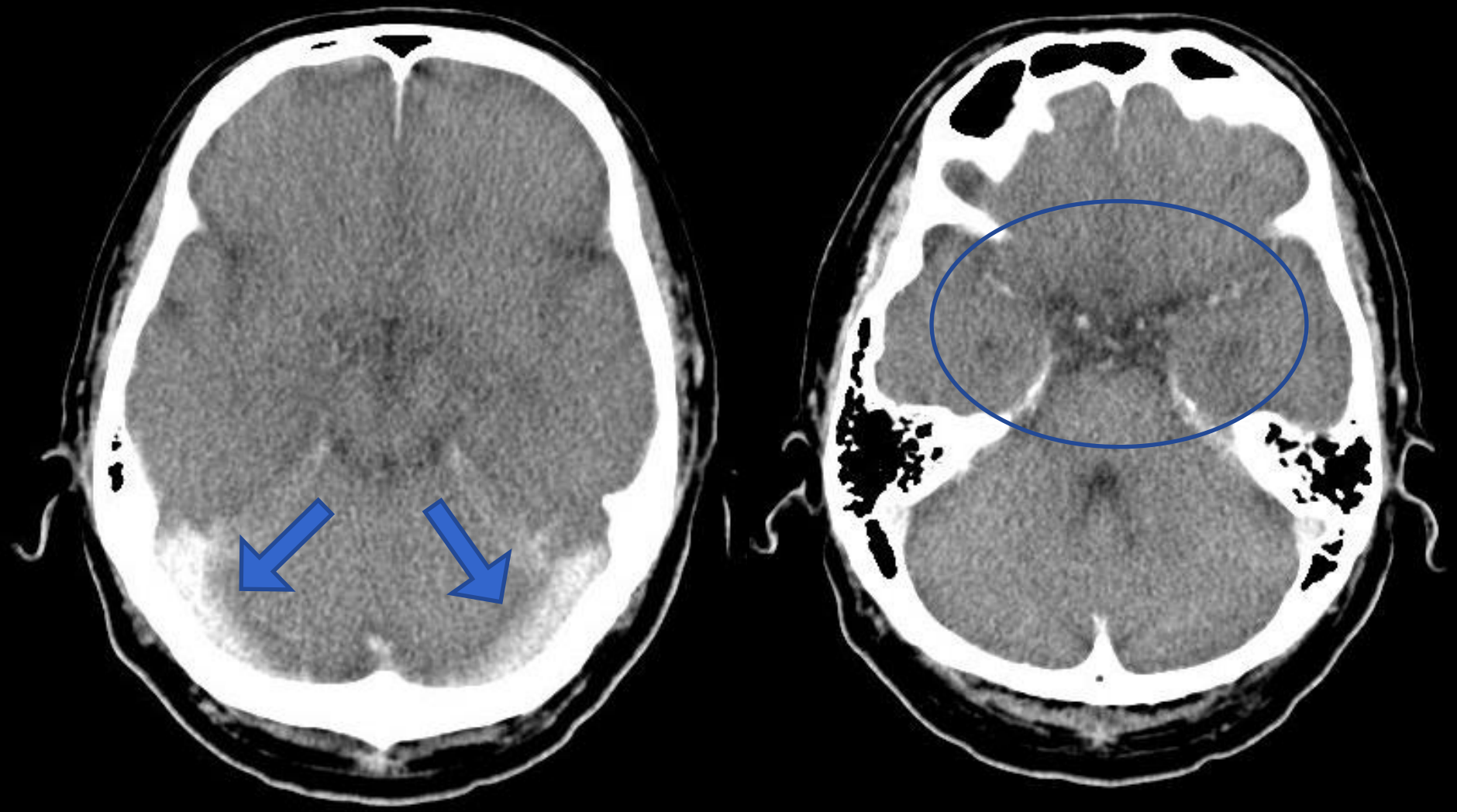

Postmortem changes are detected. No fatal hemorrhagic lesions.

PMCT（About 3 days after death）

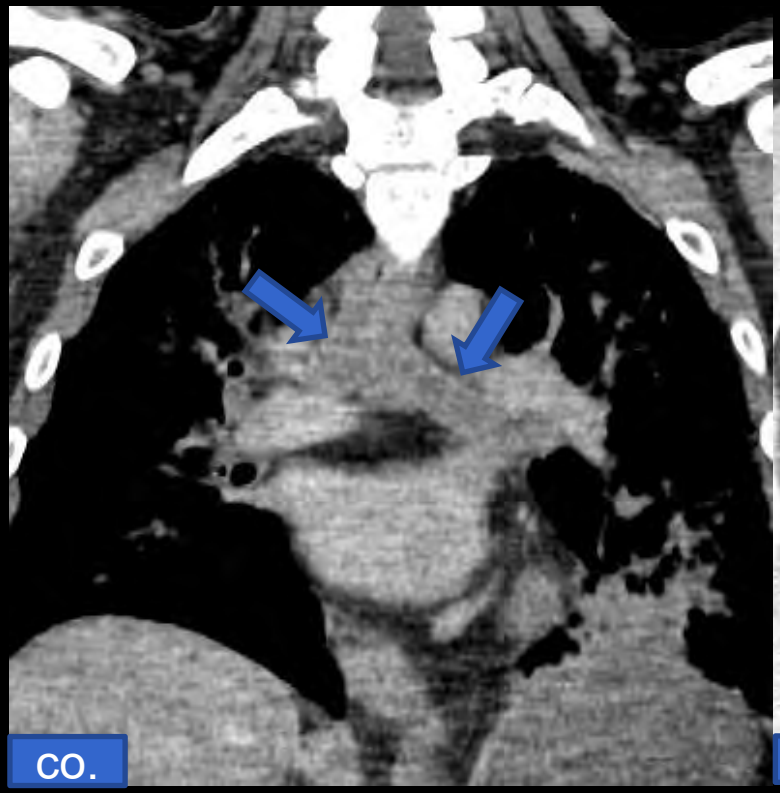

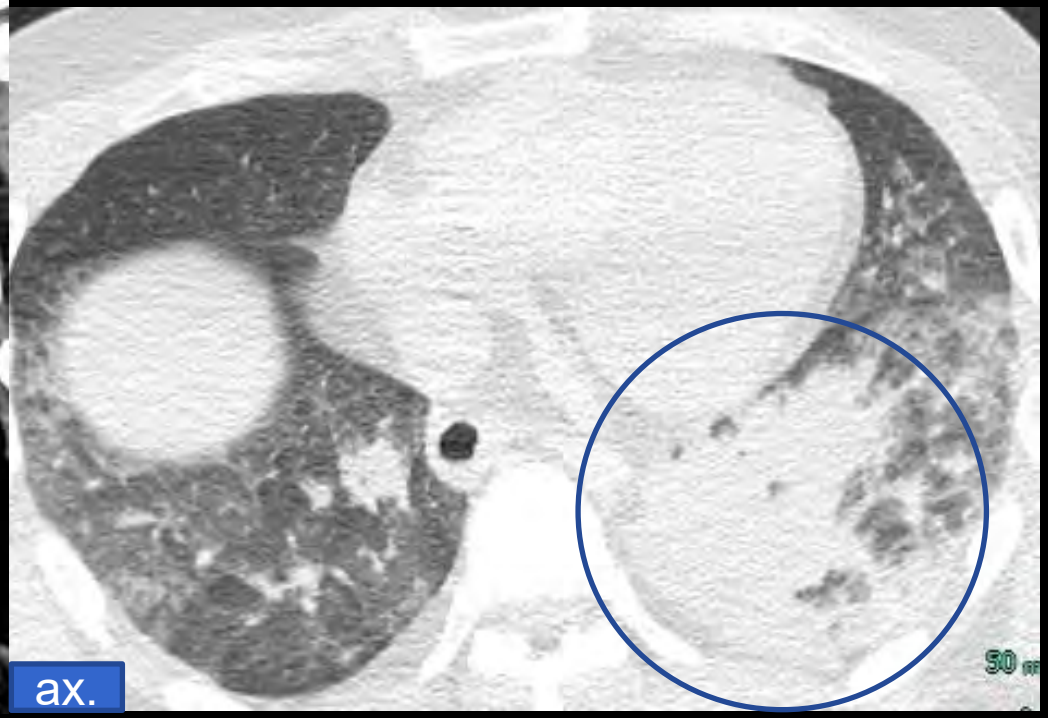

Fluid collection within the trachea and bronchi.

Massive consolidation at lt. lower lobe.

Autopsy results

（No subarachnoid hemorrhage）

- CO-Hb 20%.
- Reddish postmortem lividity.
- Food residue inside trachea and bronchi.
- Pneumonia at lt. lower lobe.

  (Neutrophil infiltration was present.）

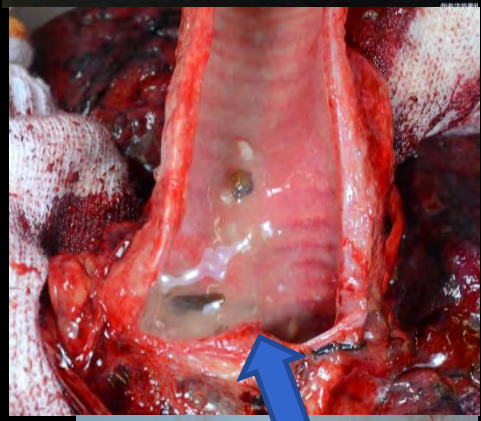

Cause of death

Suffocation by vomitus aspiration

under consciousness disorder

caused by carbon monoxide poisoning

Misinterpretation pattern of Case 1

Postmortem changes were mistaken for the cause of death.

Case 2

- A Female in her 40s.
- After she drank alcohol at a party, she found dead at a toilet of the place. She was transferred to an emergency hospital and resuscitated but died.
- PMCT was taken at the hospital and emergency doctor interpreted the image as follows; intraperitoneal bleeding (bleeding site unknown) as the cause of death

PMCT taken at the hospital

（About 4 hours after the death）

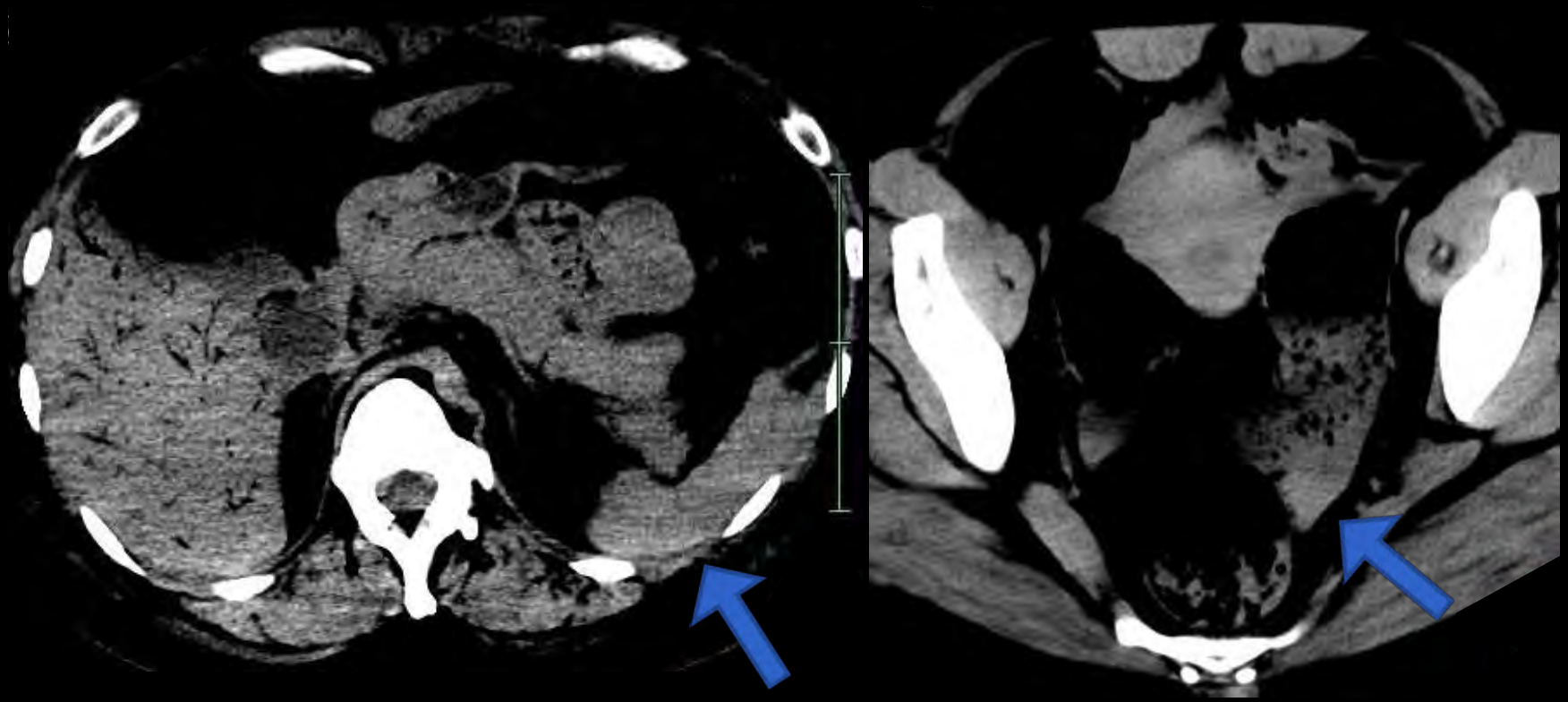

Bloody ascites is detected around the liver and spleen, pelvic space

PMCT prior to autopsy

(About 3.5 days after death)

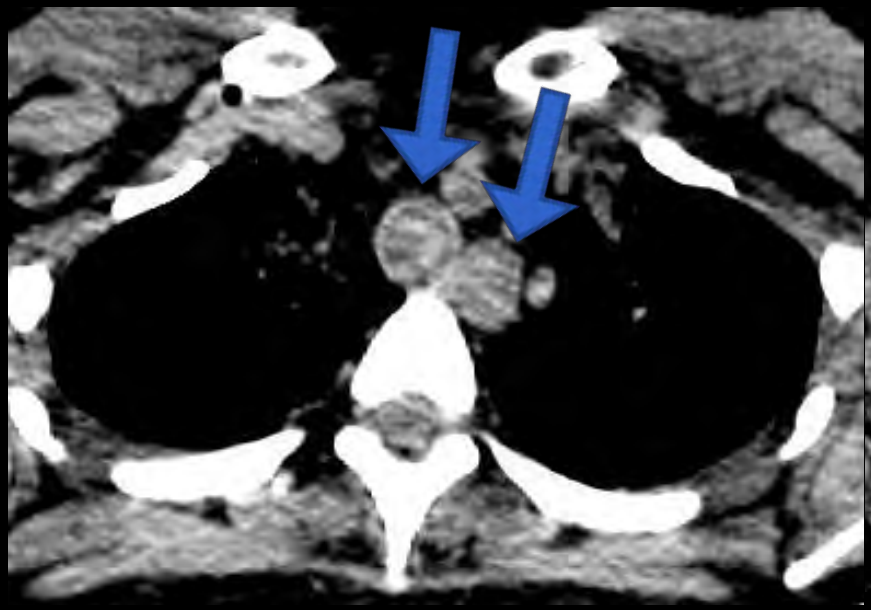

Soft tissue density is seen inside trachea and esophagus.

Soft tissue density is seen in the stomach

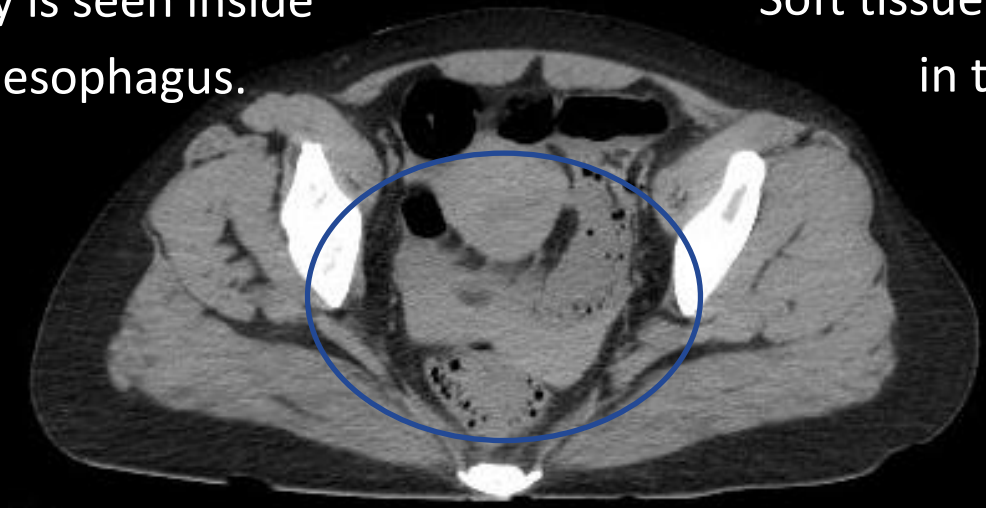

Bloody ascites is detected.

Autopsy results

- Remarkable postmortem lividity.
  Petechia at eyeball and eyelid conjunctiva and at skin.
  Liquidity of heart blood (indicating sudden death）.
- Large amount of aspiration material inside trachea and bronchi.
- High blood concentration of ethanol (4.437mg/mL).
- High blood concentration of antidepressant (0.39μg/mL).
- Bloody ascites (Dark red fluid blood）.
- Liver and spleen contusion (No coagulation）.
- Sternum fracture, multiple rib fracture

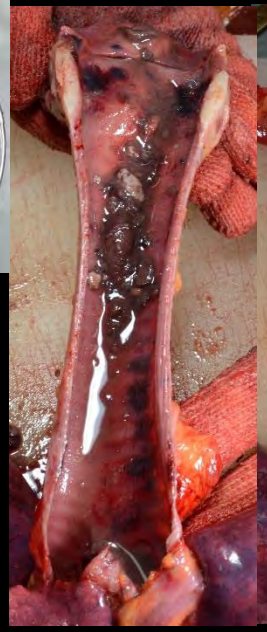

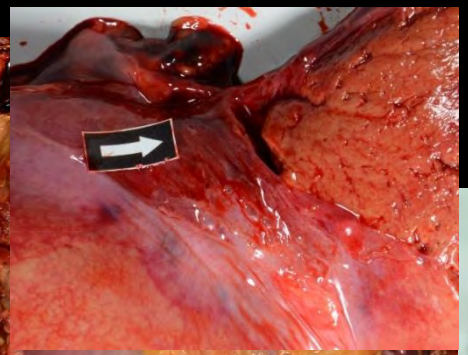

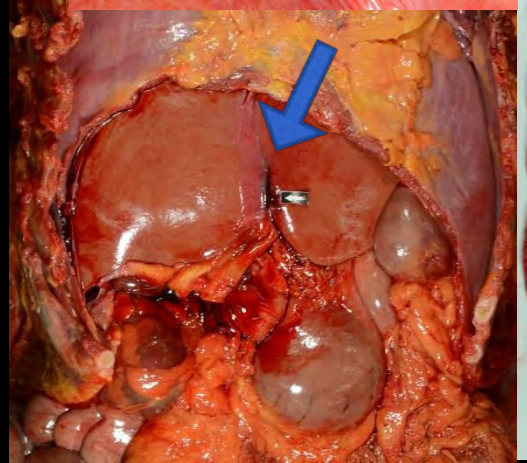

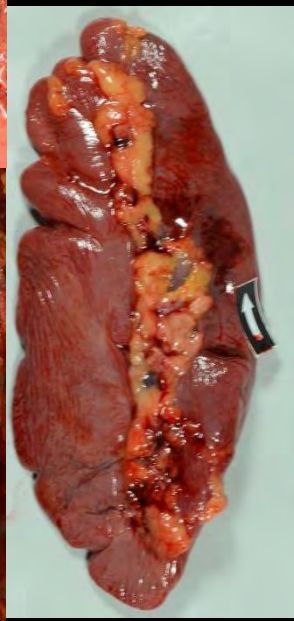

Cause of death

Suffocation by vomitus aspiration

caused by acute alcohol poisoning

（Liver and spleen contusion, ascites
⇒caused by resuscitation）

Misinterpretation pattern of Case 2

Resuscitation changes were mistaken for the cause of death.

Case 3

- A male in his 50s. A truck driver.
  He fell to the ground from 1.5m high and became unconscious. He was transferred to an emergency hospital but died.
- PMCT was taken at the hospital and interpreted as follows; no fatal traumatic lesion. The cause of death was supposed to be ‘cardiac failure’.

PMCT taken at the hospital

(About 1.5 days after death)

Cervical spine CT was not taken for PMCT.

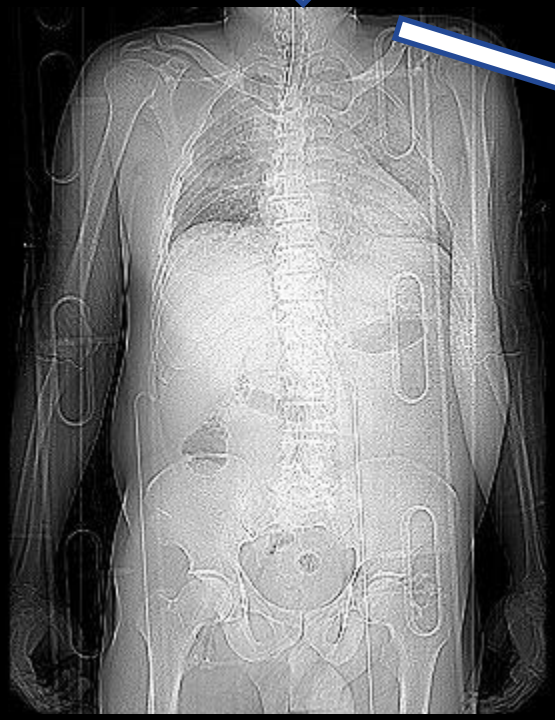

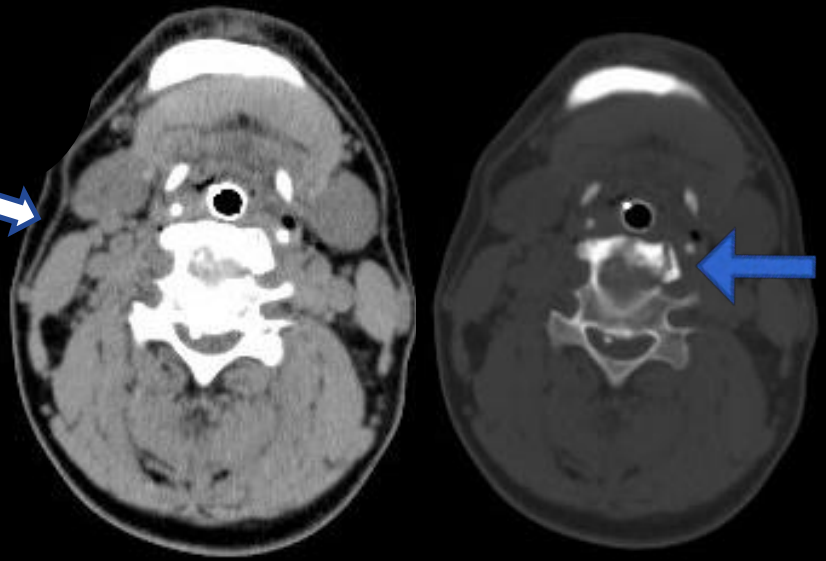

For this protocol, lower cervical spine fracture Is barely detected but subtle.

PMCT（About 3 days after the death）

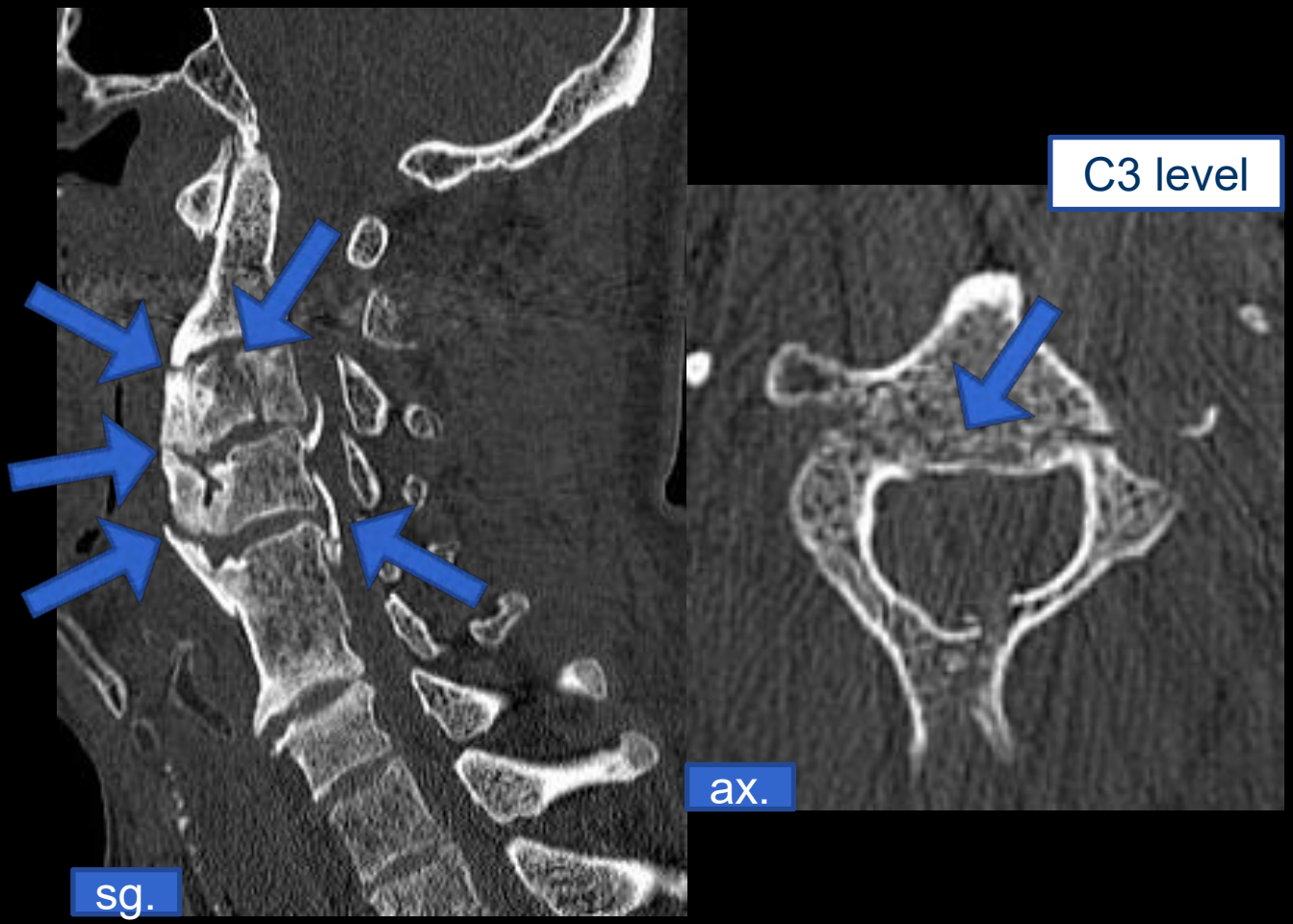

Massive calcification of vertebral osteophyte suspected DISH・OPLL

Cervical spinal fracture (C2・C3)

Cervical spinal canal stenosis

Autopsy results

Cause of death

Cervical spinal cord injury

caused by cervical spine fracture

C2 pedicle fracture、C2-3 vertebral body fracture、

C4-5,C 7-Th1 vertebral osteophyte fracture + hemorrhage

Dark-reddish discoloration of cervical spine, contusion+ hemorrhage

Misinterpretation pattern of Case 3

The cause of death was determined by insufficient examination.

(Not a misinterpretation error
but a image acquisition protocol error.)

Case 4

- A male with intellectual disability in his 10's.
- He had lived at welfare facility for 5 years.
- He began to vomit a lot and the following day, he became unconscious and cardiac arrest. He was transferred to an emergency hospital and resuscitated temporally but the following day he died.
- A Doctor at the hospital determined the cause of death as sepsis caused by bowel obstruction (endogenous). Antemortem brain CT and chest and abdominal X ray was used for the decision. No PMCT was taken.
- Judicial autopsy was performed since he died at facility.
- Past history: none.

X ray film at the hospital (antemortem)

Brain CT: intact
X ray (prone position)
CRP 20 mg/dl

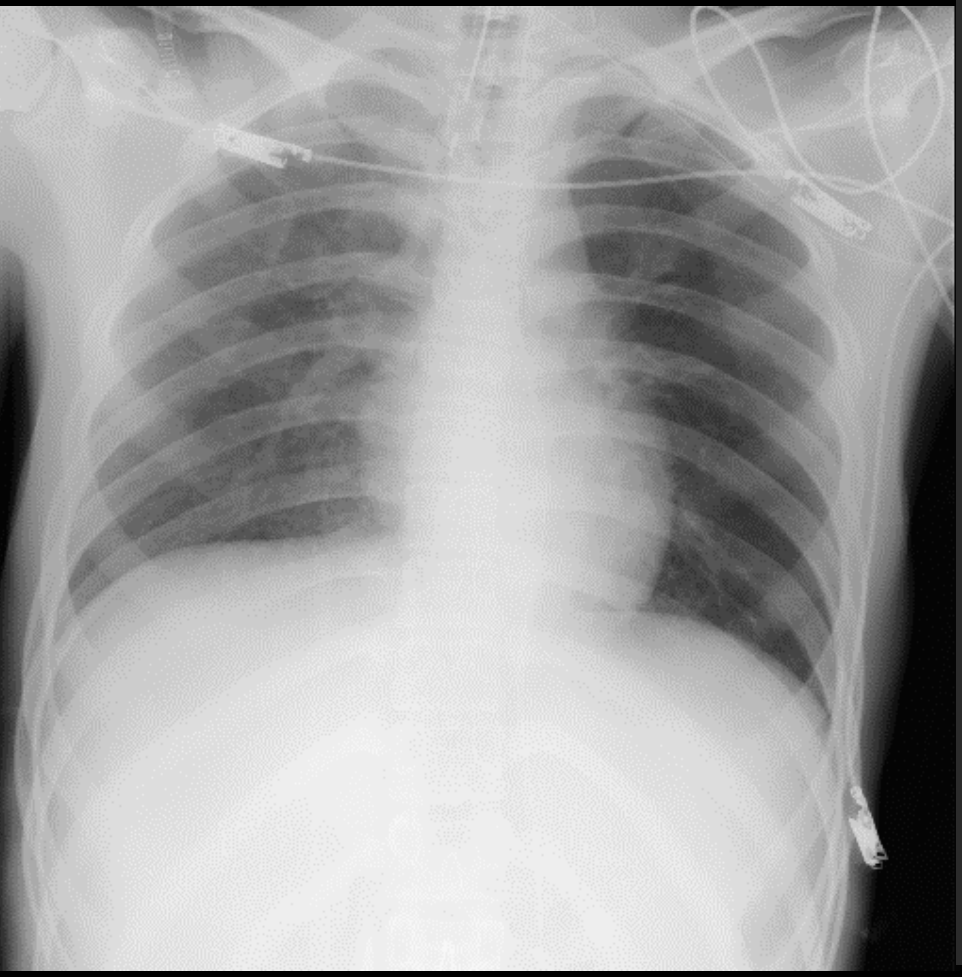

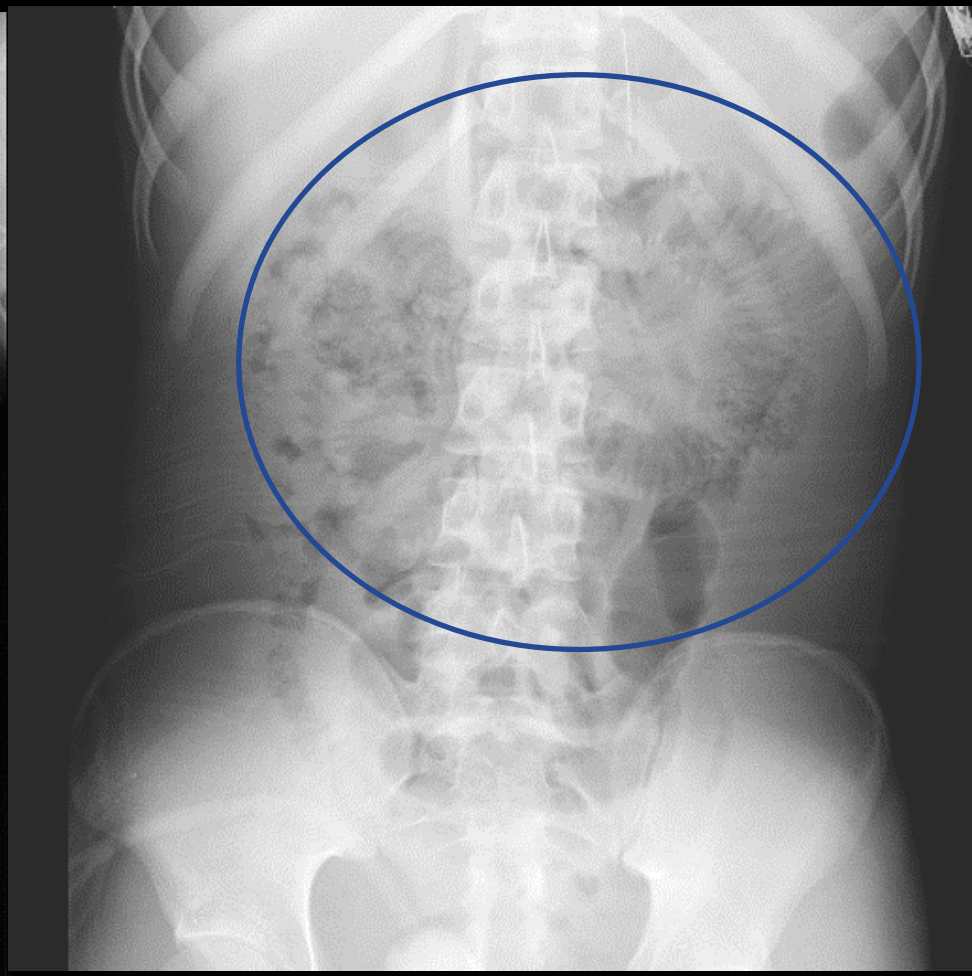

PMCT prior to autopsy

（About 3 days after the death）

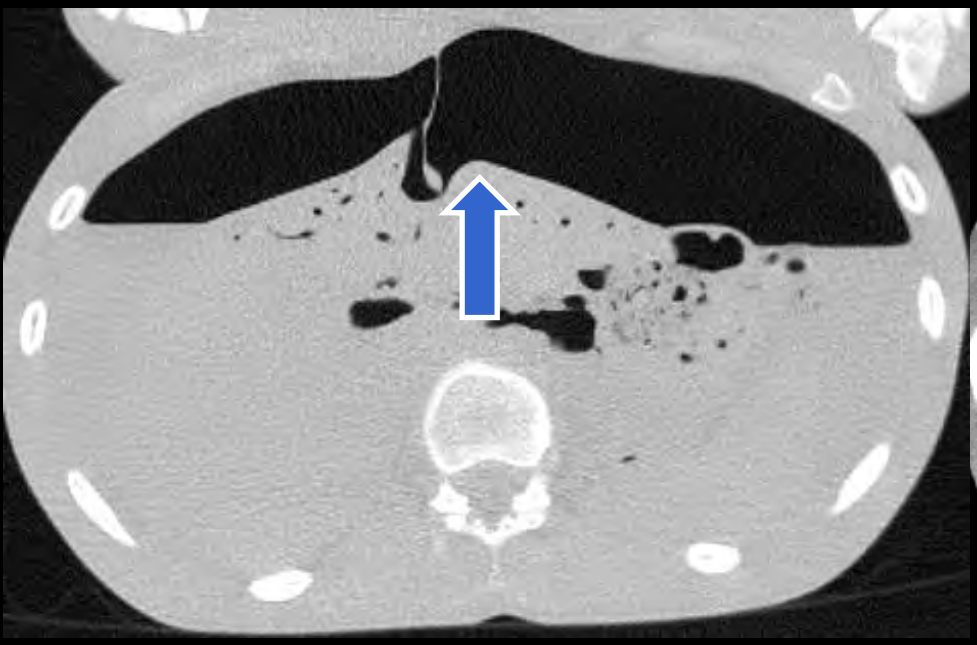

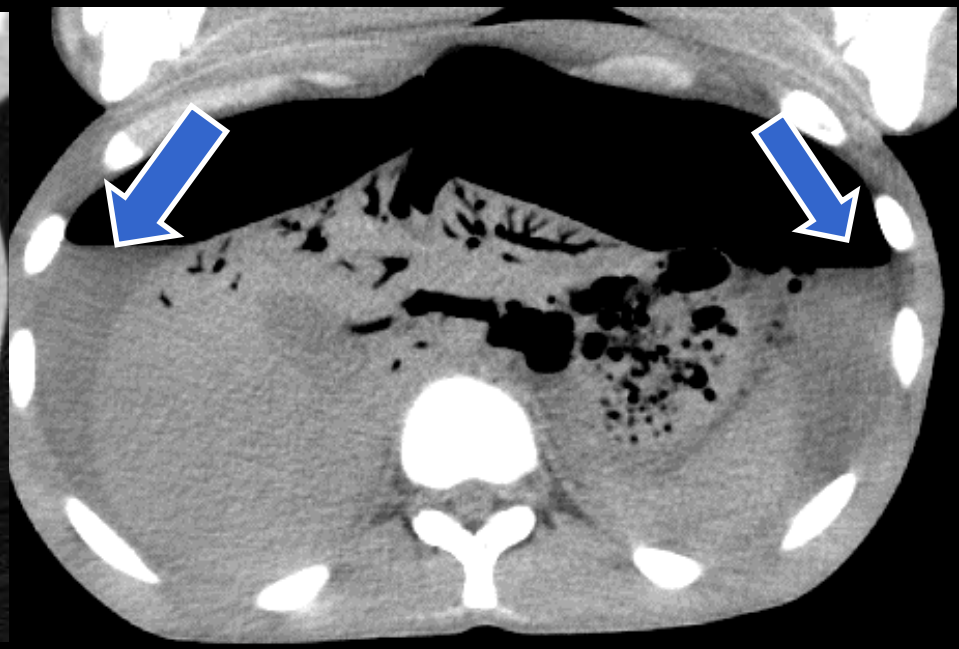

- Massive free air is detected. Perforation site cannot be detected.
- Ascites with slightly high density.
- Jejunum was slightly enlarged but no apparent findings of bowel obstruction

(→Free air was overlooked for the abdominal X ray with supine position at the hospital)

Autopsy findings

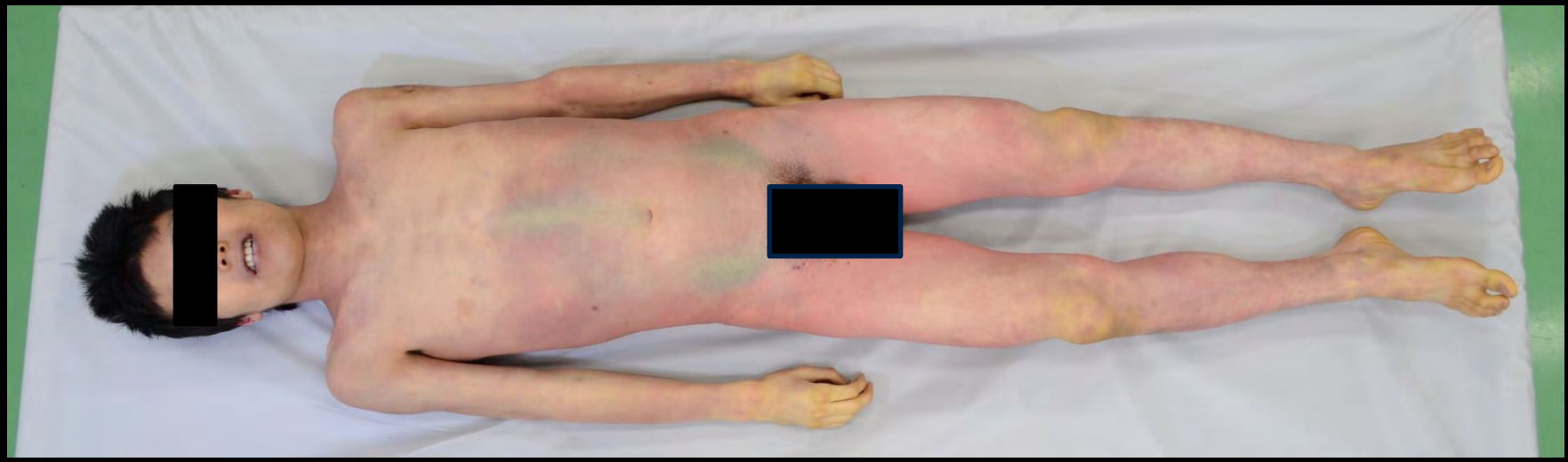

No apparent traumatic lesion.

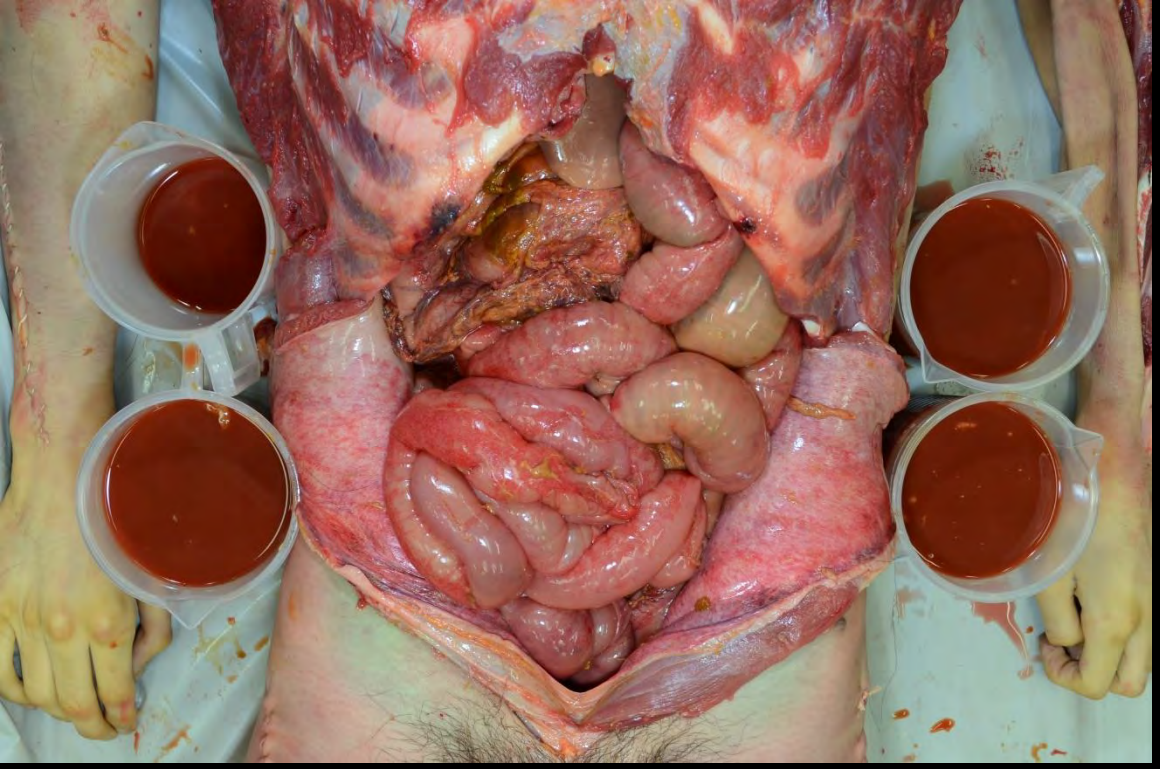

Autopsy result

- Yellowish-brown ascites 1.6L polluted by stool.
- Discoloration of peritoneum.
- Multiple reddish discoloration on the surface of the bowel (panperitonitis).
- High blood concentration of CRP, procalcitonin.

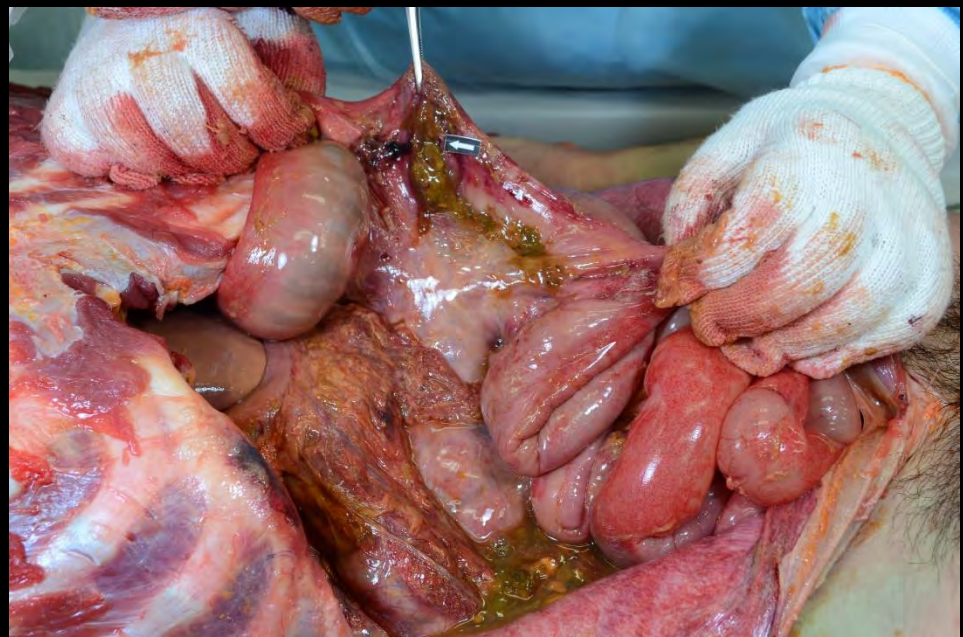

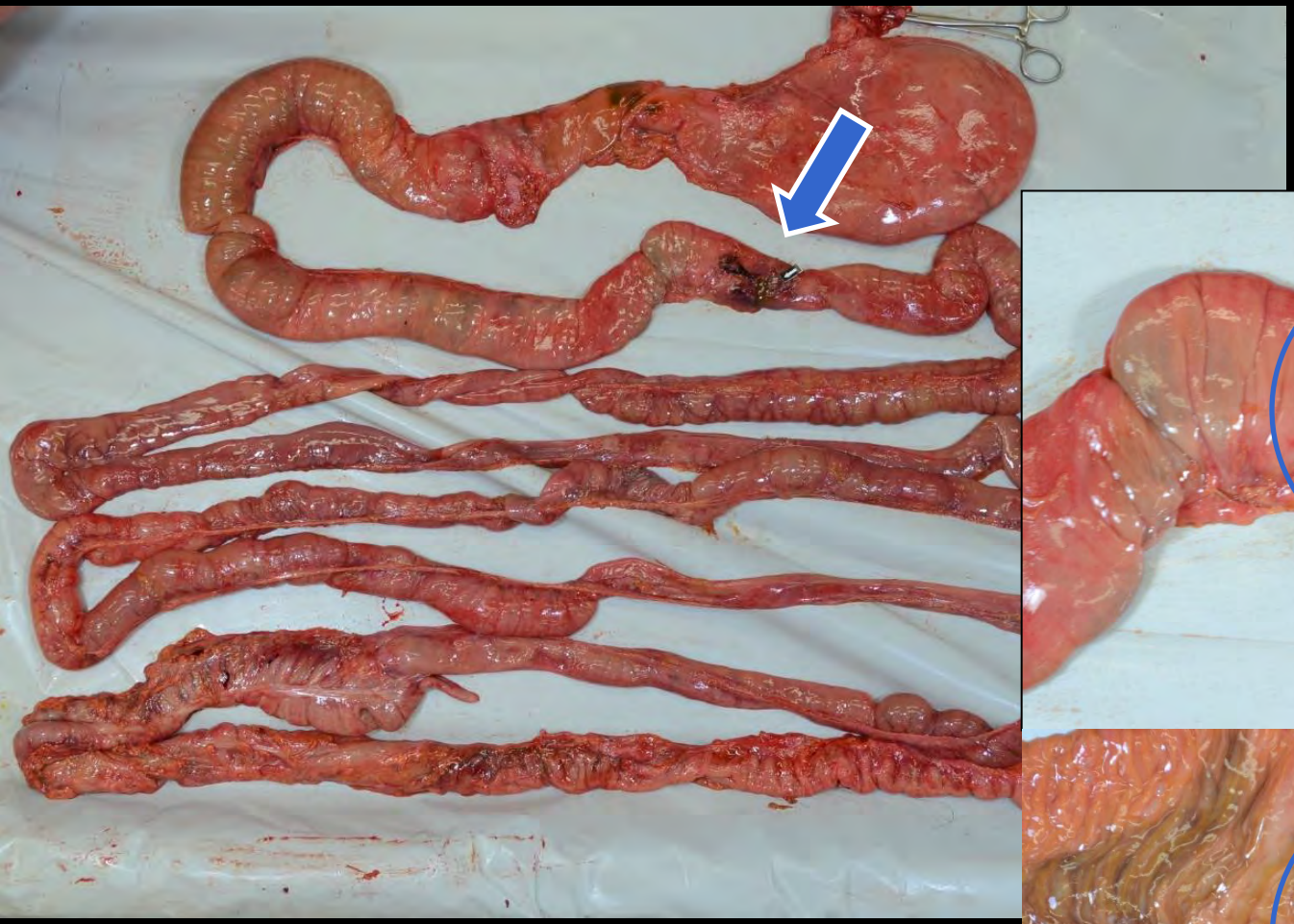

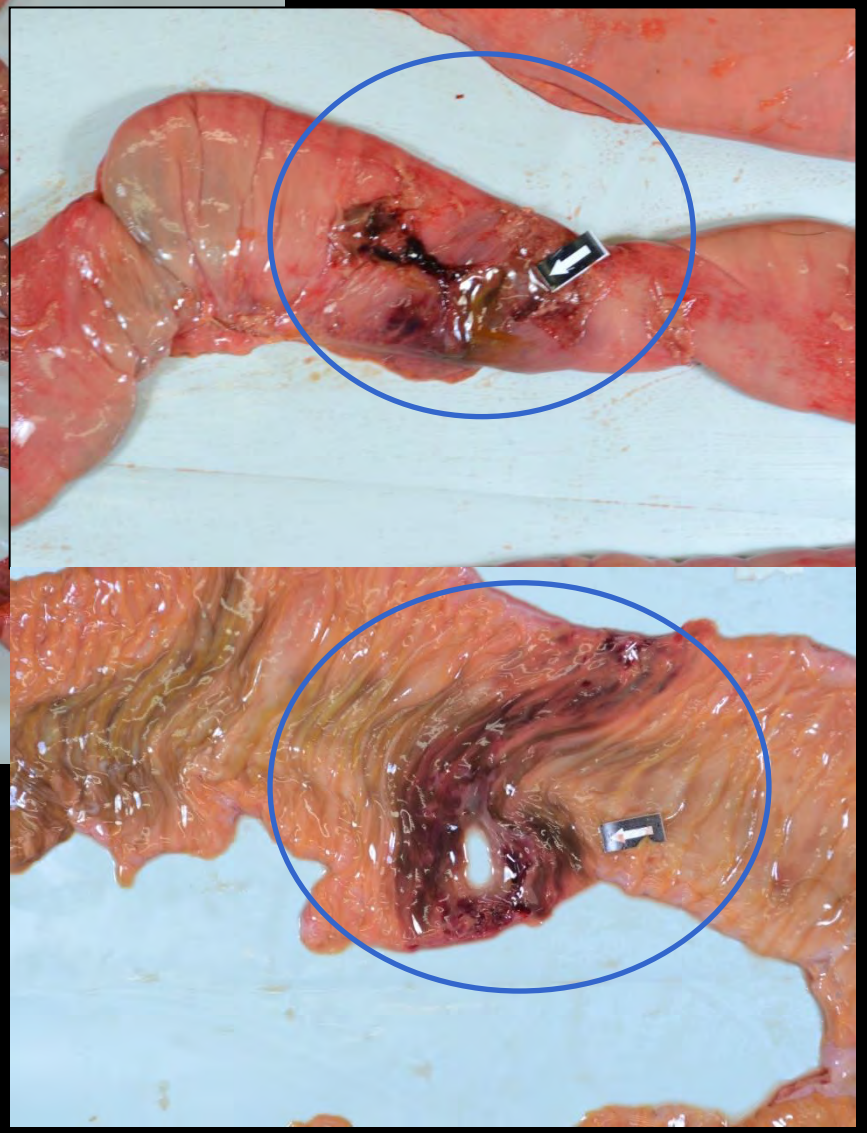

Suspected traumatic perforation at ileum and surrounding submucosal hemorrhage was detected.

Old and new traumatic fractures were detected at autopsy and PMCT

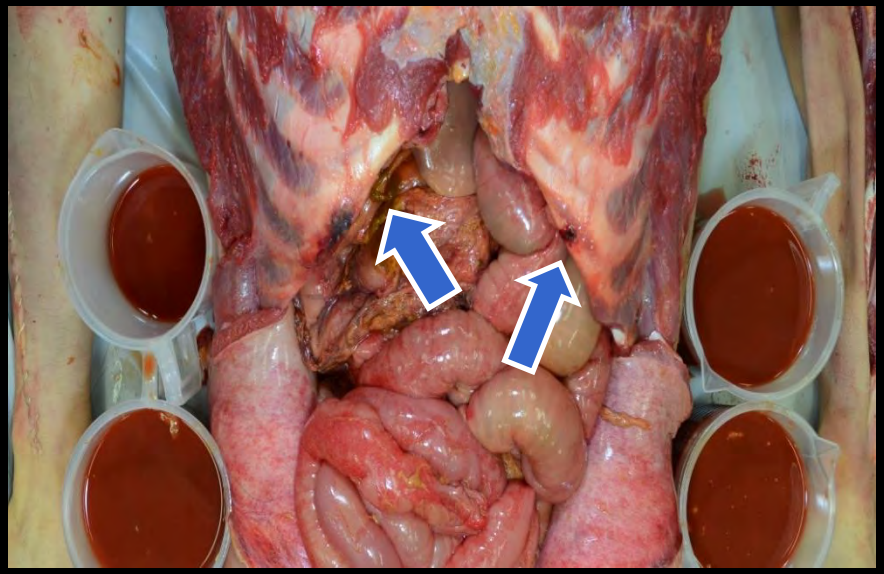

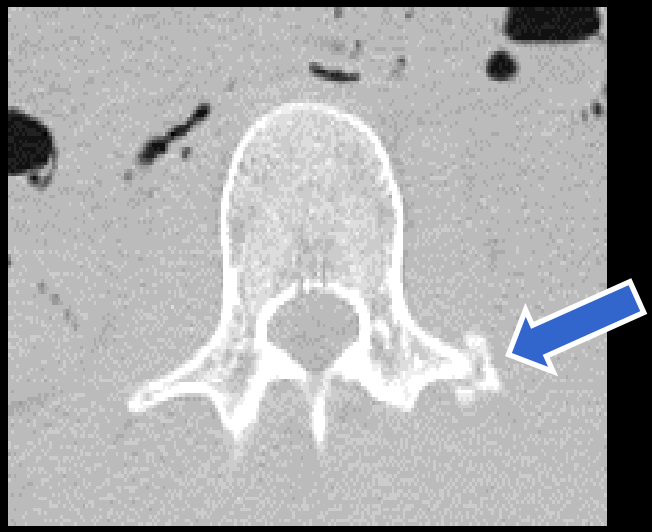

Old fracture at lt. transverse process at L3 level.
（No hematoma at autopsy.）

Lt. upper arm intramustle

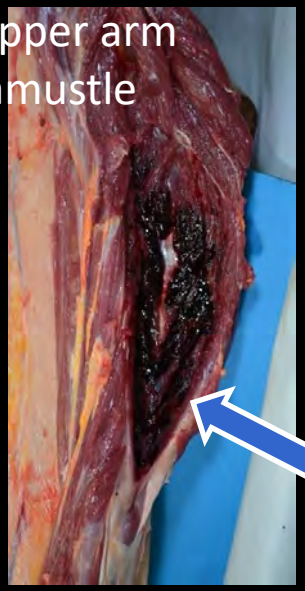

In front of Lumbar supine

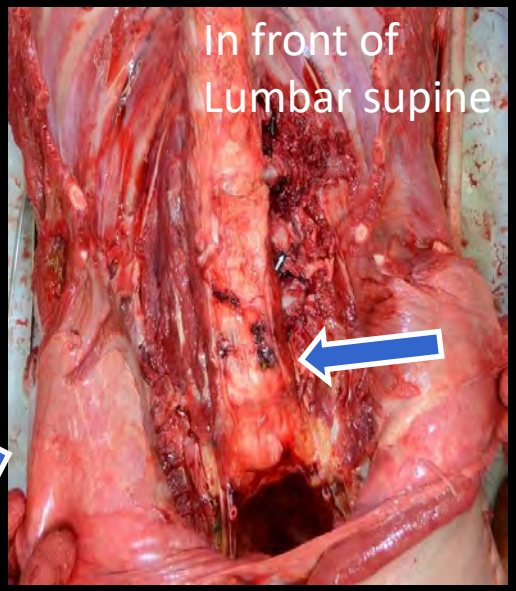

Cause of death

Sepsis caused by traumatic small bowel perforation and peritonitis

(→Staffs at facility confessed the assault on daily basis and kicked at the abdomen the day before his death.)

Misinterpretation pattern of Case 4

Exogenous death was mistaken as endogenous death.

(Insufficient antemortem images were used to determine the cause of death.)

Case 5

- A male in his 50s was found dead in a sofa of a boat being moored at a liver.
- A police doctor (not a radiologist, not a forensic pathologist) took PMCT and interpreted the image as follows; myocardial infarction was the possible cause of death because of the existence of calcification of cardiac artery.
- Since a woman together with him complaint about headache, CO poisoning was suspected and autopsy was performed.

PMCT（About 4 days after the death）

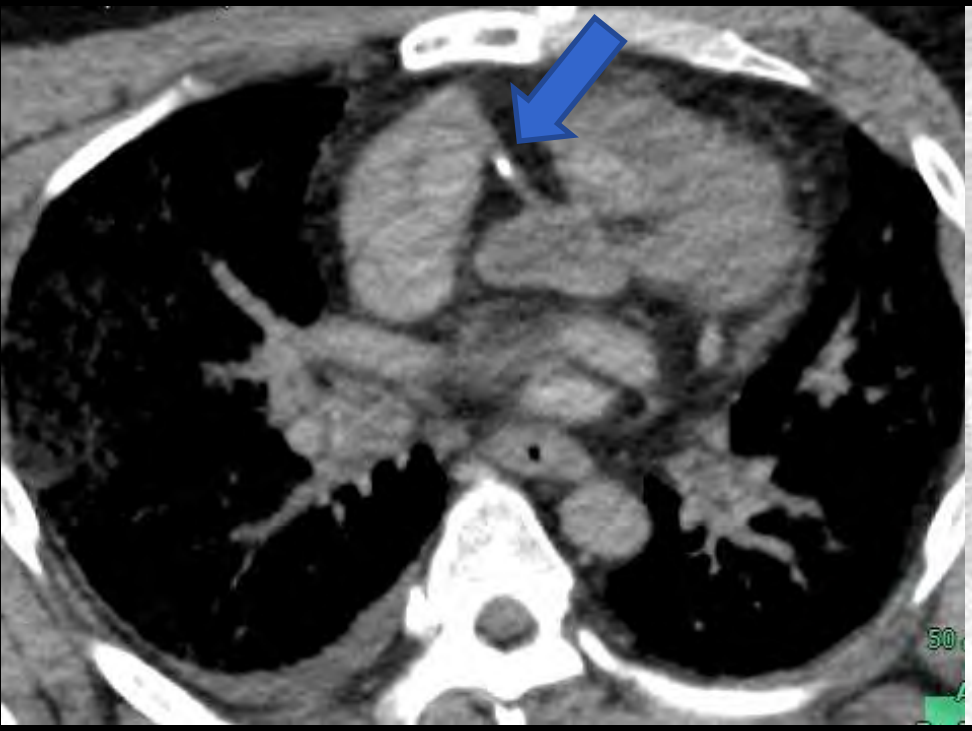

Punctate calcification of rt. coronary artery.

Diffuse ground glass opacity of bilat. lung.

Focal enhancement of coronary artery at autopsy

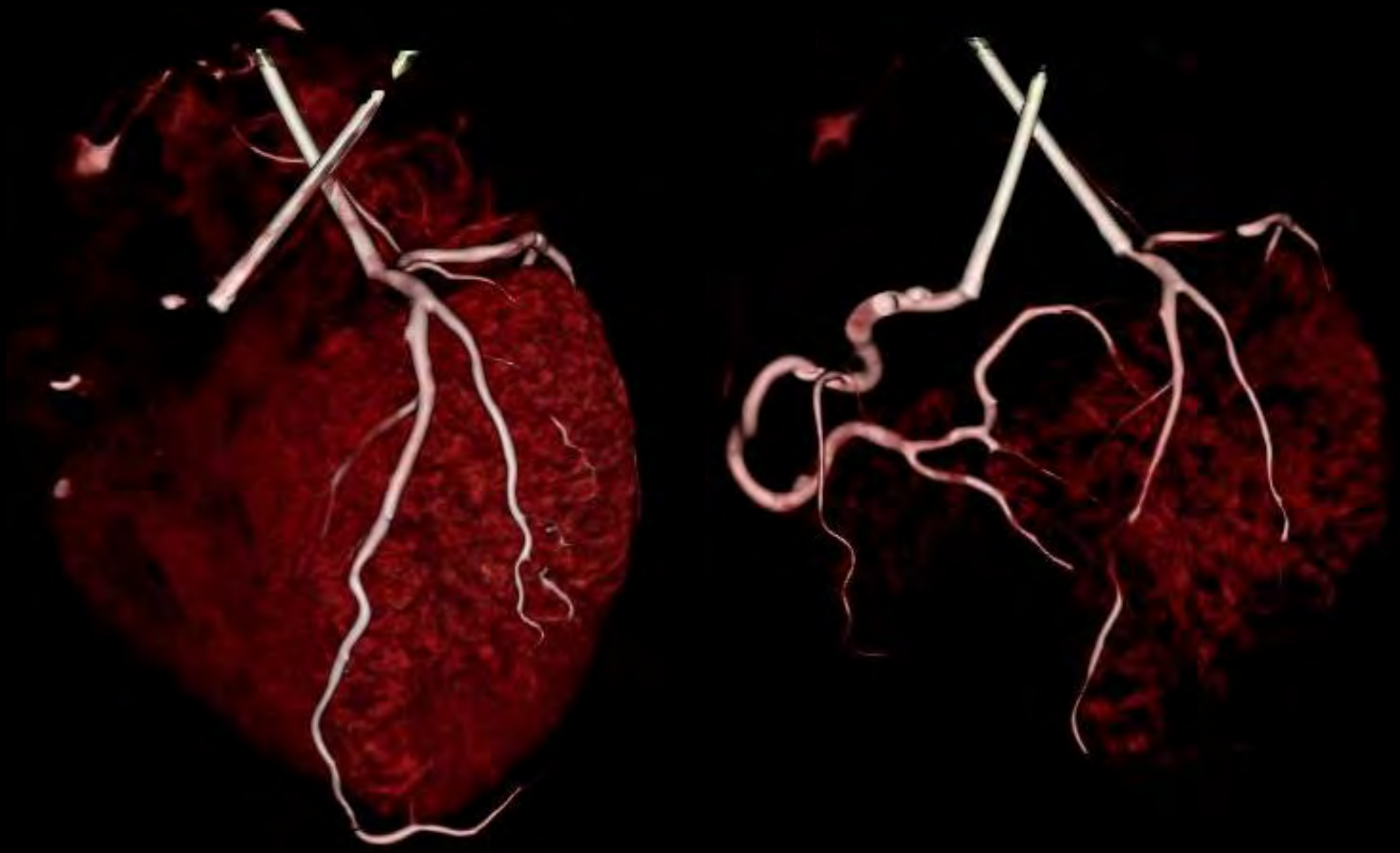

Stenosis of coronary artery(-)

Autopsy results

- Reddish postmortem lividity.
- Blood concentration of CO-Hb 70%.

（Stenosis of coronary artery(-).
Cardiac muscle was intact. ）

Cause of death

Carbon monoxide poisoning

Misinterpretation pattern of Case 5

Minor, unrelated findings obtained were considered to be the cause of death.

Discussion

We presented five misdiagnosis patterns of PMCT revealed by autopsy results.

① Postmortem changes were mistaken for the cause of death.

② Resuscitation changes were mistaken for the cause of death.

③ The cause of death was determined by insufficient examination because the pathological lesion for the true cause was not within the imaging range.

④ Exogenous death was mistaken as endogenous death.

⑤ Minor, unrelated findings obtained were considered to be the cause of death.

Various postmortem artifacts should not be misdiagnosis as cause of death

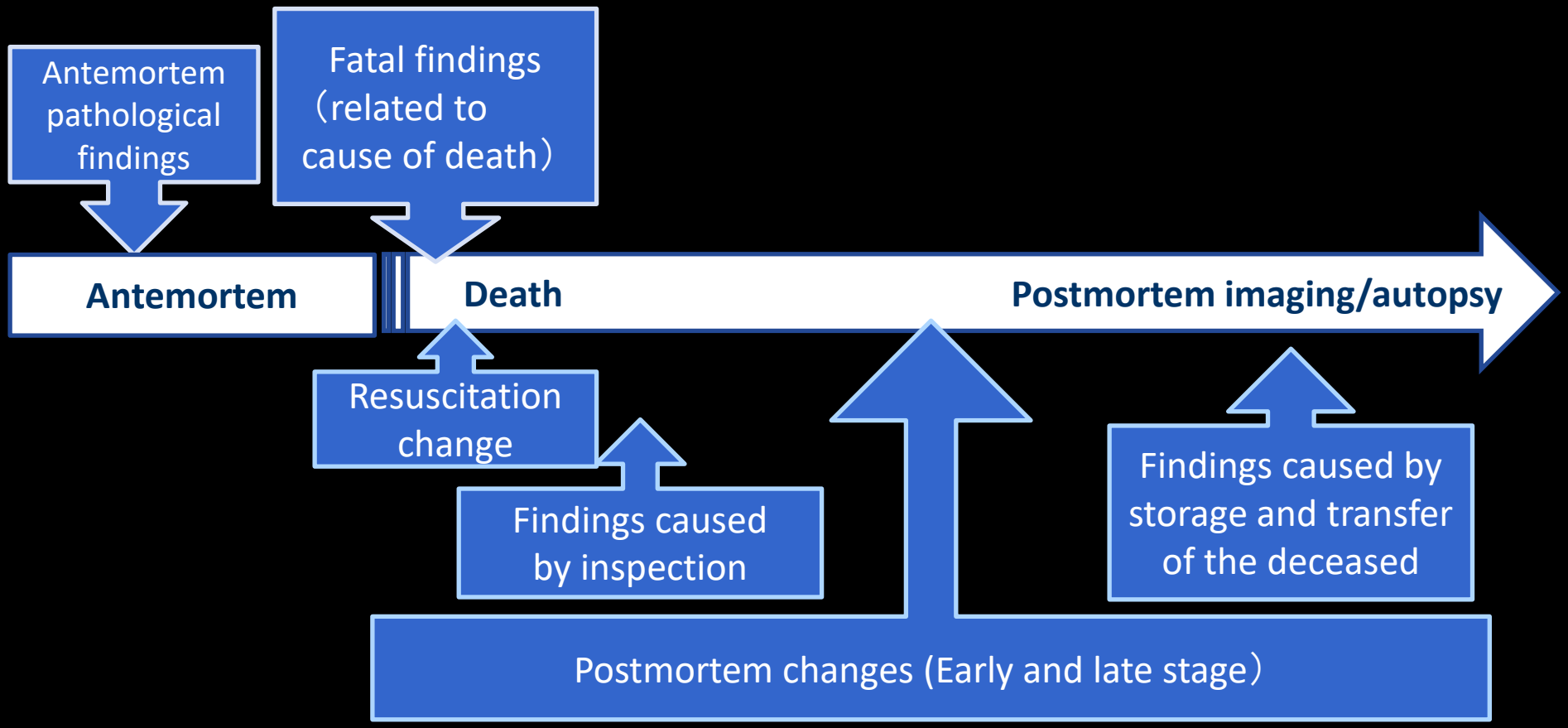

Various version of postmortem artifact

Misdiagnosis caused by recognition bias should be noted

Specialists tend to select the ‘familiar’ diagnosis

Clinical radiologists tend to select ‘endogenous cause of death’.

Postmortem changes early stages

Postmortem changes late stages

Skeleton

Forensic pathologists tend to select ‘exogenous cause of death’.

Conclusion

Proper interpretation and implementation of postmortem imaging is the crucial keystone in the death investigation system.

On the basis of comparison with autopsy, sharing the results and accumulation of evidences should be promoted. Also, collaboration with the forensic departments would be desirable.

千葉大学
CHIBA UNIVERSITY

Thank you very much for your time！

Maiko Yoshida
maikichi0711@ gmail.com

Utility of Postmortem Computed Tomography in the Identification of Intracranial Abnormality in Cases of Fatal Meningitis

Song SH[1], O'Donnell C[2], Dmetrichuk JM[1,3], Pickup MJ[1,3], Williams AS[1,3]

[1]Faculty of Medicine, University of Toronto, Toronto, Canada
[2]Victorian Institute of Forensic Medicine, Southbank, Australia
[3]Ontario Forensic Pathology Service, Toronto, Canada

Introduction

Postmortem CT (PMCT) is an increasingly available and powerful tool in death investigation with the capacity to significantly supplement or supplant anatomical dissection in some cases.

One possible application of PMCT is facilitating targeted dissection of only specific organs in the appropriate context; however, the ability of PMCT to reliably detect intracranial abnormality in cases of fatal meningitis is not known and this may have implications for approaches to targeted dissection.

This study was undertaken to assess the ability of PMCT to detect intracranial abnormality in cases of fatal meningitis.

Methods and Materials

A search was conducted of all deaths that underwent medicolegal autopsy at the Provincial Forensic Pathology Unit in Toronto, Ontario, Canada between January 1, 2013- June 1, 2019 to identify cases with cause of death containing "meningitis".

Twenty-three cases were identified. Three cases were excluded as a postmortem CT scan had not been performed. Control cases were selected for the remaining 20 cases and were matched for age, sex, and year of postmortem examination. Controls were selected such that the cause of death was not evident in the CT head. An additional 15 control cases were specifically added to introduce potentially difficult differential diagnoses (such as cases with known pseudosubarachnoid hemorrhage) as well as add cases to years and age ranges with minimal representation (so that there were more than 2 cases in a visually distinct age range, such as pediatric age). All control cases had undergone full anatomical dissection at autopsy, including removal and examination of the brain (figure 1). The PMCT accession numbers for the cases and controls were placed into a list and the list was randomized.

Four reviewers independently reviewed the CT scans of the head, categorizing them into 3 categories:

1) normal
2) benign findings – dissection not necessary
3) abnormal – dissection recommended

The reviewers were specifically instructed that the implication of categorizing a case as either (1) normal or (2) benign findings would be that the pathologist may not open the calvarium at autopsy. The reviewers had various levels of experience interpreting PMCT images. One reviewer was in their first year of practice as a forensic pathologist and had not previously trained using PMCT. Two reviewers were practicing forensic pathologists (3 and 9- years in practice) who self-identified as being comfortable interpreting PMCT images. The final reviewer was a board- certified radiologist with extensive experience interpreting PMCT images.

The cause of death as determined by the autopsy was accepted as the gold standard. Interobserver agreement was determined by Cohen kappa coefficients between observers. Sensitivity and specificity of PMCT for the detection of any intracranial abnormality requiring dissection in cases fatal meningitis was determined for each reviewer.

Figures

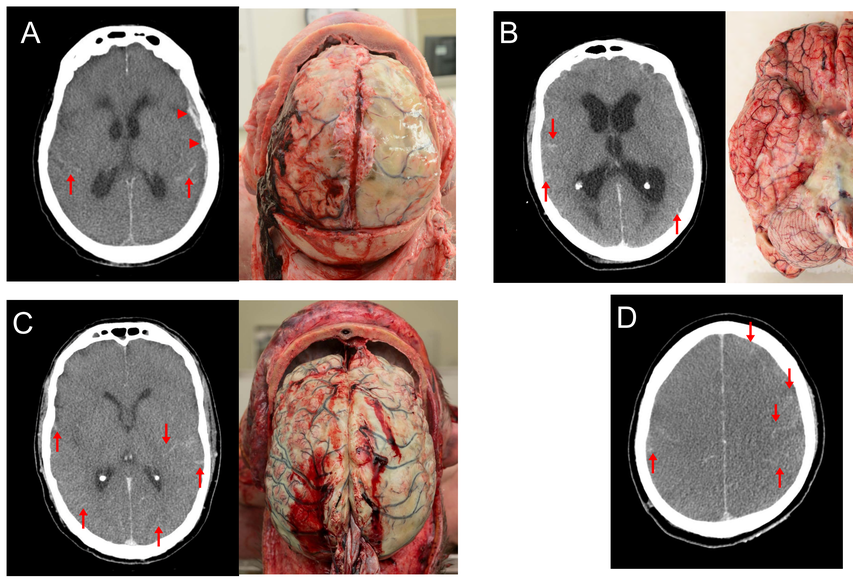

Figure 1. Postmortem CT and autopsy findings in cases of fatal bacterial meningitis compared to PMCT findings in a control non-meningitis case. A – C: PMCT finding of pseudosubarachnoid hemorrhage-like appearance (arrows) that correlated with purulent bacterial meningitis at autopsy. A – in addition, a left subdural hemorrhage is evident on PMCT (arrowheads) and in the autopsy photo. B – in addition, hydrocephalus is evident on PMCT, likely a result of obstructive phenomenon in this basal-predominant meningitis case. D: Pseudosubarachnoid hemorrhage in a case of fatal drug toxicity appearing similar to the meningitis cases (the appearance is the result of a survival interval in the intensive care unit post-resuscitation with the development of cerebral edema and increased intracranial pressure).

Reviewer	Sensitivity % (95% CI)	Specificity % (95% CI)
FP(a)	75.0 (50.9 – 91.3)	74.3 (56.7 – 87.5)
FP(b)	65.0 (40.8 – 84.6)	88.6 (73.3 – 96.8)
FP(c)	65.0 (40.8 – 84.6)	54.3 (36.7 – 71.2)
Radiologist	75.0 (50.9 – 91.3)	65.7 (47.8 – 80.9)

Table 1. Sensitivity and specificity of PMCT for the detection of any intracranial abnormality requiring dissection in cases of fatal bacterial meningitis.

Results

The sensitivity and specificity of PMCT for the detection of fatal meningitis ranged from 65-75% for all reviewers and within experienced reviewers. Specificity ranged 54.3-88.6% for all reviewers and 65.7-88.6% for experienced reviewers (table 1).

In 2 cases all reviewers did not identify an indication for dissection in cases that were found to be meningitis at autopsy and in an additional single case only the most inexperienced reviewer suggested dissection in a case of meningitis. Between experienced reviewers, in a single case only the board-certified radiologist identified an indication for dissection and in another case only the forensic pathologists identified an indication for dissection, when the radiologist did not suggest dissection.

Kappa coefficients ranged from fair (0.273-0.384; most inexperienced reviewer to other reviewers), moderate (0.487 FP(a) – radiologist), to substantial (0.656 – FP(a)–FP(b), 0.672 FP(b)-radiologist).

Discussion

PMCT is well-suited to detect skeletal trauma, intracorporal gas, and foreign bodies, but there remain limitations that prevent PMCT from entirely replacing anatomical dissection in death investigations, depending on the circumstances of the case and the specific medicolegal questions to be answered. Fatal pathology and/or injury to soft tissue and organs may not be apparent due to inherent limitations in the visualization of these processes in non-contrast enhanced studies. Cardiac, pericardial, lung, vascular, liver, kidney, spleen, and diaphragm injuries have been reported as often missed [1]. There is a relative paucity in the literature regarding the use of PMCT in determining natural causes of death. Available evidence suggests that common natural causes of death such as cardiovascular disease (myocardial infarction), pulmonary embolism, cancer, and infectious diseases can be missed if using PMCT alone [2,3].

The current study demonstrates that there is a possibility that fatal meningitis can be missed using PMCT alone, regardless of the level of training or experience of the image reviewer. Using a conservative approach, asking reviewers to seek any intracranial abnormality that they felt should be further assessed by dissection, such intracranial abnormalities were noted in the majority, but not all, cases of fatal meningitis, with an overall sensitivity of ~65-75%.

Summary

- PMCT is a powerful tool that is increasingly recognized for its capacity to supplement or supplant traditional anatomical dissection in certain medicolegal cases
- Current forensic autopsy practice may include altering the approach to anatomical dissection after consideration of the history/circumstances, death scene information, and findings of PMCT
- The current study demonstrates fatal bacterial meningitis may be missed by review of the PMCT findings alone, with a sensitivity of PMCT between 65-75% for the detection of any intracranial abnormality requiring dissection in cases of autopsy proven bacterial meningitis
- In the absence of a history to suggest meningitis, targeting anatomical dissection to exclude opening of the calvarium presents a potential risk of missing fatal bacterial meningitis

***Corresponding author:** Andrew S. Williams, MD FRCPC (AP & FP): andrewscott.williams@mail.utoronto.ca*

References

1. Jalalzadeh H, Giannakopoulos GF, Berger FH, et al. Post-mortem imaging compared with autopsy in trauma victims – A systematic review. Forensic Science International. 2015 Dec 1;257:29–48
2. Christe A, Flach P, Ross S, et al. Clinical radiology and postmortem imaging (Virtopsy) are not the same: Specific and unspecific postmortem signs. Legal Medicine. 2010 Sep;12(5):215–22.
3. Ross SG, Bolliger SA, Ampanozi G, et al. Postmortem CT Angiography: Capabilities and Limitations in Traumatic and Natural Causes of Death. RadioGraphics. 2014 May;34(3):830–46.

Virtual Autopsy– Challenges in implementation in Indian Medicolegal System

Dr Abhishek Yadav

Associate professor, Faculty Incharge- Mortuary, Faculty Incharge Histopathology

Department Of, Forensic Medicine, All India Institute of Medical Sciences, New Delhi

E-mail: drayad_in@yahoo.com

What is virtual autopsy

- Latin term *virtualis: "usable", "industrius", or "better."*
- Greek terms *autos* "self" and *opsomei* "I will see"
- "VIRTUAL AUTOPSY" is the method which combines and analyses: *(Term used in Book By Dr Michael Thali*)
- 3D photogrammetric surface scan of corpses.
- Images from Computed tomography (CT)
- Magnetic resonance imaging (MRI)
- With minimal invasive technique for taking for Autopsy Samples.

Benefits in Indian Medicolegal System

- Immense help In Sudden Non Violent Deaths
- All body parts can berecorded for further additional in-detail examination.
- Reproducibility.
- 2nd and 3rd Opinion.
- Infection and Biohazard control.
- Humanitarian Aspect.
- Less man power / resource required
- The whole body scan Data will stored with a digital interface like PACS.

Legal Status in India

- Autopsy Conducted under Section 174 & 176 of The Code of Criminal Procedure, 1973
- No Section in IPC, CrPC and IEA describes the manner an Autopsy will be conducted.
- Digital Autopsy report will be Valid in Court;
- Sec. 45 of the Indian Evidence Act deals with the Expert opinion related to the interpretations of Radiological Investigations including X-ray, CT and MRI admissible as report, subjected to cross examination
- Section 65B of the Indian Evidence Act relates to admissibility of electronic records asevidence in a Court.

AIIMS SET-UP


12/4/2019 AIIMS and ICMR working on developing 'virtual autopsy' technique, Harsh Vardhan says

AIIMS and ICMR working on developing 'virtual autopsy' technique, Harsh Vardhan says

The medical institutes are working on a technique that allows doctors to conduct postmortems without dissecting the body.

PTI
3 December, 2019 5:49 pm IST

Union Health Minister Harsh Vardhan at Parliament house | Photo: Praveen Jain | ThePrint

Myths Vs Realities In Indian Scenario

Myths:

- It will replace conventional Autopsy
- Cost Effectiveness
- Radiologist is required for reporting
- A CT film has to be read and reported

Reality:

- It is the same Autopsy, methods of conventional autopsy will not be discarded
- Only internal dissection will limited, that too on case to case basis.
- Advanced technology will be used in conventional Autopsy
- Autopsy surgeon will have more detailed study of the case by additional radiological element in autopsy.
- 16 slice CT Scanner with accessories with 5 years warranty: 3.30 cr.
- Health of doctors and the mortuary assistants is important and valuable
- New technology of CT Scanning 60% less (Nanonex Israel Technology).
- Only required for training, consultation and academic collaboration
- Forensic doctors will do a complete examination of CT data in 3D Approach.
- No Automatic Film will be generated.
- Doctor will select the images which he want include in his report.
- He may write only his finding and may not include any image also

Challenges

- Inertia.
- Additional Work.
- Hostile Colleagues.
- Fear of Failure /Unexplored Domain.
- Fear of unknown.
- Un-Interested Radiologists
- Collaboration.
- Lack of Finances:

Way forward

- Start reading books.
- Basic CT reading experience/Training .
- Dual Approach
- Use Radiologist for training, consultation and academic guidance but not as solitary reporting Person .
- Identify Interested Individual/ Departments/ Authorities.
- Establish 2-3 Centers at state level.
- Procure CT Machines.

COST –NEVER A FACTOR BUT WILL POWER IS